A STUDY OF NICKEL MOLYBDENUM OXIDE CATALYSTS FOR THE OXIDATIVE DEHYDROGENATION OF *n*-HEXANE

By

Bavani Pillay

Submitted in fulfilment of the academic requirements for the degree of
Doctor of Philosophy in the School of Chemistry
University of KwaZulu-Natal
Durban,
South Africa

June 2009

As the candidate's supervisor I have/have not approved this thesis/dissertation for submission.

Signed: _____ Name: _____ Date: _____

ABSTRACT

Nickel molybdenum oxide catalysts with different chemical compositions have been synthesized and tested for the oxidative dehydrogenation of *n*-hexane. The co-precipitation method was used for the synthesis and several methods were used to characterize these catalysts. These include inductively-coupled plasma optical emission spectroscopy, Raman spectroscopy, infrared spectroscopy, energy dispersive X-ray spectroscopy, scanning electron microscopy, temperature programmed reduction, temperature programmed desorption, X-ray photo-electron spectroscopy and X-ray diffraction spectroscopy techniques as well as the Brauner-Emmet-Teller technique for surface area determination. The phase composition of the catalysts was largely dependent on the chemical composition.

Catalyst testing on *n*-hexane feed was done with a fixed bed continuous flow reactor and experiments were performed with feed/air ratios above and below the flammability limit. Varied reaction conditions were used for the catalytic testing. Prior to the catalytic testing, blank experiments were performed. Analysis of the products were done both online and offline in conjunction with gas chromatography employing FID and TCD detectors.

The influence of the catalyst on the conversion of *n*-hexane and selectivity to dehydrogenation products is reported. Products observed were the carbon oxides (CO and CO_2), isomers of hexene (1-hexene, 2-hexene and 3-hexene), cyclic C_6 products (cyclohexene and benzene), cracked products: alkanes/alkenes (propane/ene, butane/ene) and oxygenates (ethanal, acetic acid and propanoic acid). β-$NiMoO_4$ was most selective to the hexenes, especially, 1-hexene and a reaction scheme is proposed.

PREFACE

The experimental work described in this thesis was carried out in the School of Chemistry, University of KwaZulu-Natal, Westville Campus, Durban from July 2003 to December 2007, under the supervision of Prof. H. B. Friedrich.

The studies represent original work by the author and have not otherwise been submitted in any form or degree or diploma to any tertiary institution. Where use has been made of the work by other authors it is duly acknowledged in the text.

DECLARATION 1- PLAGARISM

I, Bavani Pillay declare that

1. The research reported in this thesis, except where otherwise indicated, is my original research.
2. This thesis has never been submitted, in part or in whole for any degree or examination at any university.
3. This thesis does not contain any person's data, pictures, graphs or other information unless specifically acknowledged as being sourced from other persons.
4. This thesis does not contain any person's writing, unless specifically acknowledged as being sourced from other researchers. Where other written sources have been quoted, then:

a. Their words have been re-written but the general information attributed to them has been referenced.
b. Where their exact words have been used, then their writing has been place in italics and inside quotation marks and referenced.

5. This thesis does not contain text, graphics and tables copied and pasted from the internet, unless specifically acknowledged, and the source being detailed in the thesis and in the reference sections.

Signed…….

DECLARATION 2- PUBLICATIONS

Publication 1: The oxidative dehydrogenation of *n*-hexane over Ni-Mo-O catalysts, First author: Bavani Pillay, Other authors: Mfanuwenkosi R. Mathebula and Holger B. Friedrich, Appl. Catal. A, 361 (2009) 57.

Publication 2: The oxidative dehydrogenation of *n*-hexane over β-$NiMoO_4$ catalysts, First author: Bavani Pillay, Other authors: Mfanuwenkosi R. Mathebula and Holger B. Friedrich submitted for publication in Applied Catalysis A.

Signed:…….

CONFERENCE CONTRIBUTIONS

Catalysis Society of South Africa conference 2008, Parys, Poster presentation, "Effect of promoters on nickel molybdate catalysts on *n*-hexane oxidation".

Catalysis Society of South Africa conference 2007, Richard's Bay, Poster presentation, "A catalytic study of nickel molybdate on *n*-hexane above and below the flammability range".

38th South African Chemical Institute Convention 2006, Durban, South Africa, oral presentation, "Investigation of nickel molybdate in hexane oxidation".

Catalysis Society of South Africa conference 2006, Mossel Bay, Oral presentation, "A Study of nickel molybdate in hexane oxidation".

1st International IUPAC conference on Green-sustainable chemistry, Dresden, Germany, September 10-15 2006, poster presentation, "Investigation of nickel molybdate in hexane oxidation".

Catalysis society of South Africa conference 2005, Eskom Convention Centre, Midrand, South Africa, Oral presentation, "An Investigation of $NiMoO_4$ in hexane oxidation".

Catalysis society of South Africa conference 2004, North-West University, Potchefstroom, South Africa, poster presentation, "Investigation of molybdates in the oxidative dehydrogenation of paraffins".

ABBREVIATIONS

ATR	attenuated total reflection
BET	Brunauer, Emmet and Teller
BUT	butane/ene
CAT	catalyst
CO_x	carbon oxides
CT	contact time
Cyc C6	cyclic C_6
EDX	energy dispersive X-ray analysis
ESR	electron spin resonance
FID	flame ionization detector
FTIR	Fourier transform infrared
GC	gas chromatograph
GC-MS	gas chromatography mass spectrometry
HPLC	high performance liquid chromatography
HT-XRD	high temperature x-ray diffraction
ICP-OES	inductively-coupled plasma optical emission spectroscopy
LFL	lower flammability limit
ODH	oxidative dehydrogenation
1-HEX	1-hexene
PROP	propane/ene
SEM	scanning electron microscopy
TCD	thermal conductivity detector
THF	tetrahydrofuran
T cracked	total cracked
TPD	temperature programmed desorption
TPO-MS	temperature programmed oxidation-mass spectrometry
TPR	temperature programmed reduction
2-HEX (c)	2-hexene (*cis*)
2-HEX (t)	2-hexene (*trans*)
UFL	upper flammability limit
X	conversion
XRD	X-ray diffraction

XPS	X-ray photo-electron spectroscopy

DEFINITIONS AND CALCULATIONS

1. % Hexane conversion:

$$X_H = \frac{(N_{Hin} - N_{Hout})}{N_{Hin}} \text{ x } 100$$

(where X = conversion, N = moles of hexane, $_{Hin}$ and $_{Hout}$ referring to concentration of hexane in the feed and concentration of hexane in product stream)

2. % Selectivity to specific product:

(where S = selectivity of product, Np = moles of carbon product, N_{Hin}-N_{Hout} = Hexane conversion)

$$S_P = \frac{N_P}{(N_{Hin} - N_{Hout})} \text{ x } 100$$

3. % Yield of a specific product:

(where Y_p = yield of product, Sp = selectivity of product, X = conversion)

$$Y_P = \frac{N_P}{S_p - X_p} \text{ x } 100$$

4. Contact time (s):

$$CT = \frac{\text{Volume of catalyst (mL)}}{\text{flow rate of gaseous feed (mL/hr)}} \text{ x } 60(s)$$

5. % Carbon balance: $(\sum NC_p)/NC_{Hin}$ x 100

(where NC_p = mol carbon product x carbon number, N_{Hin} = moles hexane in feed x carbon number)

$$NC_P = \frac{\sum NC_P}{NC_{Hin}} \text{ x } 100$$

LIST OF TABLES

LIST OF FIGURES

LIST OF SCHEMES

CONTENTS

Chapter 2: $NiMoO_4$ catalysts

Chapter 3: Experimental

Chapter 4: Characterization: Results and discussion

Chapter 5: Non-catalytic studies on *n*-hexane

ACKNOWLEDGEMENTS

First and foremost I thank God for guidance and blessings. You have bestowed upon me knowledge and strength and courage to complete this piece of work. I extend my heartfelt gratitude to my supervisor, Prof. H. B. Friedrich for his guidance, valuable advice, kindness and constant motivation. You have been an aid in helping me realize my true potential. I would like to thank the NRF, THRIP and SASOL in particular, for their financial support throughout the duration of this project. I would also like to thank Dr. C. Dwyer, Dr. R. Meyer, Mrs L. Hattingh, Dr. F.F. Prinsloo, Dr. C. Nicolaides, Dr. F. Otto and Dr. N. Mnqanqeni from SASOL R & D for advice and support.

Thank you to the late Dr. Fiona. Graham from the Electron Microscope Unit, University of KwaZulu-Natal (UKZN) for EDS and SEM analysis, Pat and Roy from the Geology department, UKZN for the XRD analysis and Bret Parel, form the Chemistry department, UKZN for GC-MS analysis. Denzil Moodley (Sasol, Eindhoven) is thanked for the XPS and TPO-MS results and Sabine Verryn from University of Pretoria is acknowleged for the high temperature XRD scans. I thank Monica Corbeanu and Kuselwa Vundisa for their assistance with temperature programmed desorption and temperature programmed reduction.

I would like to thank all the technical staff at the University of KwaZulu-Natal who has assisted me in some way or the other during the duration of my studies. A special thanks to Jayambal Govender for her efficiency in administrative and financial matters, Gregory Moodley for placing of orders, Rickey Parasam for his assistance with building and maintaining a workable reactor system, Harvey Sishi and Jodie Couling for helping with setting up the reactor system. I would like to especially thank Anita Naidoo for valuable input with regard to instrumental techniques as well as her invaluable advice.

I would like to express my deep appreciation to Mr. Mfanuwenkosi R. Mathebula for his time, effort and enthusiasm in assisting me in the lab. Thank you Zibuyile for your assistance too.

During my years as a postgraduate I have forged many friendships. Thanks to you my experience at UKZN has been a pleasant one. Evans and Saroj thanks for your words of wisdom and help through difficult times.

To the two most special people in my life, my mum and dad, Babs and Saroj, you have been my guiding angels, my pillar of strength and my blanket of hope. My journey through life has been difficult at times but thanks to your love and care my path has become clearer. You have shown me that through a relaxed mind, a peaceful soul and joyful spirit you achieve your greatest successes. My dear siblings Pravani and Naven thank you for your respect and warmth. It's really comforting to know that I can depend on you. There were times that your mere presence was uplifting.

CHAPTER 1
INTRODUCTION

Catalysis is a concept that is associated with pioneers of modern physics and chemistry [1, 2] and can be considered a multidisciplinary science and one of the most important research frontiers in chemistry [3].

1.1 Economic aspects

Catalysis is of great importance for developing revolutionary new technologies for the chemical industry as well as for many other industries [3]. More than 90% of chemical manufacturing processes worldwide are catalyzed reactions [1]. Catalysis has been applied in many fields, but the two most popular areas are in energy conversion and in the production of hydrocarbon feedstocks. **Table 1.1** refers to the present and future processes used to produce energy sources and hydrocarbon feedstocks [4]. Other uses include production of foodstuffs, pharmaceuticals and other manufactured goods [1].

Catalysis also plays a role in atmospheric pollution control such as in the abatement of industrial odours, NO_x abatement and the control of motor vehicle exhaust gases [4]. All this underlies the fact that catalysis is of central importance and will remain so in the foreseeable future, especially in generating environmentally benign products and as a key to safer and cheaper manufacture of desirable products [1].

1.2 Heterogeneous catalysts

Heterogeneous catalysts or contact catalysts [2, 5] are favoured industrially because reactants and products are easily separated from the catalyst. These catalysts have been utilized in the medical, fabric, building and food industry [1]. Many heterogeneous catalysts are currently under research and development for paraffin oxidation processes [6, 7]. Selective oxidation by heterogeneous catalysis is an important chemical process for the production of fine chemicals, bulk organic chemicals and for environmental applications [8].

Table 1.1: Present and future routes to organic chemicals and hydrocarbon fuels [4].

Source	Treatment	Chemical product	Fuel product
Crude oil	Refining Reforming Hydrodesulphurization	Alkenes Aromatics	High octane petrol Aviation gasoline Diesel oil Fuel oil
Natural gas			Natural gas
	Oxidation	Methanol	Alkenes and aromatics
	Dehydrogenation	Alkenes, alkynes	
	Steam reforming	Synthesis gas	
Coal	Distillation	Aromatics, phenols	Coke
	Water gas reaction	Synthesis gas	
	Water gas shift	Hydrogen	
	Liquefaction to crude oil substitute		
Biomass	Hydrolysis Fermentation	Ethanol	Ethanol
	Hydrogenolysis	Alkanes	Alkanes

1.2.1 Classification of heterogeneous catalysts

In heterogeneous catalysts the chemical properties of the surface of a chosen substance reflect its ability to act as a catalyst in a specified system. It is important to know the capabilities of various classes of substances to select an effective catalyst for a desired application. **Table 1.2** shows the classification of solids according to their catalytic abilities. For catalysis to take place there must be a chemical interaction between the catalyst and the reactant-product system and the transformation of reactant molecules must occur without any alteration in character or quantity of the catalyst [4].

Table 1.2: Classification of heterogeneous catalysts [4].

Class	**Functions**	**Examples**
Metals	hydrogenation dehydrogenation hydrogenolysis	Fe, Ni, Pd, Pt, Ag
Semiconducting oxides and sufides	oxidation dehydrogenation desulphurization	NiO, ZnO, MnO_2, Cr_2O_3, Bi_2O_3-MoO_3, WS_2
Insulator oxides	dehydration	Al_2O_3, SiO_2, MgO
Acids	polymerization isomerization cracking alkylation	H_3PO_4, H_2SO_4, SiO_2-Al_2O_3, zeolites

Transition metals are good catalysts for reactions involving hydrogen and hydrocarbons because they readily adsorb at the surfaces of metals. Base metals are not attractive for oxidation because at necessary temperatures they are rapidly oxidized throughout their bulk. Many oxides are excellent oxidation catalysts because they interact with oxygen and other molecules. Alumina, silica and magnesia oxides do not interact much with oxygen and are poor oxidation catalysts [4].

1.3 Kinetics of catalyzed reactions

The two different modes in which catalyzed reactions can be studied are the static mode or the dynamic mode. In the static mode the reaction is monitored by measuring the decrease in concentration or pressure of reactants or corresponding increase in the products with time. In this mode reactants are confined within a particular volume of space. The dynamic mode forms the basis of the continuous flow reactor, where gaseous reactants flow through a bed of catalyst particles. There are many varieties of these two basic types of catalytic reactors. With the continuous flow reactor, there are practical limits to the upper and lower flow rates which can be measured and the desired conversion [4].

1.4 Other features of heterogeneous catalysts

1.4.1 General requirements for catalysts employed for industrial processes

An ideal catalyst is one that has high activity, long term stability and, more importantly, high selectivity to a desired product. Depending on the type of catalyst employed, product selectivity generated from a particular reactant varies [2]. The current trends in applied catalysis are 'green catalysis', extension of pure research, and the general need to produce useful products from precursors that are widely available. The most important considerations for industrial catalysts are activity and durability and the prime requirements are: firstly, the catalyst must be able to effect the desired reaction at an acceptable rate under conditions of temperature and pressure that are practicable and secondly, have a long lifetime [4].

1.4.2 Catalytic reactors

The type of reactor employed is determined by the choice of reactants and dictates the physical form of the catalyst used (**Table 1.3**) [4]. It is of crucial importance to predict the performance of commercial reactors to help improve the success of an industrial process [3].

Table 1.3: Compatibility between reaction systems, reactor types and catalyst forms [4].

Reaction system	**Reactor types**	**Catalyst forms**
Gases only	Fixed bed	Coarse particles or monolithic structure
	Fluidized-bed	Fine particles
Gas + Liquid	Batch reactor	Fine particles
	Bubble column reactor	Fine particles
	Continuous stirred-tank reactor	Coarse particles
	Trickle column reactor	Coarse particles or monolithic structure

A **fixed bed reactor** is basically a tube packed with porous solid catalyst through which reactants can flow [3, 4]. It may consist of a single cylindrical vessel or assemblies of smaller diameter tubes [3]. Usually a pressure drop occurs across the bed as a result of obstruction of gas flow by the particles. The pressure drop is dependent on the flow rate, bed length and particle size. The form of catalysts used in fixed bed reactors may vary in size and shape. Since many catalyzed reaction are exothermic, fixed bed reactors usually have facilities for removing the enthalpy of the reaction. One way of doing this is by flowing cooling gas or liquid between the reactor tubes, as in the case of multi-tubular reactors. Another way is to split the bed into sections and pass

cooling gas in the spaces between them [4]. **Fig. 1.1** shows diagrams of fixed bed catalytic reactors.

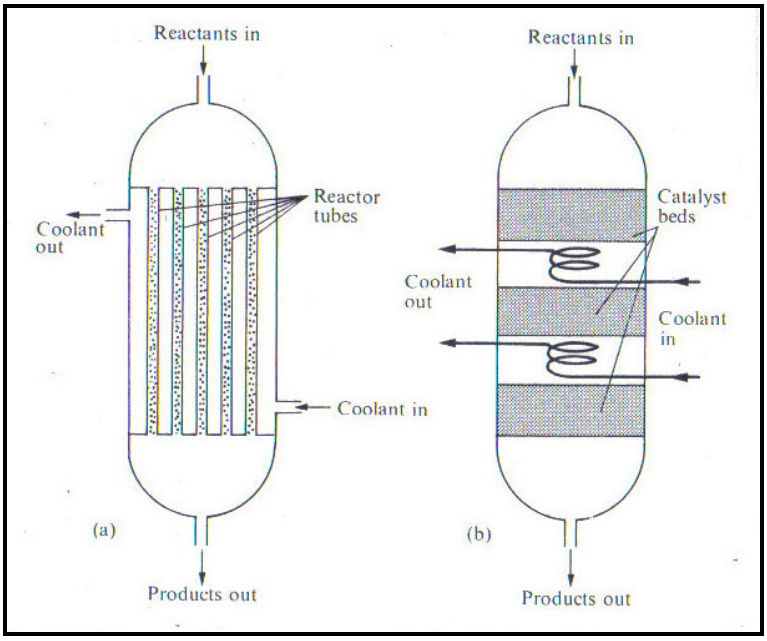

Fig. 1.1: Diagram of fixed bed catalytic reactors a) multi-tubular, b) sectioned bed reactor [4].

1.4.3 Choice of oxidant

For paraffin activation a good oxidant must have the ability to limit undesired consecutive reactions under relatively mild conditions and hence a very active, but selective oxidizing species is required. The most preferred oxidant to date is molecular oxygen because of its affordability and due to lower environmental issues [9, 10]. N_2O is also becoming a popular oxidant from an environmental perspective since it is considered to be a greenhouse gas [10]. It is produced as a co-product in the industrial synthesis of adipic acid. The use of N_2O has been reported for the selective oxidation of ethane over a silica supported molybdenum catalyst [11] and for the selective oxidation of methane to methanol and formaldehyde over molybdenum and vanadium catalysts [12-14].

1.5 Oxidation catalysis

1.5.1 Non selective oxidation reactions

There is much difficulty in finding correlations between the catalytic activity of oxides and their chemical and physical properties. Many transition metals have variable valency and therefore many oxides are possible, each with distinctive structure, stability and catalytic ability. P-type oxides are usually better catalysts for oxidation reactions than n-type oxides because the adsorbed oxygen species are more reactive than the lattice oxide ions [4].

1.5.2 Selective oxidation reactions

Selective oxidation is a reaction in which C-H bonds in the organic substrate are ruptured and oxygen insertion occurs to yield the corresponding aldehyde, ketone and carboxylic acid [8]. In the modern petrochemical industry, selective oxidation is one of the most widely used reactions and products derived from crude oil are converted into a multiplicity of useful products [4]. Majority feed stocks are made from aromatics to alkenes and are used for the plastic and polymer industry and are selectively oxidized to a range of useful products [4, 8]. Since these products are largely available and cheap there has been major growth of the petrochemical industry [4].

Selective oxidation of organic compounds produces more than sixty percent of the chemicals and intermediates [10]. It is estimated that forty billion US dollars worth of organic chemicals are produced annually by selective oxidation [10, 15].

Pure oxides catalyze deep oxidation reactions yielding carbon dioxide and water as products and this is of little practical interest except in the control of environmental pollution. Selective oxidation requires catalysts of a more complex nature.

The main classes of selective hydrocarbon oxidation reactions are given in **Table 1.4.** In reactions belonging to Class I the hydrocarbon is oxidized by dehydrogenation, either intramolecularly to give a diene or a cyclic molecule or intermolecularly to give a dimer. It is possible to use a metal catalyst for dehydrogenation but the high temperatures needed to obtain appreciable product yields may cause the hydrocarbon to decompose completely, giving carbon on the surface. If, however, the thermodynamics allow the reaction at a sufficiently low temperature, then the process may be successful.

Table 1.4: Classification of catalyzed reactions of hydrocarbons with oxygen.

Class I: Oxidative dehydrogenation 1. Dimerization of propene to hexadiene or benzene 2. Dehydrogenation of butane or butene to butadiene 3. Dehydrocyclization of hexane to cyclohexane
Class II: Formation of oxygenated products without carbon-carbon bond fission 1. Oxirane from ethene 2. Acetaldeyde from ethene 3. Acrolein and acetone from propene 4. Allyl alcohol from propene 5. Acrylic acid from propene 6. Maleic anhydride from butadiene, phthalic anhydride from *o*-xylene
Class III: Formation of oxygenated products with carbon-carbon bond fission 1. Acetaldehyde and acetic acid from propene 2. Maleic anhydride from benzene, phthalic anhydride from naphthalene
Class IV: Deep oxidation

The reaction of a hydrocarbon and oxygen produces a highly unsaturated molecule plus water, e.g.

$$2C_4H_8 + O_2 \rightarrow 2C_4H_6 + 2H_2O$$

This is thermodynamically favoured because of the high enthalpy of formation of water. This reaction is typically called *oxidative dehydrogenation*. A suitable selective catalyst would give good yields to butadiene at lower temperatures than would be possible with dehydrogenation [4]. The reaction is exothermic and coke and cracked product formation are very low [9, 16].

The oxidation of olefins (Class II) involves the incorporation of one or more oxygen atoms and it is usually preferable to preserve the original unsaturation and activate one of the carbon-hydrogen bonds instead. This is usually a challenge, since the double bond is usually the most reactive part of the molecule.

In Class III reactions (**Table 1.4**) it is necessary to oxidize the double bond in order to achieve the desired products. These reactions, however, have low selectivities and are wasteful as a fraction

of the carbons is lost to carbon oxides [4]. Generally, catalysts known to be effective for reactions in Class I and II contain either molybdenum or antimony and for Class III, vanadium [4].

The formation of nitriles through oxidative coupling with ammonia (ammoxidation) is another example of a selective paraffin catalytic oxidation reaction, and the direct conversion of propane to acrylonitrile is a reaction that is at the pilot stage of development [10, 17].

Bismuth molybdate was the first selective oxidation catalyst discovered in the 1950's by Sohio laboratories [4, 10]. This catalyst gave an exceptionally high selectivity to acrolein in the oxidation of propene. The principal features of the mechanism and role of the catalyst in this reaction are well understood. The only industrial application of selective paraffin oxidation by heterogeneous gas-solid catalysis is the production of maleic anhydride from butane. This is the most well-known and understood oxygen insertion reaction which uses vanadium phosphorous oxide catalysts where vanadylpyrophosphate being the active phase [4, 10, 18].

1.6 The mechanism for catalytic oxidation

The catalytic oxidation of hydrocarbons was proposed to take place in two steps. Reaction between the oxide and the hydrocarbon results in the oxide being reduced and the hydrocarbon oxidized, and the reduced oxide then reacts with O_2 to restore to its initial state. The ability of the oxide to donate its structural oxygen (electrical conductivity) determines the efficacy of a selective oxidation catalyst, *i.e.* its selectivity and activity. Thus it is a balance between ease of loss of oxygen from the solid and the ability to incorporate gaseous oxygen into the bulk oxide, as well as the mobility of the entities in the solid [1]. The catalyst must have a viable redox couple (M_1^{n+} and M_2^{m+}). This mechanism is referred to as the Mars -van Krevelen mechanism (**Fig. 1.2**) [19].

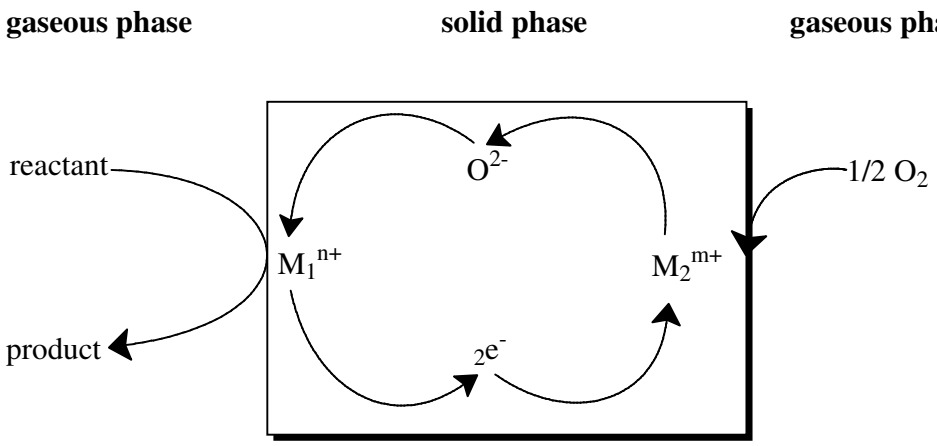

Fig. 1.2: The proposed Mars -van Krevelen mechanism [19].

1.7 The role of acid-base properties in catalytic oxidation

The behaviour of catalysts is dependent on the acid-base characteristics of oxide catalysts. They influence either activation of the hydrocarbon or the rate of adsorption and desorption of reactants and products. The effect of acid-base properties and the proposed mechanism on the activation of paraffins is reaction specific [10]. Heterolytic breaking of the carbon-hydrogen bond is preferable, usually, since radical sites needed for homolytic activation may cause the appearance of radical oxygen species, which may lead to total oxidation [16, 20]. The strength of interaction of products with the surface is dependent on the strength of Lewis acid and base sites on the catalyst. There is an increased probability of a product being totally oxidized to carbon oxides by a basic catalyst if the product possesses strong acidic properties. To enhance selectivity it is better to use an acidic catalyst to favour desorption of an acidic product. Likewise it would be better to use a basic catalyst to favour desorption of basic products such as olefins. It is important to have a balance between acid and base sites on the surface of the catalyst to optimize the productivity of a catalyst [21].

1.8 Reactivity of paraffins in oxidation

In terms of reactivity of alkanes, propane and butane are more reactive than ethane because secondary carbon-hydrogen bonds are more reactive then primary ones. Allylic carbon-hydrogen bonds formed from the oxidative dehydrogenation (ODH) of paraffins with three or more carbons are susceptible to further oxidation. Alcohols, aldehydes, ketones, carboxylic acids, ethers and carbon oxides may also form from oxygen insertion into the paraffin molecule and further ODH of the paraffin may also occur. The stability of partially oxidized products is dependent largely on

reaction conditions and residence time on the catalyst surface which is influenced by the basicity of the catalyst, as discussed previously. Longer length carbon chain olefins are more basic, hence it is expected that they will spend less time on the surface of a basic catalyst [22].

1.9 Paraffins as feedstocks

There is a great demand for aromatics and olefins such as ethylene, propylene and isomers of butene and butadiene in the domestic and worldwide chemical industry [23]. Steam cracking of naphtha and fluidized catalytic cracking in oil refining produces the majority of these feedstocks. However, this is only profitable on a very large scale due to high operational and environmental costs. The increasing demand for such feedstocks has led to research into alternate sources. Paraffins, being cheap and easily available, are good potential substitutes for olefinic and aromatic feedstocks. Paraffins are also cheaper to use and store than olefins and many toxic aromatics.

Paraffins are obtained from natural gas and petroleum and considerable amounts are produced from the Fischer-Tropsch process [24]. With the increasing development of gas to liquid plants worldwide, the supply of higher paraffins is expected to rise considerably, which further encourages hydrocarbon functionalization for the production of important chemical intermediates.

1.10 Advantages of oxidative dehydrogenation

Paraffin oxidation (ODH) provides an alternative route to the manufacture of important organic chemicals. The process of ODH can offer high yields of olefins through the conversion of smaller volumes of alkanes. In comparison to the conventional steam-cracking method of dehydrogenating alkanes to olefins and current catalytic dehydrogenation processes, ODH offers the advantages of reducing costs, lower greenhouse gas emissions and saving energy. Capital and operational efficiencies are gained by eliminating the need for a furnace and for decoking shutdowns, lowering operating temperatures, lessening material demands, conducting fewer maintenance operations and using a greater proportion of alkanes in the olefin conversion process [10, 25].

1.11 Catalytic systems for oxidation

Nickel molybdates, unsupported vanadium pentoxide, vanadia supported on silica, alumina or titania have been reported for the oxidative dehydrogenation of the lower paraffins [9, 16].

Lower alkane (methane, ethane, propane and butane) oxidation has been widely studied. There have been reports regarding the oxidation of methane to syngas [26-28] and its use as a source of hydrogen for fuel cell applications and internal combustion engines [29-31]. More importantly the conversion of methane to methanol and formaldehyde has been of considerable interest [32, 33].

Ethane was successively converted to ethylene using vanadium phosphorous oxide (VPO) catalysts [34] and TiO_2-anatase supported vanadium-molybdenum phosphorous catalysts was used to convert ethane to acetic acid [34, 35]. A later report shows the oxidation of ethane to ethylene and oxygenates under catalytic and non-catalytic conditions using vanadium magnesium oxide (VMgO) catalysts [36].

VMgO catalysts were also reported for the oxidation of propane [37]. With propane, propene was the most selective product. Magnesium vanadium phases and γ-Al_2O_3 supported vanadium oxide catalysts were studied in propane ODH [38-40]. The oxidation of propane to acrylic acid and isobutene to methacrylic acid over Keggin type heteropolymolybdates was also found [41-43]. Metal vanadium oxide catalysts were also investigated for the oxidative dehydrogenation of propane [44].

Butane oxidation with various catalysts results in the production of isomers of butane, butadiene, methyl vinyl ketone, methyl ethyl ketone, crotonaldehyde and maleic anhydride [10, 34, 45, 46] depending on the catalyst used. The most well understood linear alkane process is the conversion of butane to maleic anhydride.

VMgO catalysts were reported for the ODH of C_4 alkanes to alkenes [37]. Promoters such as MoO_3, Cr_2O_3, TiO_2 [46], Mg and Zr [47] were also added to the system to improve the selectivity particularly for the ODH of *n*-butane to butadiene.

There are fewer reports for the oxidation of hydrocarbons above C_5. *n*-Pentane oxidation yielded maleic anhydride and pthalic anhydride [7, 48-50]. Pt single gauze reactors were investigated for the partial oxidation of $C_{1\text{-}5}$ alkanes, yielding mainly oxygenated products [51]. Pentane oxidation with VMgO catalysts gave pentenes and promotion with antimony improved the selectivity to this product [52, 53].

The oxidation of *n*-hexane was reported with VPO catalysts yielding maleic anhydride, phthalic anhydride, benzoic acid, cracked products and carbon oxides as respective products [54]. *n*-Hexane hydrogenolysis with Pd/Al_2O_3 and Pt/Al_2O_3 catalysts gave methylpentanes, methylcyclopentanes and hydrogenolysis products as major products, and benzene and cyclohexane as the minor products [55]. More recently the partial oxidation of *n*-hexane to C_6 oxygenates in a single gauze reactor [56] and *n*-hexane to CO and H_2 on Rh-coated alumina monoliths in short contact time reactors were reported. For stoichiometric C/O ratios 100% conversion was achieved for the hydrocarbon [29]. Most recently the oxidation of *n*-hexane using Mn-exchanged zeolites was reported [57, 58]. The nature of ROOH-mediated kinetically relevant steps in alkane oxidation on Mn zeolites showed that terminal selectivity for linear alkane-O_2 oxidation is strongly influenced by three factors: ROOH regeneration, spatial constraints around Mn cations, and competitive oxidation between heterogeneous and unselective noncatalytic pathways. Synthesis rates for hexanols (ROH), hexanal/hexanones (R(–H)=O), and acids were proportional to hexylhydroperoxide (ROOH) concentrations on all Mn-zeolite catalysts, except Mn-ZSM-58, on which products formed exclusively *via* noncatalytic autoxidation because of restricted access to Mn cations present within small channels (0.36 nm) [57]. Titanium silicate molecular sieves as catalysts were found to be selective for the liquid-phase selective oxidation of *n*-hexane to secondary alcohols and ketones [59, 60]. The kinetics of *n*-hexane total oxidation has also been investigated using $LaCo(1-x)FeO_3$ perovskites [61] and Pt/Al_2O_3 catalysts [62]. *n*-Hexane has been selectively oxidised to *n*-hexanoic acid and adipic acid using aluminophosphates (AlPO) molecular sieves [63, 64].

n-Octane, *n*-decane and *n*-hexadecane, which are important components of gasoline and diesel fuels, were studied over rhodium-coated monoliths to obtain maximum syngas yields [65] and contributions of heterogeneous and homogeneous chemistry for the catalytic partial oxidation of *n*-octane was further investigated [66]. The partial oxidation of *n*-decane to H_2, ethylene and higher α-olefins, over rhodium, platinum and platinum-rhodium alloys in monolith autothermal reactors at short contact times was also reported [67].

The advantage of using paraffins as feedstocks for producing high value products has been highlighted in **Section 1.9**. The aim of this work was to investigate the oxidative dehydrogenation of longer chain paraffins using a heterogeneous catalytic system for the production of high value olefins. In the area of paraffin activation, a small yet growing interest has been placed on the molybdate-based systems. In particular, the $NiMoO_4$ system may provide a promising route to

these high value products. This catalyst based system shall be discussed in detail in the following chapter.

References

[1] J. M. Thomas and W. J. Thomas, "Principles and Practice of Heterogeneous Catalysis", VCH Verlagsgesellsschaft mbh, Weinheim, 1996.

[2] "Catalyst Handbook", Wolfe Scientific Books, London, WC, 1970.

[3] J. M. Thomas and K. I. Zamaraev, "Perspectives in Catalysis", 1992.

[4] G. C. Bond, "Heterogeneous Catalysis, Principles and Application", Oxford Science Publication, 1987.

[5] K. W. Whitten, R. E. Davus and M. L. Peck, "General Chemistry with Quantitative Analysis", Saunders College Publishing.

[6] F. Cavani and F. Trifiro, Catal. Today, 36 (1997) 431.

[7] F. Cavani and F. Trifiro, Catal. Today, 51 (1999) 561.

[8] B. K. Hodnett, "Heterogeneous Catalytic Oxidation", John Wiley and Sons Ltd.

[9] L. M. Madeira and M. F. Portela, Catal. Rev. - Sci. Eng., 44 (2002) 247.

[10] G. Centi, F. Cavani and F. Trifiro, "Selective Oxidation by Heterogeneous Catalysis", Kluwer Academic/ Plenum Publishers, New York, 2001.

[11] L. Mendelovici and J. H. Lunsford, J. Catal., 94 (1985) 37.

[12] M. M. Khan and G. A. Shrader, J. Catal., 91 (1985) 263.

[13] H. F. Liu, R. S. Liu, K. Y. Liew, R. E. Johnson and J. H. Lunsford, J. Am. Chem. Soc., 106 (1984) 4117.

[14] K. J. Zhen, M. M. Khan, C. H. Mak, K. B. Lewis and G. A. Somorjai, J. Catal., 94 (1985) 501.

[15] S. T. Oyama, A. N. Desikan and J. W. Hightower, in "Catalytic Selective Oxidation", S. T. Oyama and J. W. Hightower (Editor), American Chemical Society, Washington. D. C, 1993.

[16] E. A. Mamedov and V. C. Corberan, Appl. Catal. A, 127 (1995) 1.

[17] B. Grzybowska-Swierkosz, Top. Catal., 11/12 (2000) 23.

[18] R. K. Grasselli and J. D. Burrington, Adv. Catal., 30 (1981) 133.

[19] P. Mars and D.W.van Krevelen, Chem. Eng. Sci. Special Suppl., 3 (1954) 41.

[20] V. D. Sokolovskii, Catal. Rev. - Sci. Eng., 32 (1990) 1.

[21] M. Ai and T. Ikawa, J. Catal., 40 (1975) 203.

[22] T. Blasco and J. M. L. Nieto, Appl. Catal. A, 157 (1997) 117.

[23] F. Cavani and F. Trifiro, Appl. Catal. A., 88 (1992) 115.

[24] M. E. Dry, "Applied Industrial Catalysis", Academic Press Inc., London, 1983.

[25] G. Centi, Catal. Lett., 22 (1993) 53.

[26] J. H. Lunsford, in "Natural Gas Conversion II", R. F. Howe, H. E. Curry-Hyde (Editor), Elsevier, Amsterdam, 1994, p. 1.

[27] K. Fujimoto, in " Natural Gas Conversion II", R. F. Howe, H. E. Curry-Hyde (Editor), Elsevier, Amsterdam 1994, p. 73.

[28] Z. Zang, X. E. Verykios and M. Baerns, Catal. Rev. - Sci. Eng., 36 (1994) 507.

[29] L. D. Schmidt, E. J. Klein, C. A. S. Leclerc, J. J. Krummenarcher and L. N. West, Chem. Eng. Sci., 58 (2003) 1037.

[30] D. A. Hickman and L. D. Schmidt, Science, 259 (1993) 343.

[31] S. S. Bharadwaj and L. D. Schmidt, Fuel Process Technol., 42 (1995) 109.

[32] G. A. Fould and B. F. Gray, Fuel Process Technol., 42 (1995) 129.

[33] T. J. Hall, J. S. J. Hargreaves, G. J. Hutchings, R. W. Joyner and S. H. Taylor, Fuel Process Technol, 42 (1995) 151.

[34] P. M. Michalakos, M. C. Kung, I. Jahan and H. H. Kung, J. Catal., 140 (1993) 226.

[35] M. Roy, M. Gubelmann-Bonneau, H. Ponceblanc and J. Volta, Cat. Lett., 42 (1996) 93.

[36] Z. Chao and E. Ruckenstein, J. Catal., 222 (2004) 17.

[37] H. H. Kung, P. Michalakos, I. Owens, M. Kung, P. Anderson, O. Owen and I. Jahan, J. Am. Chem. Soc., (1993) 389.

[38] X. Gao, P. Ruiz, Q. Xin, X. Guo and B. Delmon, J. Catal., 148 (1994) 56.

[39] S. Sugiyama, T. Hashimoto, N. Shigemoto and H. Hayasi, Cat. Lett., 89 (2003) 229.

[40] J. G. Eon, R. Olier and J. C. Volta, J. Catal., 145 (1994) 318.

[41] J. B. Moffat, Appl. Catal., 146 (1996).

[42] I. V. Kozhevnikov, J. Mol. Catal. A: Chem., 117 (1997) 151.

[43] M. Ai, J. Mol. Catal. A: Chem., 114 (1996) 3.

[44] P. Rybarczyk, H. Berndt, J. Radnik, M.-M. Pohl, O. Buyevskaya, M. Baerns and A. Bruckner, J. Catal., 202 (2001).

[45] G. Centi, F. Trifiro, J. R. Ebner and V. M. Franchetti, Chem. Rev., 88 (1988) 55.

[46] D. Bhattacharyya, S. K. Bej and M. S. Rao, Appl. Catal. A, 87 (1992) 29.

[47] M. E. Harlin, V. M. Niemi, A. O. I. Krause and B. M. Weckhuysen, J. Catal., 203 (2001).

[48] G. Centi, J. Lopez Nieto, D. Pinelli and F. Trifiro, Ind. Eng. Chem. Res., 28 (1989) 400.

[49] G. Busca and G. Centi, J. Am. Chem. Soc., 111 (1989) 46.

[50] G. Centi, G. Golinelli and G. Busca, J. Phys. Chem., 94 (1990) 6813.

[51] D. I. Iordanolglou, A. S. Bodke and L. D. Schmidt, J. Catal., 187 (1999) 400.

[52] S. A. Korili, P. Ruiz and B. Delmon, Symposium on Heterogeneous Hydrocarbon

Oxidation Presented before the Division of Petrochemical Chemistry Inc. 211th National Meeting, New Orleans, L. A, 1996.

[53] L. T. Weng, P. Ruiz and B. Delmon, "New Developments in Selective Oxidation by Heterogeneous Catalysis", Elsevier, Amsterdam, 1991.

[54] G. Centi and F. Trifiro, Catal. Today., 3 (1988) 151.

[55] M. Skotak and Z. Karpinski, J. Chem. Eng., 90 (2002) 89.

[56] R. P. O'Connor and L. D. Schmidt, J. Catal., 191 (2000) 245.

[57] B. Zhan, B. Moden, J. Dakka, J. G. Santiesteban and E. Iglesia, J. Catal., 245 (2007) 316.

[58] B. Moden, B. Zhan, J. Dakka, J. G. Santiesteban and E. Iglesia, J. Phys. Chem., 111 (2007) 1402.

[59] J. S. Reddy, S. Sivasanker and P. Ratnasamy, J. Mol. Catal., 70 (1991) 335.

[60] J. K. Kim, Y. S. Ko, T. J. Kim and W.S. Ahn, J. Korean Inst. Chem. Eng., 33 (1995) 511.

[61] V. Szabo, M. Bassir, J. E. Gallot, A. Van Neste and S. Kaliaguine, Appl. Catal. B, 42 (2003) 265.

[62] N. Raic, B. Grbic and A. Terlecki-Baricevic, Appl. Catal. B, 50 (2004) 153.

[63] J. M. Thomas, R. Raja, G. Sankar and R. G. Bell, Nature, 398 (1999) 227.

[64] R. Raja, S-O. Lee, M. Sanchez-Sanchez, G. Sankar, K. D. M. Harris, B. F. G. Johnson and J. M. Thomas, Top. Catal., 20 (2002) 85.

[65] R. Subramanian, G. J. Panuccio, J. J. Krummenacher, I. C. Lee and L. D. Schmidt, Chem. Eng. Sci., 59 (2004) 5501.

[66] G. J. Pannancio, K. A. Williams and L. D. Schmidt, Chem. Eng. Sci., 61 (2006) 4207.

[67] J. J. Krummenacher and L. D. Schmidt, J. Catal., 222 (2004) 429.

CHAPTER 2
NICKEL MOLYBDATE CATALYSTS

2.1 Introduction

Nickel molybdates, $NiMoO_4$, are classed as molybdates because they belong to a group of minerals consisting of the molybdate radical, MoO_4, and a metallic element [1]. Alternatively molybdates are naturally occurring inorganic compounds that are salts of molybdic acid, H_2MoO_4 [2] and chemically these are compounds containing an oxoanion with molybdenum in its highest oxidation state of 6 [3]. Minerals of this chemical class fall mainly into two isostructural groups: the wolframites or scheelites. Depending on temperature or pressure conditions, $NiMoO_4$ may have a wolframite or scheelite structure. $NiMoO_4$ is more likely to have a scheelite structure, since it was reported that compounds with the formula $AMoO_4$ (where A is a metal cation) normally have the scheelite structure, whereas pressure is required to form molybdates with the wolframite structure [4]. In the scheelite structure, the A cation has a coordination number of eight, while the Mo cation is in an approximately tetrahedral coordination to oxygen. The wolframite structure has hexagonally closed-packed oxygen with some octahedral sites occupied by the A and Mo cations [4].

2.2 Transition of phases

Three different structures can exist for $NiMoO_4$, of which only two are stable at atmospheric pressure [5]. These are called the α-$NiMoO_4$ and β-$NiMoO_4$ phases. The structural type depends on the conditions of synthesis, as well as the temperature and pressure [6]. α-$NiMoO_4$ is stable at room temperature and has molybdenum in the octahedral configuration. β-$NiMoO_4$ is the high temperature phase, which is metastable, and has molybdenum in the tetrahedral configuration [6].

The two polymorphs were first identified by Plyasova et al. in 1973 and were found to have a monoclinic crystalline network with the α-phase initially termed the P-phase and the β-phase, then termed the N-phase. Both the P- and N-phases were reversible. The P-phase when heated to a temperature of 650 °C converted to the N-phase and the N-phase when cooled reverted back to the P-phase [7].

Thermal analysis was used to confirm the α-β transition [8, 9]. **Fig. 2.1** shows a DTA cycle for a catalyst with a Ni:Mo ratio of 1 having two transitions, an endotherm at 720 °C due to conversion

of the low temperature phase to the high temperature phase when the catalyst was heated, and an exotherm at 200 °C when the catalyst was cooled was attributed to the reverse transformation of the N-phase to the P-phase [8].

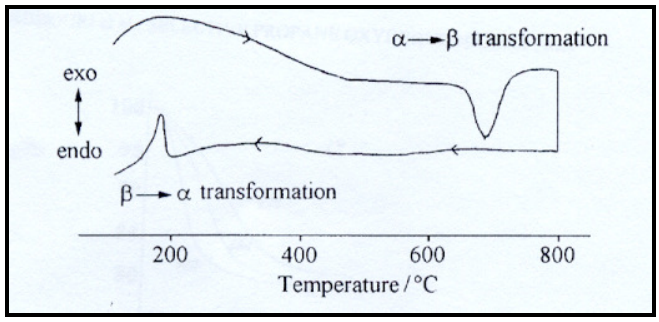

Fig. 2.1: DTA cycle of stoichiometric $NiMoO_4$ phase transitions [8].

Coordination of the molybdenum atoms was confirmed by Rietveld refinement of XRD and DFT measurements, which showed Mo atoms are in a tetrahedral environment in β-$NiMoO_4$, however, in the case of α-$NiMoO_4$, Mo is in a pseudo-octahedral environment with two very long Mo-O distances (2.35-2.40 Å) [9], unlike what was previously thought to be an octahedral environment [10]. Factors influencing the phase transition were recently reported [11].

2.2.1 Structural properties: crystal and magnetic structure of α-$NiMoO_4$

α-$NiMoO_4$ is composed of Ni and Mo ions in oxygen octahedra (**Fig 2.2**) and crystallizes in the monoclinic space group C2/m. Below 19K anti-ferromagnetic ordering is observed. The magnetic unit cell has a doubled c-axis and the magnetic space group is $C_{2c}2/m'$. Ni ions occupy two different sites and therefore two sub-lattices are distinguished. By neglecting the small canting angle between these sub-lattices the magnetic structure is collinear and all moments within one chemical cell are parallel. The magnetic structure can be described as a sequence of such cells with alternating signs along the c-direction [12].

2.3 Stability of the phases

Density functional theory calculations have shown that the α-phase is ~9 kcal/mol more stable than the β-phase [9] and an energy barrier of ~50 kcal/mol for the α-β transition [9]. Time resolved-XRD measurements indicated an activation energy of ~80 kcal/mol [10].

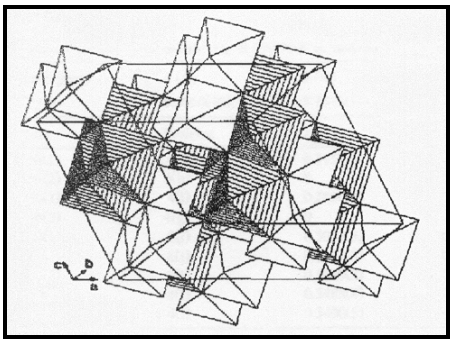

Fig. 2.2: Arrangement of the oxygen octahedra in α-$NiMoO_4$ [12].

2.4 Synthesis of $NiMoO_4$

There are several ways of synthesizing $NiMoO_4$ catalysts but the most commonly used method is co-precipitation [13]. This method, however, lacks reproducibility since both the chemical and phase composition of the precipitate is strongly dependent on the precipitating conditions, such as concentration of reactant ions in solution, pH, duration of aging of the precipitate in the mother liquor, temperature of filtration and temperature of precipitation [14]. There were several attempts to improve the method of co-precipitation and perhaps the most successful of these was the patented procedure [15]. Changes in experimental parameters in the precipitation process can lead to different precursors with the general formula: xNiO $y$$MoO_3$ $n$$H_2O$ $m$$NH_3$ [15-18]. When equimolar solutions of ammonium molybdate and nickel nitrate were mixed with stirring at 85 °C and a pH of 5.6, a yellow precursor was obtained, which, after drying at 120 °C for 5 hours and then thermal decomposition for 2 hours at 550 °C, yielded the $NiMoO_4$ catalyst [15]. The effect of precipitation conditions on the type of precursor obtained is illustrated in **Fig. 2.3**.

Other techniques have been developed for the preparation of catalysts which allow better control of contact between the phases and to control the thickness and structure of the superficial layer. For instance, the advanced reactive sputtering technique produces $NiMoO_4$-MoO_3 catalysts with controlled compositions and structures which can be easily characterized. Thin films of MoO_3, $NiMoO_4$ and combinations of both were prepared over different supports. This technique revealed that the multilayer films of $NiMoO_4$ on α-MoO_3 included the interfacial β-$NiMoO_4$ in the bilayer structures at low temperatures [19].

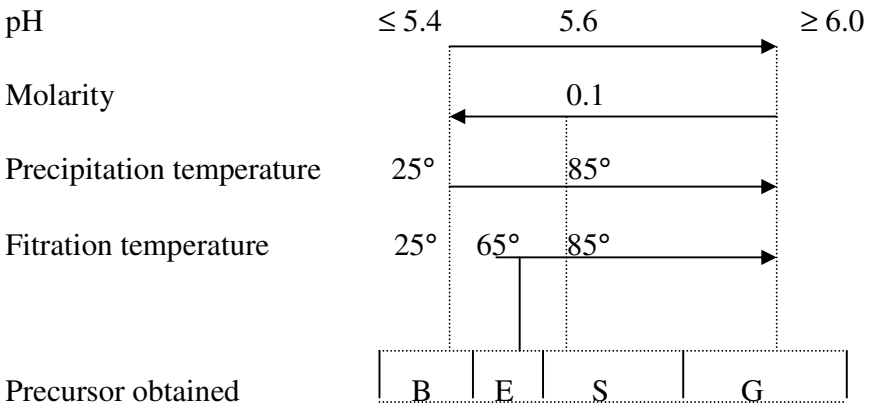

B (blue) = $(NH_4)_4H_6NiMo_6O_{24}.nH_2O.mNH_3$

E = S + B (S= stoichiometric)

S (yellow) = $NiMoO_4.nH_2O.mNH_3$

G (green) = $Ni_{1+\delta}MoO_4.H_2O.mNH_3$

Fig. 2.3: Effect of precipitation conditions on the type of precursor obtained [16].

Physical mixing, impregnation, the sol-gel method, synthesis from organic salts and the use of natural polymers or substances can also be used to prepare these catalysts. The advantage of using organic salts (such as oxalic acid) is that it allows for lower crystallization temperatures [20]. A recent cheap and simple method involving the use of polymers to prepare the catalyst involves creating a polymer network containing ions of the active catalyst of appropriate concentrations in aqueous solution inside the organic matrix (for instance agar-agar gel) [21]. The sol-gel technique is a low-temperature method which is also cheap and simple and allows control of the catalysts composition [21, 22].

2.4.1 Doped and supported catalysts

To enhance the catalytic performance of Ni-Mo-O systems in the selective oxidation of alkanes, several metal ions were used as dopants [23-31]. For *n*-butane ODH, alkali [24] (lithium, sodium, potassium or caesium) or alkali-earth [23, 24] (calcium, strontium and barium) metals were used. These catalysts were prepared through the wet impregnation of α-$NiMoO_4$ using different loadings of nitrate salts. Filtration, drying, crushing and calcination in air for 2 hours at 550 °C gave rise to the final form of the catalyst.

For propane ODH, promoters such as K, Ca, and P were used and also synthesized by the wet impregnation of pure α-$NiMoO_4$ [8, 25, 26].

Elements such as phosphorous, antimony, bismuth or arsenic were also effective as dopants in the oxydehydrogenation process leading to a higher quantity of unsaturated products [27]. Methods for preparation included co-precipitation, impregnation and dry mixing. The impregnation method results in dopants on the catalyst surface, while the sol-gel method produces surface and structural modifications. This allows for compositional homogeneity.

Tellurium and phosphorous were also used to improve the application of Ni-Mo catalysts in the direct oxidation of propane to acrolein and acrylic acid. Mechanical mixing of Te_2MoO_7 or telluric acid with $NiMoO_4$-MoO_3 and impregnation of nickel molybdate with ammonium telluromolybdate were reported techniques for the preparation of Te-doped catalysts [28-30]. For P-doped catalysts the wet impregnation technique of $(NH_4)_2HPO_4$ was used [28, 29]. Antimony was also reported as a promoter for $NiMoO_4$ in *n*-butane oxidation [31].

The use of supported nickel molybdate catalysts in ODH reactions is rare. However, there were reported investigations using TiO_2 (anatase) [32] and SiO_2 [33-36] to support the active phase. TiO_2-supported catalysts were prepared either by wet impregnation of the support with an aqueous suspension of $NiMoO_4$ or the direct precipitation of $NiMoO_4$ on the support surface using solutions of nickel nitrate and ammonium heptamolybdate [32]. SiO_2-supported catalysts were also prepared by wet impregnation [36], by direct precipitation of $NiMoO_4$ on the support or by sol-gel routes [34, 35].

Hydrotreatment catalysts make use of γ-Al_2O_3 as supports which are prepared by depositing transition metals salts onto the support, followed by calcinations to produce oxidic materials that are stable and must be sulfided prior or during the start up of the hydrotreatment process [37].

2.5 Characterization

$NiMoO_4$ catalysts have been characterized by techniques which include infrared spectroscopy, X-ray diffraction, Raman spectroscopy, scanning electron microscopy, BET surface area measurements, X-ray photo-electron spectroscopy, X-ray fluorescence spectroscopy, temperature programmed reduction, temperature programmed desorption, differential thermal analysis, electron spin resonance spectroscopy, X-ray absorption near-edge spectroscopy and density functional theory calculations.

2.5.1 X-ray diffraction

X-ray powder diffraction is one of the most diagnostic tools for the identification of phases in crystals of $NiMoO_4$ catalysts.

There are distinct differences in the XRD patterns between the precursor and α-$NiMoO_4$ (**Fig. 2.4**) [24].

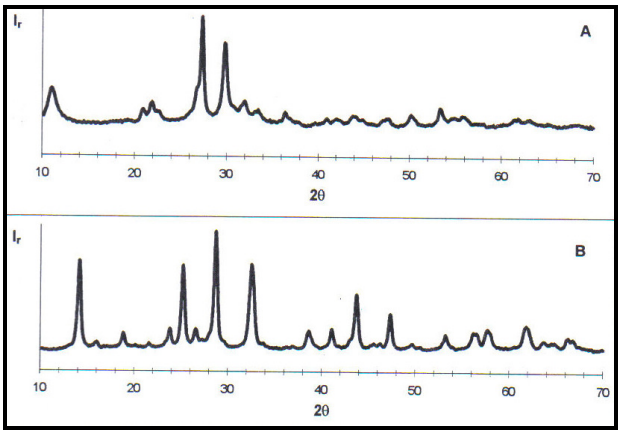

Fig. 2.4: XRD patterns for the $NiMoO_4$ precursor (A) and α-$NiMoO_4$ (B) [24].

Both phases of the stoichiometric nickel molybdate catalyst also show a different X-ray pattern (**Fig. 2.5**). The characteristic peak of the α-phase is at 2θ = 28.7° and for the β-phase at 2θ = 26.4° [38].

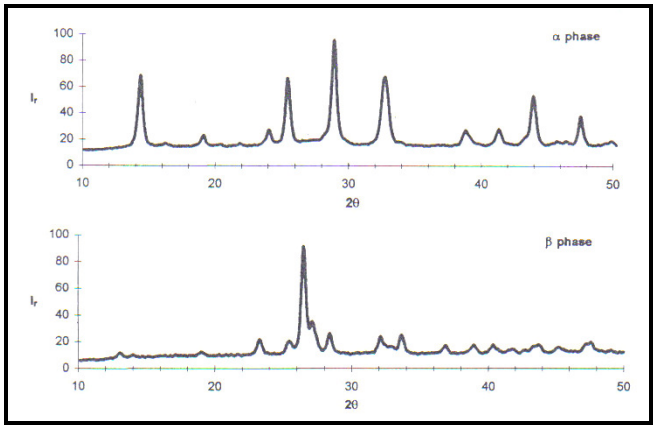

Fig. 2.5: X-ray diffractogram for the α-$NiMoO_4$ and β-$NiMoO_4$ phases [38].

The XRD technique was also used to study the composition of the NiO-MoO_3 system with a wide range of Ni:Mo ratios [7, 39, 40]. Four phases were identified: nickel oxide, molybdenum

trioxide, normal nickel molybdate and nonstoichiometric nickel molybdate [40]. Samples with Ni:Mo ratio < 1 presented the two phases, α-$NiMoO_4$ and MoO_3, whereas species with a ratio of 1 were composed mainly of the $NiMoO_4$. Catalysts with Ni:Mo > 1 consisted of a mixture of nickel oxide, normal nickel molybdate and nonstoichiometric nickel molybdate phases [40]. However, when the Ni:Mo > 1.6, then only NiO and nonstoichiometric nickel molybdate was detected [7].

When catalysts with Ni:Mo ratios > 1 were heated to 650 °C, and then cooled back to room temperature, instead of observing peaks characteristic of the α-phase and NiO in the XRD, the existence of the β-phase at room temperature was observed. This was because the β-phase reacts with excess nickel to form a solid solution of nonstoichiometric composition that is stable at room temperature [7]. The solubility limit for the solid solution formed in nickel is at Ni:Mo = 1.1-1.2 in catalysts containing excess nickel relative to the stoichiometric $NiMoO_4$ [39]. A solid solution of the vacancy type is formed *i.e.* the excess of dissolved Ni ions occupies the normal octahedral positions in the β-phase, while some tetrahedral positions of the Mo remain empty [39].

In another study of Mo- and Ni-rich catalysts, the identification of phases was confirmed [41]. In Ni-rich catalysts only a solid solution of nickel and both phases of nickel molybdate were detected but not nickel oxide [41]. It was concluded that the β-phase is stabilized at room temperature due to the incorporation of excess of nickel in the crystalline lattice of the molybdate [41, 42]. Formation of a nickel-rich solid solution increases the lattice parameters and leads to an increase in the reducibility of the system [42].

Nickel-rich samples, when heated to 550 °C and cooled to room temperature, show the β-phase. The longer the treatment lasts, the higher the percentage of this phase and the smaller the percentage of the NiO phase, however, when the temperature is increased the opposite effect is observed. At very high temperatures the solid solution separates. X-ray data have shown that at 800 °C much NiO is present, at 900 °C contraction of the β-phase occurs and the sample comprises, after being heated to 1000 °C and cooled to room temperature, only of α-$NiMoO_4$ and NiO [42].

2.5.2 IR spectroscopy and Raman spectroscopy

Vibrational spectroscopy of $NiMoO_4$ was studied to understand the nature of the metal-oxygen coordination and the structural transformations of the system as well as the stoichiometry. **Fig. 2.6** shows the tetrahedral and octahedral coordination of Mo in the two $NiMoO_4$ phases [43].

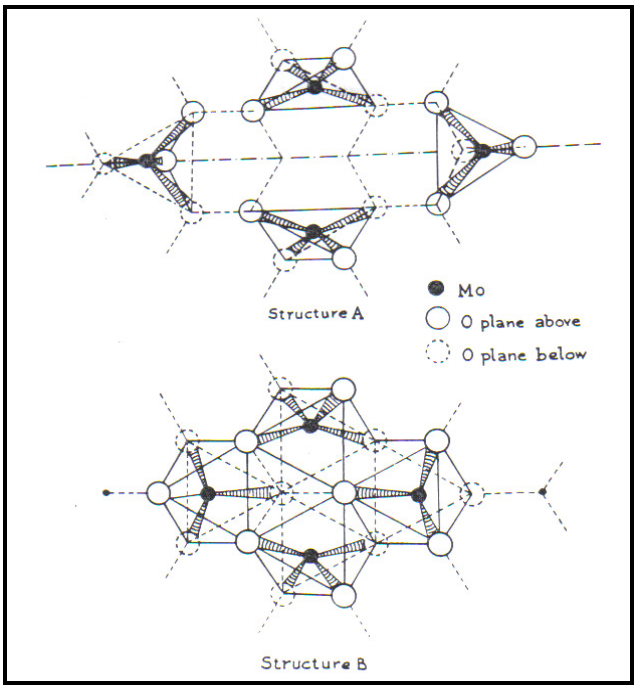

Fig. 2.6: Representation of the tetrahedral and octahedral coordination in $NiMoO_4$ [43].

The IR spectrum of α-$NiMoO_4$ exhibits bands at 600, 935 and 960 cm^{-1} (**Fig. 2.7**) [7, 44]. When the β-phase is stabilized due to presence of NiO at room temperature, a strong band at 950 cm^{-1} and two new characteristic bands at 800 and 880 cm^{-1} (**Fig. 2.7**) are observed due to a change in Mo coordination from 6 to 4 and the possibility of absorption of a second metal. A strong absorption at 945 cm^{-1} is typical of molybdenum in the octahedral configuration [44].

Characteristic bands of MoO_3 in the FTIR spectra are at 980 cm^{-1}, attributed to the vibration of the Mo=O bond, and at 870 and 812 cm^{-1}, attributed to the Mo-O bond [44]. Both these and the absence of bands characteristic of the β-phase are a good indication if there is an excess of either Ni or Mo [41, 44]. Any shifting of the Mo=O band to lower frequencies implies a decrease in the double bond characteristics, and an increase in labilization of the double bond [45].

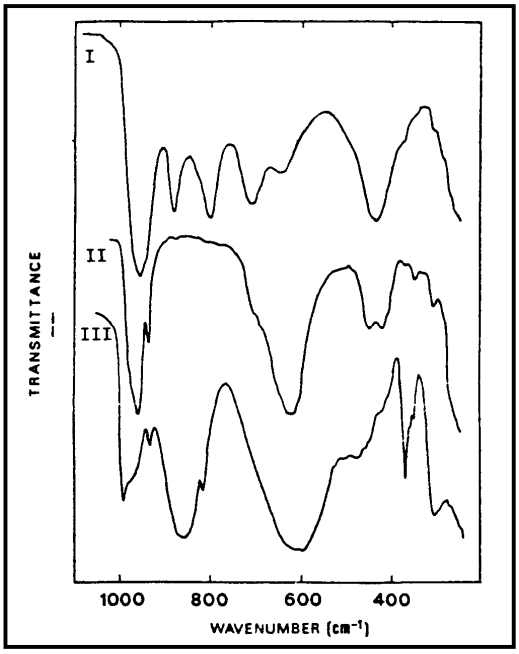

Fig. 2.7: I β-$NiMoO_4$ stabilized with excess NiO, II pure α-$NiMoO_4$, III $NiMoO_4$·5MoO_3 [44].

No specific correlations between the infrared absorptions and catalytic activities in oxidative dehydrogenation of alkanes has been reported for α-$NiMoO_4$ [44], unlike the V_2O_5/MgO catalytic system in which the presence of V=O bonds found in pure V_2O_5 cause the formation of oxygen containing products [44]. The band at ~ 930 cm^{-1} has been found to be due to lattice oxygen [23]. For β-$NiMoO_4$, a multifunctional Ni-O-Mo linkage nature of the active site was postulated in propane oxidative dehydrogenation [44].

Raman spectroscopy is a particularly useful technique for characterizing stoichiometric $NiMoO_4$ catalysts or those with a Ni:Mo < 1, as small amounts of segregated phases such as MoO_3 in the Ni-Mo-O system can be determined since MoO_3 is an excellent Raman scatterer [24, 46].

A Mo-O-Mo deformation mode band around 260-230 cm^{-1} and a band around 390 cm^{-1} could be associated with the Mo-O bending mode. The major feature is the Mo-O stretching mode at around 962 cm^{-1}. Raman bands around 965-944, 880, 390 and 240-210 cm^{-1} are consistent with octahedrally coordinated polymolybdates [24].

The Raman microprobe technique together with SEM allows the differentiation between the two crystallite shapes of $NiMoO_4$ and MoO_3 and indicates the existence of two separate phases. Spectra obtained for catalysts with Ni:Mo < 1 show the presence of $NiMoO_4$ on the surface of individual MoO_3 particles [46].

2.5.3 SEM

The SEM technique provides an understanding of the nature of the active form of $NiMoO_4$ catalysts by giving information about the morphological structure of the surface. Two crystallite forms have been identified. MoO_3 crystallites have well-defined easily recognized hexagonal shapes (**Fig. 2.8a**) and $NiMoO_4$ crystallites are of porous, round and irregular form (**Fig. 2.8b**). The $NiMoO_4$ particles appear to cluster together forming a "sponge-like" structure. With non-stoichiometric Ni/Mo ratios the phase characters are apparent, *i.e.* have distinct particle identity. Separate $NiMoO_4$ and MoO_3 are easily identified. The surface of MoO_3 is covered with $NiMoO_4$ [46].

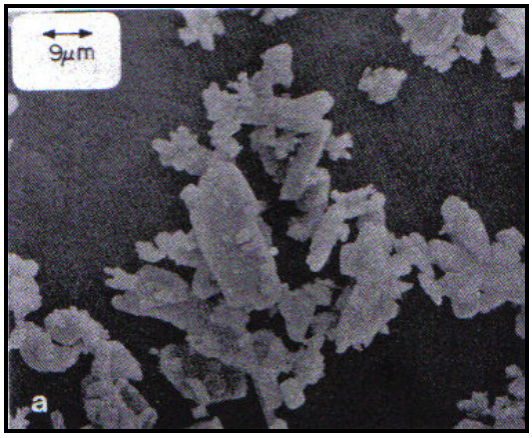

Fig. 2.8a: SEM of pure MoO_3 [46].

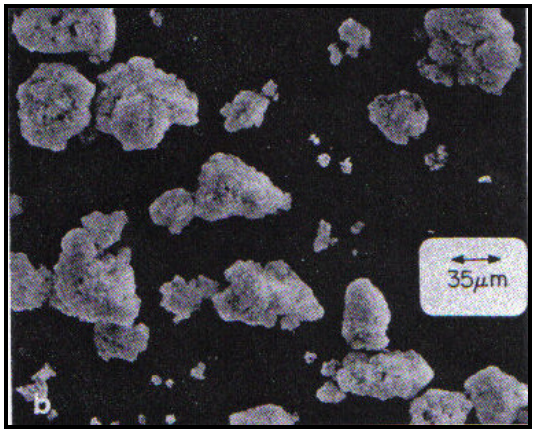

Fig. 2.8b: SEM of pure $NiMoO_4$ [46].

2.5.4 Surface area measurements

BET surface areas for stoichiometric catalysts varied among the different reports [23, 46]. The surface areas for catalysts with Ni:Mo < 1 decrease when the percentage MoO_3 excess increases, varying between 37 m^2/g for the pure $NiMoO_4$ and 3 m^2/g for pure MoO_3 [46]. Catalysts with $NiMoO_4$ as the dominant phase exhibited the largest surface areas. When NiO and particularly MoO_3 increased, the surface area decreased [47].

Promoters such as alkali and alkali-earth metals affect $NiMoO_4$ surface areas [23, 24]. The surface area of the promoted catalyst was found to be smaller than that of the unpromoted catalyst. Also, the surface area of the $NiMoO_4$ catalyst decreases with increase in the ion size and concentration of the promoters [23].

2.5.5 Temperature programmed methods

2.5.5.1 Temperature programmed reduction

The widespread application of nickel molybdate in hydrodesulfurization of petroleum has encouraged studies on the reducibility of this system [48]. The mechanism of $NiMoO_4$ reduction by hydrogen was determined by temperature programme reduction [49]. The profile is shown in **Fig. 2.9**. It shows two maxima, one at 545 °C and one at 725 °C. Reduction was proposed to start at low temperatures, resulting in metals Ni and Ni_4Mo and amorphous MoO_2. Ni^{2+}, after being reduced to metallic nickel, activates molecular hydrogen which favours Mo^{6+} reduction to Mo^{4+} which accounts for the first TPR peak. The second peak is attributed to Mo^{4+} reduction. Metallic nickel activates molecular hydrogen and induces molybdenum reduction with formation of metallic Mo and a Ni-Mo alloy and thus at 725 °C a mixture of Mo, Ni-Mo alloy and Ni_3Mo were found [49]. Reducibility of the catalysts decreases with Cs loading [49].

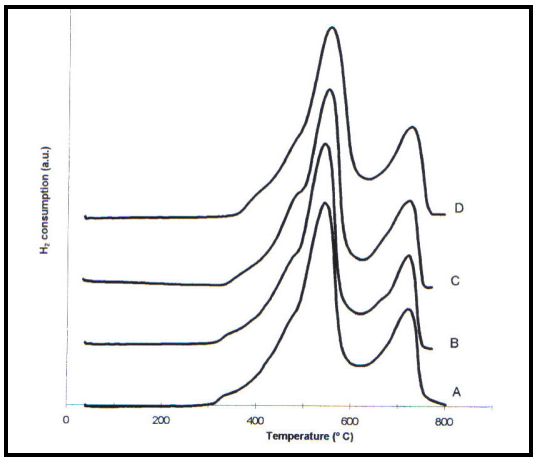

Fig. 2.9: TPR profile of unpromoted (A) and Cs-promoted α- $NiMoO_4$, 1% Cs (B); 3% Cs (C) and 6% Cs (D) [49].

2.5.5.2 Temperature programmed desorption

CO_2-TPD was used to characterize the basicity of the surface of Cs-doped catalysts. The TPD profiles for the doped $NiMoO_4$ shows that doping increases the surface basicity and that an overdoping effect was found for catalysts with a 6% Cs promoted $NiMoO_4$ [50].

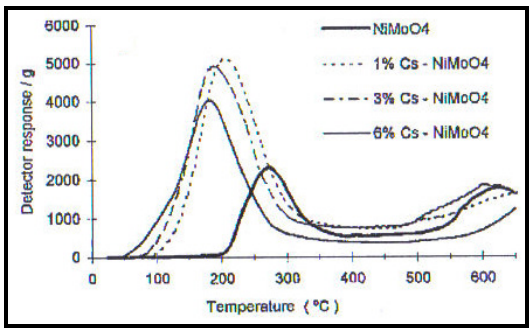

Fig. 2.10: TPD profile of CO_2 adsorbed at 30 ℃ [50].

2.5.6 X-ray photo-electron spectroscopy (XPS)

XPS was used to determine variations in oxidation states of samples with nonstoichiometric compositions. Band positions and bandwiths are identical for samples with or without excess MoO_3, irrespective of the preparation method. Mo 3d binding energies for $NiMoO_4$ are the same as those of MoO_3. The Ni 2p band positions are similar for Ni-Mo-O catalysts, but are very different from those of NiO. Oxidation states in samples with different Ni:Mo ratios do not change unless the NiO phase is present [46].

XPS was also used to quantify the promoter found on the surface of doped $NiMoO_4$ catalysts since alkali and alkali-earth metals are commonly used as promoters of mixed oxides and these were found to remain on the catalyst surface as in the case of alkali metal salts [24].

2.5.7 Electrical conductivity measurements

Both α-$NiMoO_4$ and β-$NiMoO_4$ are n-type semiconductors. The values obtained from electrical conductivity measurements indicate that the main surface defects are in accordance with the model of doubly ionized vacancies for the α-phase and singly ionized vacancies for the β-phase which can be described by the following equilibria [44, 51]:

$$(O_o)_s \leftrightarrow ½\ O_2\ (g) + V_o \qquad (1)$$

$$V_o \leftrightarrow V_o^{\circ} + e^- \quad (2)$$

$$V^{\circ}_o \leftrightarrow V_o^{\circ\circ} + e^- \quad (3)$$

Where

$(O_o)_s$ = surface anion

V_o = anion vacancy with the two electrons trapped

V°_o = singly ionized anionic vacancy

$V_o^{\circ\circ}$ = doubly ionized anionic vacancy

The α-phase has two conduction regimes, the one at 450-650 °C is a p-type semiconductor and at higher temperatures an n-type semiconductor is observed. The β-phase also behaves as a p-type semiconductor in the temperature range 450-650 °C [52]. It was concluded that the electrical transport for both nickel molybdate phases takes place *via* a classical intrinsic band conduction mechanism [52].

2.6 Applications of $NiMoO_4$

Nickel molybdenum catalysts have been applied to many industrial processes ranging from hydrodesulfurization of petroleum distillates [37, 53-60], hydrodenitrogenation of petroleum distillates [60, 61], steam reforming of hydrocarbons, reforming, hydrogenolysis and cracking of *n*-butane [62], water gas shift reactions [63], oxidative coupling of methane [64], hydrogenation [65] and other hydrotreating reactions [48, 66, 67].

2.7 $NiMoO_4$ in selective oxidation reactions

The oxidation reactions in which Ni-Mo-O catalysts are involved include dehydrogenation, isomerization, oxidation with oxygen insertion, partial oxidation and total oxidation. Their catalytic behaviour in oxidative dehydrogenation and partial oxidation processes is influenced by their physicochemical properties.

2.7.1 Oxidation of hydrocarbons

2.7.1.1 Unpromoted Ni-Mo-O catalysts

Selective oxidation of C_4-hydrocarbons with simple $NiMoO_4$ catalysts was found to be most effective in the presence of excess MoO_3 [17, 46]. This was particularly true for the production of maleic anhydride from 1-butene [68], butadiene and furan [69] which showed high selectivities with catalysts with a specific excess of MoO_3. It was established that carbon oxides and maleic

anhydride formation occur *via* competing processes which occur at different MoO_3 sites. The $NiMoO_4$ phase is responsible for 1-butene ODH which selectively blocks MoO_3 sites that lead to total oxidation, allowing selective oxidation to maleic anhydride [69]. In the presence of the pure $NiMoO_4$ high selectivity to butadiene was achieved. This was due to defects on the Ni-O-Mo sites [13].

Pulse feed experiments have shown that ODH of 1-butene to butadiene involves the intervention of reticular oxygen, while different forms of adsorbed oxygen are responsible for the formation of partial and total oxidation products. Mo^{+5} sites that exist in catalysts when MoO_3 is present in the $NiMoO_4$ matrix are able to activate the oxygen molecule resulting in high selectivity to maleic anhydride [17].

Mazzocchia et al. [41], from their investigation involving the oxidation of butane to butadiene and maleic anhydride, obtained significantly different results by changing the reaction conditions such as temperature, contact time and the fuel: oxygen ratio. They found that Mo-enriched compounds gave a higher activity, but reduced formation of dehydrogenation products and increased selectivity to carbon oxides. The butane pulse experiment revealed that the yield of butene was the same when the number of pulses was increased. From this, it was concluded that dehydrogenation occurs without the intervention of lattice oxygen, whereas maleic anhydride is formed by activated oxygen at specific centers that disappear on strong reduction and can be regenerated by reoxidation. These sites were thought to correspond to Mo^{+5} sites [41].

The effect of the Ni:Mo ratio on Ni-Mo-O catalyst was also examined for the oxidation of propene. Catalysts containing excess MoO_3 produced acrylic acid in better yields because MoO_3 increases the superficial acidity which allows the formation of this product. β-$NiMoO_4$ has the ability to convert propene to acrylic acid and oxidizes acrolein to acrylic acid, while α-$NiMoO_4$ is not very reactive in both these reactions [18].

Although excess MoO_3 is the key ingredient for oxidation reactions, the preparation method of the precursor affects the properties of the catalyst and its performance. For instance, preparation using the coprecipitation method yields a catalyst with a smaller electrical conduction activation energy and is more active than one prepared by physical mixing of the two components $NiMoO_4$ and MoO_3 [70].

2.7.1.2 Promoted Ni-Mo-O catalysts

Catalytic properties of Ni-Mo-O systems were found to improve with use of promoters. Ni-Mo-based catalysts formed from one or two crystalline phases and at least one promoter proved effective in the oxidation of propene. When one of the phases was the β-form, a conversion of 95.3% and a selectivity of 95.6% for acrolein and acrylic acid resulted at the relatively low temperature of 370 °C [31].

Binary $NiMoO_4$ and MoO_3 systems promoted with tellurium showed enhanced catalytic performance in propene oxidation, which was attributed to both the synergetic effects generated by the combination of the Mo- and Te-oxides with $NiMoO_4$. Tellurium was found to decrease conversion yet increase the selectivity to acrylic acid, while the selectivity and activity of $NiMoO_4$ increased due to the presence of molybdenum oxide. The decrease in the activity observed with tellurium, may be due to tellurium molybdate accelerating the α- to β-$NiMoO_4$ transformation [71]. The surface coverage of $NiMoO_4$ on MoO_3 was confirmed by the large amount of Ni found on the surface of the catalyst as determined by XPS suggesting the synergism of the two phases [46].

The role of tellurium as a promoter is to keep Ni and Mo in a high oxidation state (eg. $Mo^{5+} + Te^{4+} \rightarrow Mo^{6+} + Te^{3+}$) which is necessary to facilitate the desorption of acrolein, whose formation is assumed to be the rate-determining step [13]. Further studies suggest that the oxygen partial pressure rather than lattice oxygen plays a role and that the presence of tellurium increases the catalyst reducibility [29]. In this case the proposed redox mechanism does not exist and the yields of acrolein can be improved by lowering propene and increasing the oxygen partial pressures [29].

Rather than using propene as the starting material for acrylic acid production, a direct route *via* propane was established using a phosphorous doped Ni-Mo-Te-O catalyst. The reaction pathway proposed for propane oxidation to acrylic acid is given in **Scheme 2.1**. A variety of intermediate products are observed, however, the yields obtained are low [28, 30].

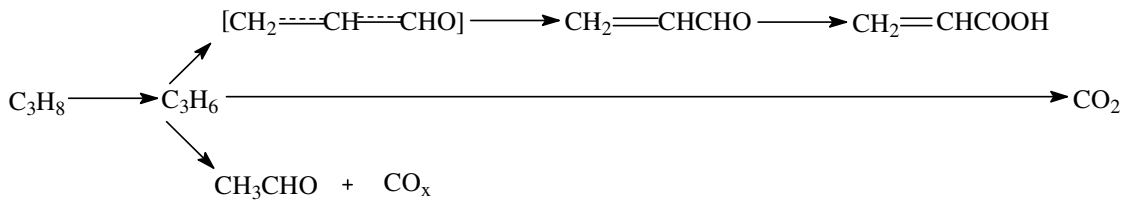

Scheme 2.1: Reaction pathway proposed for propane oxidation with Ni-Mo-O based systems [28].

Sb-doped Ni-Mo catalysts were prepared with the aim of producing maleic anhydride from *n*-butane oxidation. These catalysts proved to be selective and stable and had a long lifetime [72]. The search for new catalysts in this area is ongoing and in this light a process using nickel-molybdenum-based oxides to produce maleic anhydride from *n*-butane oxidation was patented [73].

There are other important oxidation processes in which Ni-Mo-containing catalysts have been used. These include the oxidation of toluene [74], propene and isobutene oxidation to acrolein and methacrolein [75] and the ammoxidation of olefins (propene and isobutene) to unsaturated nitriles [76].

2.7.2 Oxidative dehydrogenation of hydrocarbons

2.7.2.1 Unpromoted $NiMoO_4$ catalysts

Ni-Mo catalysts have been used in the oxidative dehydrogenation of the light alkanes ethane [77], propane and butane [78-80].

There are several diverse reports for the production of mono-olefins (butenes) and diolefins (butadienes) through the ODH of butane. The compositions of the preferred catalysts varied and there appear to be differences regarding the postulated active component [78-80].

Stepanov et al. found that catalysts with a molybdenum:nickel ratio of 1:2 were most effective, providing a 4.5% yield of butenes and 21.6% of butadiene at 590 °C with a molar ratio of *n*-butane to oxygen to steam of 1:0.25:10 and a 100 hr^{-1} space velocity of *n*-butane [78]. Pilipenko et al. found that catalysts with a Ni:Mo ratio of 1.92-1.28 had the greatest selectivities to butadiene [79]. For a molar ratio of C_4H_{10}:O_2:H_2O = 1:0.25:20 mole% the overall yield and selectivity of butadiene and *n*-butenes was 22.6% and 70.5%, respectively. They concluded that

the catalyst with the three phases: nickel oxide, normal and nonstoichimetric nickel molybdate were most effective for the ODH of butane and that an oxygenated nickel oxide compound that exists in different forms was responsible for the catalytic activity. Furthermore, it was proposed that nickel oxide is also responsible for the butane to butenes conversion step [79].

When the ODH of butane was studied by Itenberg et al., catalysts with a Ni:Mo ratio 1.0-1.2 showed maximum selectivity to olefins [80]. Both MoO_3 and NiO showed poor activity and selectivity to the dehydrogenation products in this reaction. It was concluded that these oxides are not responsible for the catalytic activity of $NiMoO_4$ catalysts. Instead the active ingredient was nickel molybdate or a solid solution of nickel oxide in the molybdate lattice. For Ni:Mo ratios lower than 1.0 or greater than 1.2 a decrease in selectivity was observed, probably due to the presence of the individual oxides. These authors also reported that the α- and β-nickel molybdate phases presented the same catalytic behaviour [80]. Thus the crystalline modification of the molybdate lattice does not affect its performance [80].

In contrast, Mazzocchia et al. found that the two phases of $NiMoO_4$ had quite different catalytic behaviour. The α-phase was found to be more active and the β-phase was more selective in butane ODH [23]. Evidence to further support the behaviour of these two phases was found from their work on propane ODH [15, 44]. The selectivity varies because of the different types of oxygen bonds at the active sites. The presence of M=O bonds is usually associated with the formation of oxygen-containing compounds. In the β-phase the character of this bond is weaker than in the α-phase and therefore higher selectivity to dehydrogenation products is expected [44]. The different behaviour of the two phases was also accounted for by the reducibility of the two phases [29]. The relationship between this factor and catalytic behaviour indicates that lattice oxygen plays a critical role in ODH, *i.e.* it is governed by a redox mechanism [81].

In the oxidative dehydrogenation of propane with catalysts with a Ni:Mo < 1, it was found that the α-form was the active phase and that these catalysts have better catalytic performance than the β-form. An interfacial synergetic effect between the planes, (010) of $NiMoO_4$ and (102) of MoO_3, was found [22].

Another report on propane ODH has shown that catalysts with excess molybdenum had a better activity and were five times more efficient than those with excess nickel although they had lower surface areas. Measurement of the change in kinetic constants for propene formation during

propane ODH counterbalances lower surface areas, and the existence of Mo atoms in interstitial positions accounts for this effect [82].

Stern and Grasselli have studied the conversion of propane to propene over molybdate catalysts supported on SiO_2 which showed that the reaction is catalytic and is not initiated by free radicals in the gas phase. The rate-determining step is the breaking of a C-H bond by abstraction of hydrogen from the methylene group of the propane molecule [83]. Of the simple molybdates tested ($AMoO_4$ with A = Ni, Co, Mg, Mn or Zn), the nickel containing catalyst gave the best activity. The molybdenum-oxygen bonds are influenced by the nature of the A metal and is assumed to be responsible for the activation of propane and therefore Ni-O-Mo-O bonds were considered to be the most active [83].

2.7.2.2 Promoted catalysts

The use of doped Ni-Mo catalysts in the ODH of butane was also extensively studied to try and meet the demand for butenes and butadienes. In this area several promoters were explored. With work involving bismuth, antimony and arsenic as promoters, arsenic gave the best yield under similar conditions [27]. More efficient was the Ni-Mo-O catalyst containing cobalt as the third metal [84].

Extensive work was carried out using alkali and alkaline-earth metals as promoters [23, 24]. It was shown that the alkali metals Li, Na, K and Cs significantly improve the selectivity of butenes and butadienes with both α and β phases of $NiMoO_4$ catalysts and this effect increases in the order unpromoted < Li-doped < Na doped < K-doped < Cs-doped. With Cs-doped β-molybdate catalysts the yield of the C_4 olefins was 14.5% at a 28.2% conversion level [23]. This has encouraged further studies on the promotional effects of caesium [50, 51]. The increase in selectivity of ODH products observed when catalysts were doped can be explained by the fact that alkali metals increase the basicity of the surface. This facilitates desorption of nucleophilic olefins/diolefins from the surface of the catalyst preventing overoxidation to carbon oxides. A good correlation between surface basicity and selectivity of C_4 products exists. The dopant is effective only up to a certain concentration, thereafter overdoping is observed [50].

When alkaline earth promoted catalysts (Ca, Sr and Ba) were studied, they revealed a much lower increase in selectivity to the C_4 olefins as opposed to the alkali promoters and this was accounted for by their less basic nature compared to the alkali promoters. However, it was interesting to note

that a very high selectivity to butadienes was achieved. In fact these catalysts exhibited selectivity to the butadienes twice that of the unpromoted catalysts [24]. Again an overdoping effect was observed for the 9% (Ba: Mo) barium-doped catalysts [24]. Similar observations were made when these catalysts were tested in propane ODH. The selectivity to propene increased from 1-9 barium loading % (9% loading giving a 30.5% yield to propene) and then decreased from 12-15% barium loading.

It was found that although alkali and alkaline earth metals improve the selectivity of dehydrogenation products from the ODH of butane with $NiMoO_4$ catalysts, the conversion decreases as the promoter loading or size increases. This may be due to the decrease in the BET surface area after doping [23, 24].

Some ternary molybdate catalysts with the formula $Ni_{0.5}A_{0.5}MoO_4$ (with A = Co, Mg, Mn or Zn) were tested in propane ODH. These catalysts were not as effective as $NiMoO_4$, but from all of them $Ni_{0.5}Co_{0.5}MoO_4$ was the most active and selective [83].

K-, Ca-, and P-doped nickel molybdate catalysts have also been used for propane [8, 25, 26] or isobutene conversion [26]. Propane conversion decreased and propene selectivity increased when calcium and potassium were used as dopants, indicating that basic sites are extremely important for the ODH process. Doping with phosphorous (acidic metal) resulted in an increase in conversion, probably due to increased adsorption on the more acidic catalyst surface [8, 25]. It was suggested that catalytic activity of Ni-Mo-O based catalysts for the ODH of light alkanes is related to catalyst reducibility, while selectivity to dehydrogenation products is dependent mainly on the acid-base character of the catalyst surface [8, 25]. Promoters significantly increase the reduction resistance of nickel molybdate, suggesting that the mobility of the lattice oxygen is not as important. It was proposed that selectivity also depends on the degree of catalyst reduction, since propene formation is improved with the pulse period in a periodic-flow reactor operation [25].

The catalytic performance of stoichiometric nickel molybdate in isobutane ODH was reported to be improved by the addition of potassium oxide which avoids subsequent overoxidation of the reactive isobutene formed, however, methacrolein formation is negatively affected [26]. By using low partial pressure of oxygen and avoiding the use of the promoter, isobutene selectivity was improved due to decreased formation of carbon oxides.

2.7.2.3 Supported catalysts

There are only a few reports using supported catalysts in the oxidative dehydrogenation of light alkanes. These include ODH of isobutene using TiO_2 [32] and SiO_2 as supports [33, 36]. These catalysts were shown to be more selective to isobutene than the unsupported catalysts and this may be due to the acid-base properties of the catalyst surface [36] or to β-phase stabilization at a low temperature [32, 33]. This route to obtain stable β-phase catalysts is very attractive since the phase is metastable at room temperature and for industrial interest it is not practical to keep the reactor operation above 250 °C to avoid the transition to the α-phase. Also, incorporation of excess nickel to stabilize the β-phase at low temperatures favours competitive side reactions. It was found in some cases that catalysts supported on silica, prepared by the sol-gel method, when tested in isobutene ODH, gave no significant yield to dehydrogenation products [34, 35]. The oxidative dehydrogenation of *i*-butane was recently investigated using nanostructured silica supported $NiMoO_4$ catalyst [85].

2.7.2.4 Effects of coke deposition

It was observed in butane ODH that when coke was deposited on $NiMoO_4$ catalysts no deactivation occurred. Instead, conversion increased, as did the selectivity to dehydrogenation products, particularly butadiene. These effects were thought to be due to the stabilization of the more selective β-phase at the low temperature and the presence of catalytically active coke [38].

2.7.2.5 Kinetics and mechanism

Few kinetic and mechanistic studies have been performed with Ni-Mo-O catalysts. The use of $Ni_{0.5}Co_{0.5}MoO_4/SiO_2$ catalysts in propane oxydehydrogenation showed that the reaction proceeded through ODH and that propene was the primary and exclusive product [86]. The propene formed was first oxidized to acrolein which was then oxidized to carbon oxides and acrylic acid. Smaller amounts of CO were also formed directly from propene. The selective oxidation of propane to propene and of propene to acrolein are both zero-order in oxygen, which is commonly found in the oxidation of hydrocarbons over metallic oxides and consistent with the redox mechanism of Mars-van Krevelen [81]. These reactions are first order with respect to the hydrocarbon, which is consistent with a rate limiting reaction between the hydrocarbon and an active site on the catalyst surface. The deep oxidation of propane into CO and CO_2 is half order in oxygen and is first order with respect to propane, while deep propene oxidation has a rate-limiting step involving a surface species that is in adsorption equilibrium with the gas phase and has a half order in oxygen.

Another study showed that partial and deep oxidation of the hydrocarbons on the Ni-Co-Mo-O system can be described through two different mechanisms [86]. The partial oxidation of propane to propene and of propene to acrolein occurs by the Mars -van Krevelen mechanism, in which the hydrocarbon reacts with the lattice oxygen (nucleophilic). Deep oxidation of propene to CO_x on the other hand occurs by a Langmuir-Hinshelwood mechanism in which the adsorbed hydrocarbon reacts with adsorbed and dissociated oxygen (electrophilic). Isotopic studies with propane and propene showed that hydrogen abstractions from a methylene group and in an allylic position (α-hydrogen) are the respective rate-controlling steps [86].

A detailed kinetic study on the ODH of propane to propene was performed to clarify some important aspects of the reaction mechanism [87]. It was found that the propene formation rate had partial orders close to one or zero with respect to propane and oxygen which suggests that gaseous oxygen is not directly responsible for ODH, which is typical of a Mars -van Krevelen type mechanism. Over α-$NiMoO_4$ it was found that a change in oxygen partial pressure does not affect propene formation, which is instead dependent on the propane partial pressure. Continuous, transient and periodic operating systems showed the involvement of lattice oxygen [88].

It was proposed for the β-phase that the following reaction takes place in six steps [87]:

$$C_3H_8 + ½\ O_2 \rightarrow C_3H_6 + H_2O \qquad (4)$$

1) propane adsorption on the catalyst surface
2) oxidation of adsorbed propane by oxygen of the $NiMoO_4$ lattice
3) , 4) desorption of the products propene and water
5) , 6) oxygen adsorption on the catalyst surface and filling of the oxygen vacancies in the solid

It was concluded that the rate-limiting step that controls the overall reaction rate can either be step 1 or step 2.

The surface of the nickel molybdate lattice has anionic vacancies as mentioned previously. Formation of propene was proposed to occur *via* the reaction of propane with anionic vacancies created by reaction with O^{2-} surface anions Eq. (5). Regeneration of the oxygen species occurs through the spontaneous reoxidation of the surface by gaseous O_2 consistent with the Mars -van

Krevelen mechanism [44]. It was then suggested that differences in propene selectivity may be accounted for by the different O_2 environments on the active catalytic sites at the surfaces of both phases [44].

$$C_3H_8 + O^{2-}{}_s \rightarrow C_3H_6 + H_2O + V_o^{\circ\circ} + 2e^- \quad (5)$$

Where $O^{2-}{}_s = O^{2-}$ surface anions

$V_o^{\circ\circ}$ = doubly ionized anionic vacancies

A kinetic study for ethane ODH was reported with the β-molybdate phase. The α-phase was both more active and selective than the β-phase [77]. For the β-phase that the overall rate of ethane conversion can be described by:

$$rC_2H_6 = d[C_2H_6]/dt = k[C_2H_6]^{1.15}\,[O_2]^{0.21} \quad (6)$$

with a reaction order of 0.16 for C_2H_4 formation with respect to oxygen [77]. It was found that lattice oxygen does not guide the reaction towards dehydrogenation, unlike propane ODH. Instead the mechanism involves the intervention of surface O^- species for the abstraction of hydrogen from the ethane molecule to give ethyl radicals [77].

A kinetic study on the selective oxidation and degradation of *n*-butane over unpromoted and Cs-promoted nickel molybdates showed that Cs doping only affects the partial order with respect to butane, which increases for dehydrogenation products and decreases for CO_x, while the partial order with respect to oxygen is almost unaffected in both undoped and Cs-doped $NiMoO_4$, again suggesting the existence of a Mars -van Krevelen mechanism [49].

Evidence for the existence of the Mars -van Krevelen mechanism operating in nickel molybdate for *n*-butane ODH includes: 1) the zero order dependence on the oxygen partial pressure for C_4 formation [49], 2) the relationship between catalytic activity and reducibility of several Cs-doped catalysts [49], 3) the similar apparent activation energies for butane conversion with and without gas phase oxygen [89], 4) the fact that no oxygen adsorption was observed by O_2-TPD [90] and 5) catalytic tests without oxygen in the feed, which showed that butane can be converted to C_4 products with high selectivity even without gas phase oxygen [89].

Experiments conducted without oxygen showed that lattice oxygen plays an important role for selectivity in both propane and butane ODH. Low butane conversion levels indicate that alkane conversion is limited by the reducibility of the catalyst or by lattice oxygen availability and mobility [88]. Low conversion levels (< 1%) are usually consistent with oxygen consumption that corresponds to a small percentage of the mobile oxygen content of the catalyst monolayer [88]. Thus the ODH reaction appears to be controlled by the reducibility of the catalyst (oxygen diffusion within the solid).

Electrical conductivity measurements of nickel molybdate catalysts provided further evidence of a redox mechanism in *n*-butane ODH [91]. When catalysts were exposed to a sequence of gaseous atmospheres of the type: oxygen-butane-oxygen, a reversible redox process was observed for both undoped and Cs-doped catalysts [91]. The sharp increase in electrical conductivity (σ) observed when pure butane is introduced into the cell is due to the release of electrons into the conduction band during surface reduction:

$$C_4H_{10} + (O_o)_s \rightarrow C_4H_8 + H_2O + Vo^{oo} + 2e^- \quad (7)$$

Where $(O_o)_s$ = surface oxygen anion

$V_o^{\circ\circ}$ = doubly ionized anionic vacancies

When oxygen is reintroduced σ reversibly decreases and virtually returns to its initial value. This corresponds to the filling of the lattice vacancies by gas phase oxygen in accordance with the following equation:

$$Vo^{oo} + 2e^- + ½\ O_2\ (g) \rightarrow (O_o)_s \quad (8)$$

Where $V_o^{\circ\circ}$ = doubly ionized anionic vacancies

$(O_o)_s$ = surface oxygen anion

Under steady state conditions, the electrical conductivity of the $NiMoO_4$ catalyst in the reaction mixture is much closer to the oxidized state than of the reduced state, which is in agreement with faster reoxidation as compared to reduction of the catalyst [91].

In the recent investigation of the kinetics and mechanism of $NiMoO_4$ in the ODH of isobutane it was deduced that isobutene is formed through a redox mechanism with participation of lattice oxygen, while the formation of carbon oxides occurs with participation of chemisorbed oxygen [92].

2.7.2.6 Nature of Active sites

The nature of the active catalytic sites in molybdenum containing catalysts and their role in selective oxidation was investigated [93]. Surface-sensitive techniques such as ESR deserve special attention for their use in studies involving changes in Mo^{5+} species upon contact with propane [94].

Mo^{5+} is the active species, as was suggested in Mg-Mo-O catalysts in propane ODH [95, 96]. Several characterization techniques, particularly XPS and EPR showed that the active site would be a co-ordinatively saturated form of Mo^{5+}, which could be generated on the surface by propane reduction.

It was proposed that active sites in molybdenum based catalysts are coupled pairs of Mo^{5+} and Mo^{6+} species which are responsible for the redox mechanism [13].

Although there is some agreement with regard to the active species in molybdenum-containing catalysts, there are possibilities of other active species. One claim is that the active oxidation state of the molybdenum in the dehydrogenation of *n*-butane, is either Mo^{5+} or Mo^{4+}, which on reduction to lower oxidation states leads to cracking or coke formation [97].

For Ni-Mo-O catalysts it is generally accepted that Mo^{5+} species are the active species. During butane oxidation to butadiene and maleic anhydride it was suggested that butane dehydrogenation occurs without the intervention of lattice oxygen [41]. It seems that maleic anhydride formation is related to gaseous oxygen activation over sites that disappear by deep reduction and that can not be regenerated by reoxidation. These sites were assumed to correspond to Mo^{5+} sites. There is no conclusive proof that establishes the nature of the active or selective sites involved in selective oxidation reactions, however other authors seem to think that the redox couple Mo^{6+}/ Mo^{5+} is necessary for the ODH step, especially in propane conversion [22].

2.8 Summary and conclusion

There are two stable structures at atmospheric pressure for $NiMoO_4$. These are the α- and β-$NiMoO_4$ phases. α-$NiMoO_4$ has molybdenum in the octahedral coordination sites and β-$NiMoO_4$ has molybdenum in the tetrahedral coordination sites. These phases undergo reverse transformation on heating and cooling.

Several methods can be used to synthesize $NiMoO_4$ catalysts ranging from physical mixing to impregnation and the sol-gel method. The most common method, however, is co-precipitation. These catalysts were characterized by various instrumental techniques. X-ray diffraction identified phases in $NiMoO_4$ catalysts of varying ratios. Phases that could be present include molybdenum trioxide, nickel oxide, normal nickel molybdate (α- and β-phases) and nonstoichiometric nickel molybdate. Infrared and Raman spectroscopy confirmed the phases present, the metal oxygen coordinations and bonds typical of these phases. Scanning electron microscopy gave information on particle structure, showing that MoO_3 is hexagonal in shape and $NiMoO_4$ is porous and round. Surface areas were dependent on the chemical composition, nonstoichiometric catalysts having a smaller surface area due to excess molybdenum. Temperature programmed reduction showed two reduction peaks and temperature programmed desorption showed the presence of two acid sites. Metal dopants can increase the basicity of the catalysts. X-ray photoelectron spectroscopy showed the same band positions and bandwiths for catalysts with an excess of molybdenum relative to the stoichiometric catalyst, and these were different from those with NiO present. Electrical transport for both nickel molybdate phases operate *via* an intrinsic band mechanism. Both α- and β-phases are p-type semi-conductors but at temperatures higher than 450-650 °C they become n-type semi-conductors. The α-phase has doubly ionized vacancies and the β-phase singly ionized vacancies.

$NiMoO_4$ catalysts have been used for many industrial processes, particularly selective oxidation reactions. For butane oxidation to maleic anhydride $NiMoO_4$ catalysts were most effective in the presence of excess MoO_3. Catalytic results were dependent on the reaction conditions. Different types of oxygen were responsible for the formation of different products. Also, in propane oxidation, it was found that catalysts with excess molybdenum were better for selective product formation. Promoters, such as tellurium, phosphorous and antimony were used to enhance the catalytic properties of $NiMoO_4$ in propane, propene and butane oxidation.

$NiMoO_4$ catalysts were also used extensively for the ODH of light alkanes, ethane, propane and butane. There were several discrepancies regarding the postulated active component in butane ODH and catalysts of varying ratios were selective. Some authors reported that the catalyst with nickel oxide, normal and nonstoichiometric nickel molybdate were preferred catalysts, while others believed that either nickel molybdate or a solid solution of nickel oxide in the molybdate lattice was most effective. Also, regarding the two pure phases, some considered that both had similar behaviour, while others disagreed. In propane ODH, for catalysts with Ni:Mo < 1, the α-phase was better than the β-phase in terms of product activity and selectivity and catalysts with excess molybdenum were good catalysts.

Promoted catalysts showed a marked improvement in catalytic performance in butane ODH. Of the promoters studied, antimony and arsenic, arsenic was the preferred dopant. With alkali and alkali-earth metals, alkali metals proved to be better for butene selectivity because of their more basic nature. However, alkaline-earth metals showed higher selectivity to butadienes. Potassium, calcium and phosphorous doped catalyst were reported for propane or isobutene ODH and potassium oxide for isobutene ODH.

Supported catalysts were also applied to propane and isobutene ODH. Isobutane ODH with TiO_2 and SiO_2 supported $NiMoO_4$ catalysts were found to be more selective to isobutene than unsupported catalysts.

Coke deposition on $NiMoO_4$ in butane ODH showed an improvement in catalytic activity and selectivity to dehydrogenation products.

Of the few kinetic and mechanistic studies performed with Ni-Mo-O catalysts most showed a common redox mechanism of Mars -van Krevelen for the oxidation of hydrocarbons over metallic oxides. Experiments carried out without oxygen showed that lattice oxygen is important for selectivity in both propane and butane ODH. Alkane conversion seems to be limited by catalyst reducibility or lattice oxygen availability and mobility. Most reports show that Mo^{5+}/ Mo^{6+} are active species of Ni-Mo-O catalysts.

2.9 Aims and objectives of this project

Nickel molybdenum oxide catalysts have been reported as a potential oxidative dehydrogenation catalysts for converting low value lighter paraffins like propane and *n*-butane to high value products such as olefins. To date there have been no reports for the ODH of higher paraffins with these catalysts. Hence the aim of this study was to:

1) Synthesize and characterize $NiMoO_4$ catalysts
2) Investigate the catalytic oxidation of $NiMoO_4$ catalysts in the ODH of *n*-hexane, an example of a higher paraffin
3) Optimize the selectivity to dehydrogenation products by changing reaction conditions
4) Enhance the catalytic performance by promoting the catalyst
5) Investigate the effect of non-catalytic oxidation

References

[1] http://www.minerals.net/glossary/terms/m/molybdate (date accessed January 2009).

[2] http://www.thefreedictionary.com/molybdates (date accessed, January 2009).

[3] http://en.wikipedia.org./wiki/molybdate (date accessed, January 2009).

[4] A. W. Sleight, Acta. Cryst., B28 (1972) 2899.

[5] A. W. Sleight and B. L. Chamberland, Inorg. Chem., 7 (1968) 1672.

[6] A. W. Sleight, B. L. Chamberland and J. F. Weiher, Inorg. Chem., 7 (1968) 1093.

[7] L. M. Plyasova, I. Ivanchenko, M. M. Andrushkevich, R. A. Buyanov, I. S. Itenberg, G. A. Khramova, L. G. Karakchiev, G. N. Kustova, G. A. Stepanov, A. L. Tsailingol'd and F. S. Philipenko, Kinet. Catal., 14 (1973) 882.

[8] A. Kaddouri, R. Del Rosso, C. Mazzocchia and D. Fumagalli, J. Therm. Anal. Calorim., 63 (2001) 267.

[9] J. A. Rodriquez, J. C. Hanson, S. Chaturvedi, A. Maiti and J.L. Brito, J. Chem. Phys., 112 (2000) 935.

[10] J. A. Rodriguez, S. Chaturvedi, J. C. Hanson, A. Albornoz and J. L. Brito, J. Phys. Chem. B, 102 (1998) 1347.

[11] H. M. Abdeldayam and S. A. Sadek, Thermochimica Acta, 473 (2008) 96.

[12] H. Ehrenberg, I. Svoboda, G. Wltschek, M. Wiesmann, F. Trouw, H. Weitzel and H. Fuess, J. Magn. Magn. Mater., 150 (1995) 371.

[13] L. M. Madeira, M. F. Portela and C. Mazzocchia, Catal. Rev. -Sci. Eng., 46 (2004) 53.

[14] M. M. Andrushkevich, R. A. Buyanov, V. G. Sitnikov, I. S. Itenberg and G. A. Khramova, Kinet. Katal., 14 (1973) 464.

[15] C. Mazzocchia, E. Tempesti and C. Aboumrad, "Catalyst for Oxidative Dehydrogenation of Propane", in U. S. Patent (Editor), Vol. 5,086,032, Norsolor, February 4, 1992.

[16] C. Mazzocchia, R. Anouchinsky, A. Kaddouri, M. Sautel. and G. Thomas, J. Therm. Anal., 40 (1993) 1253.

[17] C. Mazzocchia, R. Del Rosso and P. Centola, Rev. Port. Quim., 19 (1977) 61.

[18] C. Mazzocchia, F. Di Renzo, P. Centola and R. D. Rosso, in "Chemistry and Uses of Molybdenum", H. F. Barry, P. C. H. Mitchelle (Editor), Golden Co, 1983, p 406.

[19] J. Y. Zou and G. L. Schrader, Thin Solid Films, 324 (1998) 52.

[20] C. Mazzochia, A. Kaddouri, R. Anouchinsky, M. Sautel and G. Thomas, Solid State Ionics, 63-65 (1993) 731.

[21] R. Anouchinsky, A. Kaddouri and C. Mazzocchia, J. Therm. Anal., 47 (1996) 299.

[22] O. Lezla, E. Bordes and P. Courtine, J. Catal., 170 (1997) 346.

[23] R. M. Martin-Aranda, M. F. Portela, L. M. Madeira, F. Freire and M. Oliveira, Appl. Catal. A, 127 (1995) 201.

[24] L. M. Madeira, R. M. Martin-Aranda, F. J. Maldonado-Hodar, J. L. G. Fierro and M. F. Portela, J. Catal., 169 (1997) 469.

[25] A. Kaddouri, R. Del Rosso, C. Mazzocchia, P. Gronchi and P. Centola, Catal. Lett., 63 (1999) 65.

[26] A. Kaddouri, C. Mazzocchia and E. Tempesti, Appl. Catal. A, 169 (1998) L3.

[27] B. J. Bertus, "Catalyst and Process for Oxidative Dehydrogenation", United States Patent Vol. 4,094,819, Philips Petroleum Company, June 13, 1978.

[28] A. Kaddouri, C. Mazzocchia and E. Tempesti, Appl. Catal. A, 180 (1999) 271.

[29] A. Kaddouri, C. Del Rosso, C. Mazzocchia, P. Gronchi and D. Fumagalli, J. Therm. Anal. Calorim., 66 (2001) 63.

[30] N. Fujikawa, K. Wakui and K. Tomita, Catal. Today, 71 (2001) 83.

[31] N. Ferlazzo, N. Bertolini and M. Ghirga, "Catalyst for the Conversion of Unsaturated Hydrocarbons into Diolefins or Unsaturated Aldehydes and Nitriles and Process for Preparing the Same", United States Patent, Vol. 4,388,223, Euteco Impianti S. p. A, June 14, 1983.

[32] R. Zavoianu, C. R. Dias and M. F. Portela, Catal. Commun., 2 (2001) 37.

[33] C. R. Dias, R. Zavoianu and M. F. Portela, Catal. Commun., 3 (2002) 85.

[34] E.Tempesti, A. Kaddouri and C. Mazzocchia, Appl. Catal. A, 166 (1998) L259.

[35] D. Cauzzi, M. Deltratti, G. Predieri, A. Tiripicchio, A. Kaddouri, C. Mazzocchia, E. Tempesti, A. Armigliato and C. Vignali, Appl. Catal. A, 182 (1999) 125.

[36] C. R. Dias, R. Zavoianu and M. F. Portela, React. Kinet. Catal. Lett., 77 (2002) 317.

[37] J. Laine, K. C. Pratt and D. L. Trimm, J. Chem. Technol. Biotechnol., 29 (1979) 397.

[38] F. J. Maldonado-Hodar, L. M. Madeira and M. F. Portela, J. Catal., 164 (1996) 399.

[39] L. M. Plyasova, M. M. Andrushkevich, R. A. Buyanov and I. S. Itenberg, Kinet. Catal., 14 (1973) 1190.

[40] F. S. Pilipenko, A. L. Tsailingol'd, V. A. Levin, L. S. Tuktarova, G. A. Stepanov, G. K. Boreskov, R. A. Buyanov and M. M. Andrushkevich, Kinet. Catal., 14 (1973) 649.

[41] C. Mazzocchia, R. Del Rosso and P. Centola, An. Quim., 79 (1980) 108.

[42] F. Di Renzo, C. Mazzocchia, G. Thomas and M. Vernay, React. Solids, 6 (1988) 145.

[43] S. S. Saleem, Infrared Phys., 27 (1987) 309.

[44] C. Mazzocchia, C. Aboumrad, C. Diagne, E. Tempesti, J. M. Herrmann and G. Thomas,

Catal. Lett., 10 (1991) 181.

[45] F. Trifiro, P. Centola, I. Pasquon and P. Jiru, Paper 18, "Proceedings of the 4th International Congress on Catalysis", Moscow, 1968.

[46] U. Ozkan and G. L. Schrader, J. Catal., 95 (1985) 120.

[47] A. I. Vagin, N. V. Burmistrova and V. I. Erofeev, React. Kinet. Catal. Lett., 28 (1985) 47.

[48] M. A. Tsurov, P. V. Afanasiev and V. V. Lunin, Appl. Catal. A, 105 (1993) 205.

[49] L. M. Madeira, M. F. Portela, C. Mazzocchia, A. Kaddouri and R. Anouchinsky, Catal. Today, 40 (1998) 229.

[50] F. J. Maldonado-Hodar, L. M. Madeira, M. F. Portela, R. M. Martin-Aranda and F. Freire, J. Mol. Catal. A: Chem., 111 (1996) 313.

[51] L. M. Madeira, J. M. Herrmann, F. G. Freire, M. F. Portela and F. J. Maldonado, Appl. Catal. A, 158 (1997) 243.

[52] A. Steinbrunn, A. Tahri and J. C. Colson, Solid State Ionics, 49 (1991) 99.

[53] P. T. Vasudevan and J. L. G. Fierro, Catal. Rev. -Sci. Eng., 38 (1996) 161.

[54] J. L. Brito and A.L. Barboza, J. Catal., 171 (1997) 467.

[55] J. L. Brito, A. L. Barboza, A. L. Albornoz, F. Severino and J. Laine, Catal. Lett., 26 (1994) 329.

[56] T. Klimova, D. S. Casados and J. Ramirez, Catal. Today, 43 (1998) 135.

[57] Z. B. Wei, W. Yan, H. Zhang, T. Ren, Q. Xin and Z. Li, Appl. Catal. A, 167 (1998) 39.

[58] J. L. Brito, F. Severino, N. N. Delgado and J. Laine, Appl. Catal. A, 173 (1998) 193.

[59] P. Vazquez, L. Pizzio, M. Blanco, C. Caceres, H. Thomas, R. Arriagada, S. Bendezu, R. Cid and R. Garcia, Appl. Catal. A, 184 (1999) 303.

[60] D. Li, A. Nishijima and D. E. Morris, J. Catal., 182 (1999) 339.

[61] Y. Chu, Z. Wei, S. Yang, C. Li, Q. Xin and E. Min, Appl. Catal. A, 176 (1999) 17.

[62] T. Borowiecki, G. Giecko and M. Panczyk, Appl. Catal. A, 230 (2002) 85.

[63] A. A. Andreev, V. J. Kafedjiysky and R. M. Edreva-Kardjieva, Appl. Catal. A, 179 (1999) 223.

[64] S. A. Driscoll, L. Zhang, U. S. Ozkan, S. T. Oyama and J. W. Hightower, American Chemical Society; Washington DC, ACS Symposium Series No. 523 (1993) 340.

[65] H. Yasuda, M. Higo, S. Yoshitomi, T. Sato, M. Imamura, H. Matsubayashi, H. Shimada, A. Nishijima and Y. Yoshimura, Catal. Today, 39 (1997) 77.

[66] V. L. S. Teixeira da Silva, R. Frety and M. Schmal, Ind. Eng. Chem. Res., 33 (1994) 1692.

[67] Z. Sarbak, Appl. Catal. A, 207 (2001) 309.

[68] U. Ozkan and G. L. Schrader, J. Catal., 95 (1985) 137.

[69] U. Ozkan and G. L. Schrader, J. Catal., 95 (1985) 147.

[70] C. Mazzocchia, F. Di Renzo and C. Mari, in "Reactivity of Solids", P. Barret, L. C. Dufour (Editor), Elsevier, Amsterdam, 1985, p. 1061.

[71] J. C. J. Bart, A. Bossi, G. Petrini, G. Battiston, A. Castellan and R. Covini, Appl. Catal., 4 (1982) 153.

[72] W. E. Cherry, A. F. Dickason and J. A. Hedge, "Catalyst or the Oxidation of Butane to Maleic Anhydride", in U.S. Patent (Editor), Vol. Sun ventures, Inc, July 6, 1976.

[73] K. Kourtakis and J. D. Sullivan, "Molybdenum Based Oxidation Catalysts", United States patent, Vol. 6,271,169, E. I. du Pont de Nemours and company, August 7, 2001.

[74] K. L. Madhok, K. P. Srivastava and S. Yadav, Indian. J. Technol., 20 (1982) 184.

[75] S. Umemura, K. Ohdan and H. Asada, "Process for the Catalytic Preparation of Acrolein and Methacrolein, in U.S. patent (Editor), Vol. 4,267, 385, UBE Industries, Ltd, May 12, 1981.

[76] T. P. Li, "Production of Ammoxidation Catalyst", in U.S. patent (Editor), Vol. 4,168,246, Monsanto Company, September 18, 1979.

[77] A. Kaddouri, R. Anouchinsky, C. Mazzocchia, L. M. Madeira and M. F. Portela, Catal. Today, 40 (1998) 201.

[78] G. A. Stepanov, A. L. Tsailingol'd, F. D. Pilipenko, A. M. Sobolev, G. K. Boreskov, R. A. Buyanov and S. A. Veniaminov, "Process for the Production of Mono- and Diolefins", in C.p.a. Marks and Clerk, agents for the applicants (Editor), British patent, Vol. 1,197537, London, 1970.

[79] F. S. Pilipenko, A. L. Tsailingol'd and G.A. Stepanov, Kinet. Catal, 17 (1976) 842.

[80] I. S. Itenberg, M. M. Andrushkevich, R. A. Buyanov, G. A. Khramova and V. G. Sitnikov, Kinet. Catal., 17 (1976) 867.

[81] P. Mars and D. W. van Krevelen, Chem. Eng. Sci. Special Suppl., 3 (1954) 41.

[82] G. Thomas, M. Sautel, A. Kaddouri and C. Mazzocchia, Solid State Ionics, 101-103 (1997) 775.

[83] D. L. Stern and R. K. Grasselli, J. Catal., 167 (1997) 550.

[84] P. Boutry, P. Marly, J. C. Daumas, M. Montarnal, R. Montarna and M. Marly, "Process for Converting Saturated Hydrocarbons to Unsaturated Hydrocarbons by Oxidation", Vol. 3,577,477, Institut Francais du Petrole, des Carburants et Lubrifiants, Rueil Malmaison, Hauts-de-Seine, France, May 4, 1971.

[85] R. Zavoianu, C. R. Dias and Soares, Appl. Catal. A, 298 (2006) 40.

[86] D. L. Stern and R. K. Grasselli, J. Catal., 167 (1997) 560.

[87] M. Sautel, G. Thomas, A. Kaddouri, C. Mazzocchia and R. Anouchinsky, Appl. Catal. A, 155 (1997) 217.

[88] R. Del Rosso, A. Kaddouri, R. Anouchinsky, C. Mazzocchia, P. Gronchi and P. Centola, J. Mol. Catal. A: Chem., 135 (1998) 181.

[89] F. J. Maldonado-Hodar, L. M. Madeira, M. F. Portela and R. M. Martin-Aranda, Proceedings of the XVth Ibero-American Symposium on Catalysis, Cordoba, Argentina, Sep 16-20, 1996.

[90] L. M. Madeira and M.F. Portela, in "3rd World Congress on Oxidation Catalysis", R. K. Grasselli, M. Gaffney, J. Lyons Eds (Editor), Studies in Surface Science and Catalysis, Vol. 110, Elsevier, Amsterdam, 1997, p. 797.

[91] L. M. Madeira, J. M. Herrmann, J. Disdier, M. F. Portela and F. G. Freire, Appl. Catal. A, 235 (2002) 1.

[92] Y. A. Agafonov, N. V. Nekrasov and N. A. Gaidai, Kinet. Catal., 42 (2001) 821.

[93] L. M. Madeira and M.F. Portela, Catal. Rev. -Sci. Eng., 44 (2002) 247.

[94] R. B. Watson and U. S. Ozkan, J. Mol. Catal A: Chem., 194 (2003) 115.

[95] M. C. Abello, M. F. Gomez and L. E. Cadus, Ind. Eng. Chem. Res., 35 (1996) 2137.

[96] L. E. Cadus, M. C. Abello, M. F. Gomez and J. B. Rivarola, Ind. Eng. Chem. Res., 35 (1996) 14.

[97] M. E. Harlin, L. B. Backman, A. O. I. Krause and O. J. T. Jylha, J. Catal., 183 (1999) 300.

CHAPTER 3
EXPERIMENTAL

3.1 Reactor setup

For heterogeneous catalyzed reactions performed on laboratory-scale, fixed bed continuous flow micro-reactor systems are appropriate because they are cost effective and relatively simple to set up; hence this system was chosen. Non catalytic and catalytic evaluation was performed using a test rig which consisted essentially of three parts: 1) the feed delivery system, 2) the reactor and 3) the analytical system.

Two setups were designed and constructed for our work. One was for testing *n*-hexane above the upper flammability limit (UFL) and the other for testing *n*-hexane below the lower flammability limit (LFL).

3.1.1 The feed delivery system

Feed gas was made up of high purity air and hexane. Gas mixtures were further diluted with nitrogen from a separate cylinder for feed compositions requiring an excess of nitrogen. Individual gas flows were monitored and controlled with needle valves, pressure regulators, gauges (100 kPa) and flow controllers in the form of rotameters which were mounted on a control panel.

Upper flammability limit

The set up for testing above the UFL is shown in **Fig. 3.1.** *n*-Hexane, a liquid at room temperature, was introduced into the system from a reagent bottle placed on a balance with a high performance liquid chromatography (HPLC) pump which works isocratically. This feed was vaporized in heated stainless steel lines maintained at 160 °C before mixing with the air and nitrogen.

Feed lines to the reactor and outlet were made up of 1/8 inch stainless steel tubing. These lines were connected to the reactor with stainless steel Swagelok fittings. A regulator before the reactor was used to monitor any build up of pressure in the reactor and the pressure relief valve (set at 0.3 psi) served as a safety device to remove back pressure build-up in the reactor. The product line

from the reactor was connected to a 75 ml stainless steel sampling vessel cooled at 5 °C to trap the condensates.

Off-gas from the reactor continuously flowed through a wet gas flow meter which was used to record the volume of gas leaving the reactor. These gaseous products were then diverted using a three-way ball valve to a gas sampling box containing two rotary valves that operated pneumatically. In this way a sample of gas was sent to a Varian 3700 gas chromatograph equipped with a TCD detector, while another was sent to a Perkin-Elmer Autosystem gas chromatograph equipped with a FID detector.

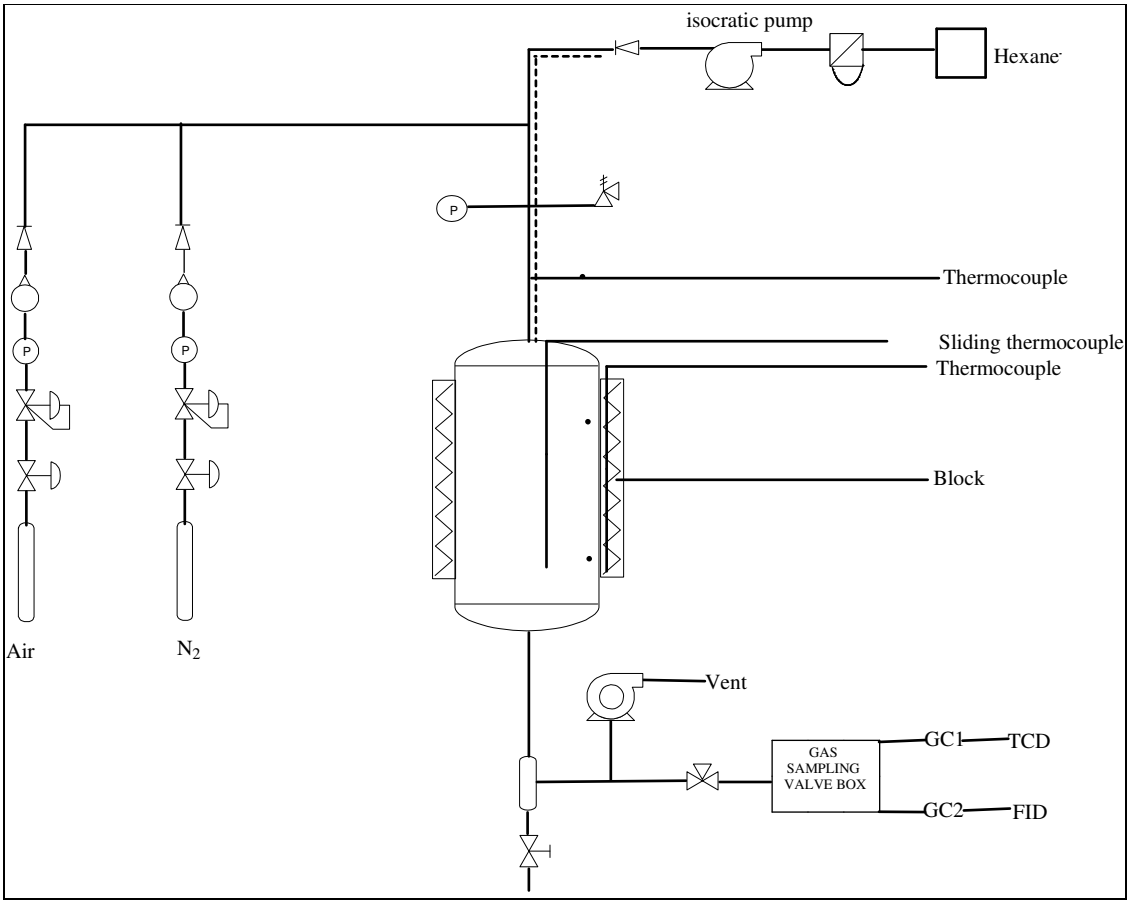

Fig. 3.1: Diagram of the test rig above the upper flammability limit.

Lower flammability limit

n-Hexane was fed from a premix cylinder containing 0.517% hexane in air. The pressure and flow rate of this gaseous mixture was controlled with a pressure regulator (100 kPa) and

rotameter before entering the reactor. A separate cylinder of instrument grade air was also connected to the system to activate the β-phase.

The inlet line to the reactor was made of copper tubing, while outlet lines were made of stainless steel, all tubing was ¼ inch in diameter.

The three-way valve immediately after the reactor was to direct the flow of gas either to the bubbler for venting the gas or to the wet gas flowmeter. **Fig. 3.2** shows the set up for testing below the LFL.

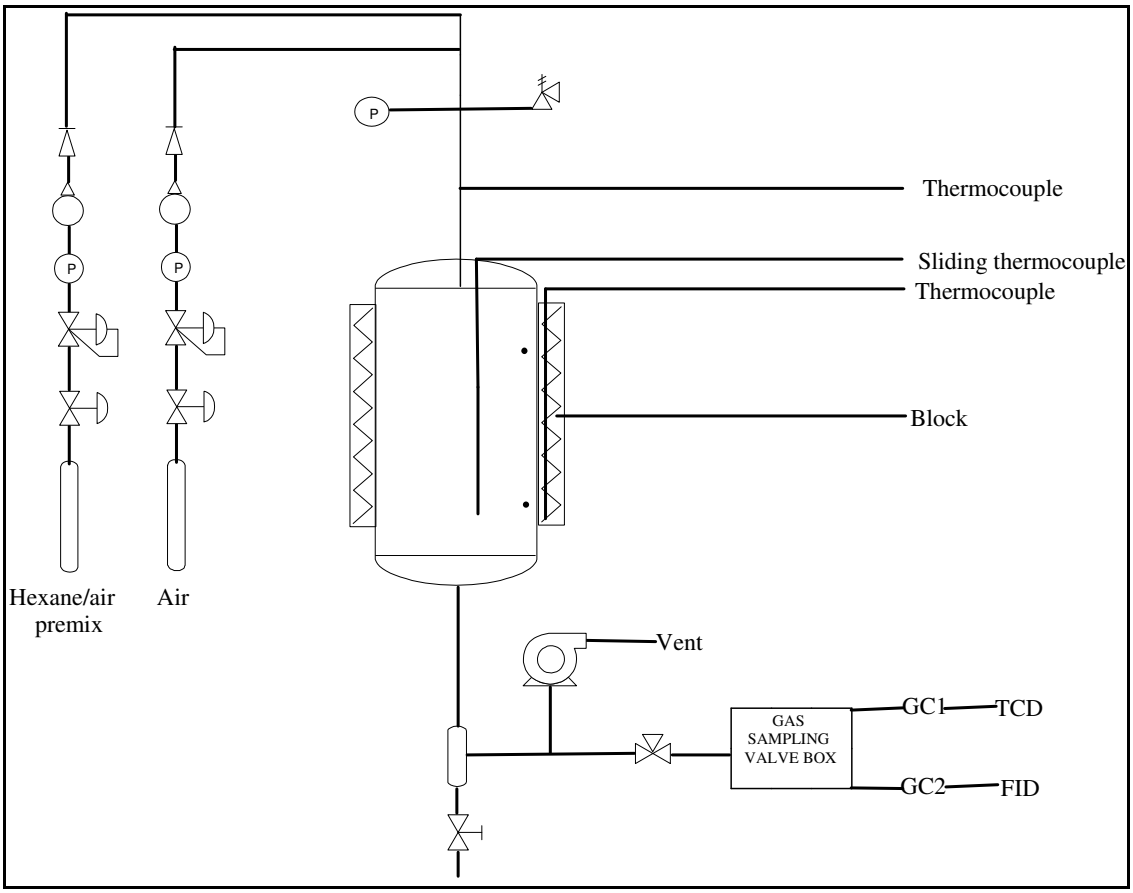

Fig. 3.2: Diagram of the test rig below the lower flammability limit.

3.1.2 Reactor

The reactor tube was a ½ inch stainless steel (grade 316) tube, 32.5 cm in length with inner diameter 15 mm. The reactor tube was positioned in a 300 mm diameter copper block. This block

operates *via* circular constructed heating elements and was used to heat the reactor. The heating is controlled and monitored using a CB-100 temperature controller with a solid state relay. The block was placed in a metal casing and insulated with glasswool. The block temperature was monitored with a fixed type K thermocouple, whereas the actual temperature inside the reactor tube was monitored with a movable thermocouple inside a closed thermowell imbedded in the reactor tube itself.

3.1.3 The analytical system

The analytical system consisted of a heated gas sampling valve box and two gas chromatographs employed for the analysis of products from the reactor. An isothermally operated Varian 3700 GC was used to separate and monitor air, methane, CO and CO_2 and a Perkin Elmer XL Autosystem GC was used to separate and monitor all other products.

The Varian 3700 GC was equipped with a chromosorb WHPSP pre-column (specifications given in the appendix pp 143) which was used to trap non-gaseous products. Thus only CO, CO_2 and air was allowed to pass through to the Carboxen ^{TM} analytical column (specifications given in the appendix pp 143) and the thermal conductivity detector.

The Perkin Elmer Autosystem GC was equipped with a CP-Sil 24 CB column (specifications given in the appendix pp 143) used to separate paraffins, olefins, aromatics and oxygenates and a flame ionization detector.

The gas sampling box contained two automated Valco rotary valves: a 10 port valve sampled effluent to the Varian 3700 GC and a 6 port valve sampled effluent to the Perkin Elmer GC. Each valve consisted of a 500 µl sampling loop which was heated at a constant temperature of 160 °C to prevent condensation of reactant effluent. The Perkin Elmer GC electronically and pneumatically controlled both these valves. Pressurized air was used to turn the valves.

Fig. 3.3 and **Fig. 3.4** illustrate the operation of the 6 port valve [1]. In the sampling mode sample flows through the sampling loop, while the carrier flows directly to the FID detector. In the standby mode the sample in the sample loop is flushed directly into the analytical column in the Perkin Elmer GC.

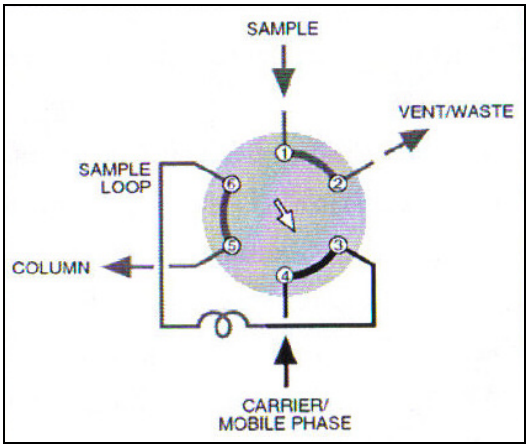

Fig. 3.3: 6 port rotary valve in standby mode [1].

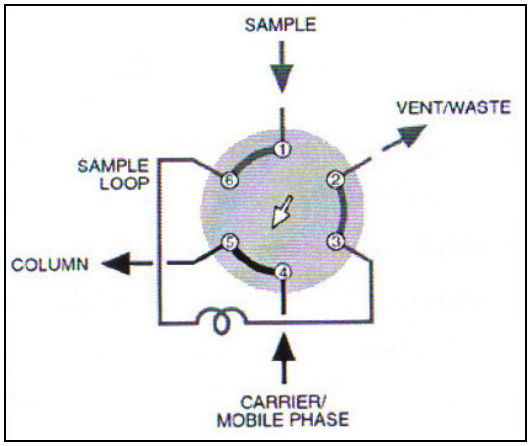

Fig. 3.4: 6 port rotary valve in sampling mode [1].

A schematic for the operation of the 10 port valve [1] is shown in **Fig. 3.5** and **Fig. 3.6** and operates similarly to the six port valve except that modification is made to allow only carbon oxides and air to pass through the analytical column, while other components are trapped in the pre-column and flushed to the wasteline. In the standby mode the sample is loaded onto the sample loop and when the valve is switched to the sampling mode the sample in injected onto the pre-column. Once carbon oxides pass through the analytical column, the valve is switched back to the sampling mode to back flush the pre-column for venting during the analysis.

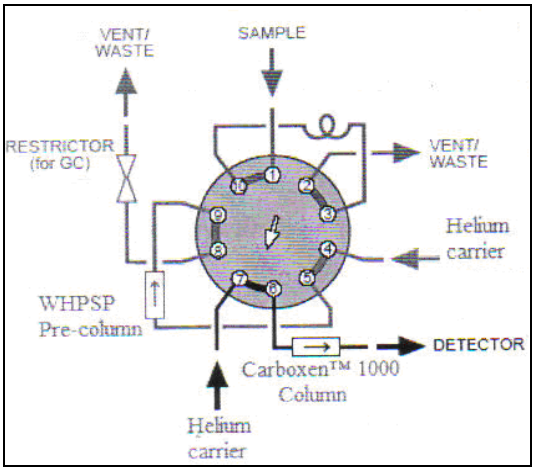

Fig.3.5: 10 port rotary valve in standby mode [1].

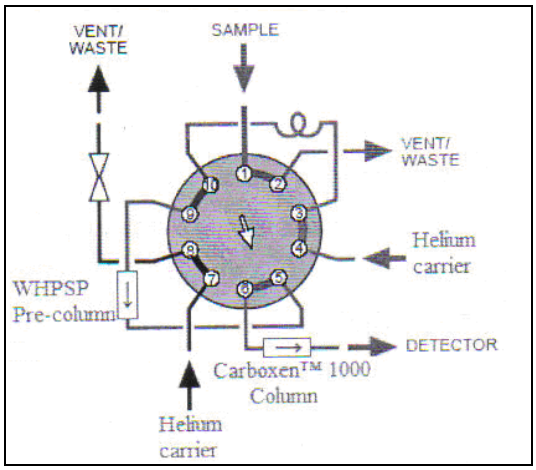

Fig.3.6: 10 port rotary valve in sampling mode [1].

Product analysis

This was done in two ways: Online analysis and offline analysis.

Products obtained from the sampling vessel for the test rig used for reactions above the flammability limit consisted of two layers, one organic and the other aqueous. These were separated and weighed. A sample of each layer was injected into the GC to identify the components present and then subjected to Karl Fischer analysis to determine the water content. The gaseous products were monitored online and at a later stage, due to inconsistencies with this method, this was also done offline.

Analysis of the products obtained from the rig used for testing below the lower flammability limit was only done offline and there was no accumulation of liquid products.

3.2 Catalyst preparation

3.2.1 Preparation of nickel molybdate precursors

Reagents used:

- Ammonium dimolybdate, $(NH_4)_2Mo_2O_7$, > 95% ACS reagent, Sigma Aldrich
- Nickel nitrate, $Ni(NO_3)_2{\cdot}6H_2O$, > 98% May and Baker
- Ammonium hydroxide, NH_4OH, 25%, Rochelle Chemicals
- HNO_3, 70%, Riedel de Haen

Procedure:

Nickel molybdate catalytic precursors were synthesized by modifying the co-precipitation method reported by Mazzocchia et al. [2]. 0.5 M solutions of $Ni(NO_3)_2.6H_2O$ (14.5 g, 0.05 mol made up with 100 ml distilled water) were mixed with 0.25 M $(NH_4)_2Mo_2O_7$ solutions (8.5 g, 0.05 mol also made up with 100 ml distilled water). Both solutions were added dropwise with continuous stirring and heating maintaining a temperature below 44^{o}C. The respective pH of the solutions (~5.7) and temperatures were monitored with a pH controller and temperature probe and the pH was adjusted with ammonium hydroxide and nitric acid. The solution was heated to 85 °C and then filtered hot under suction using a buchner funnel.

The synthesised $NiMoO_4$ precursors were dried at 100 °C in the oven for a minimum of 2.5 hours (**Fig 3.7**).

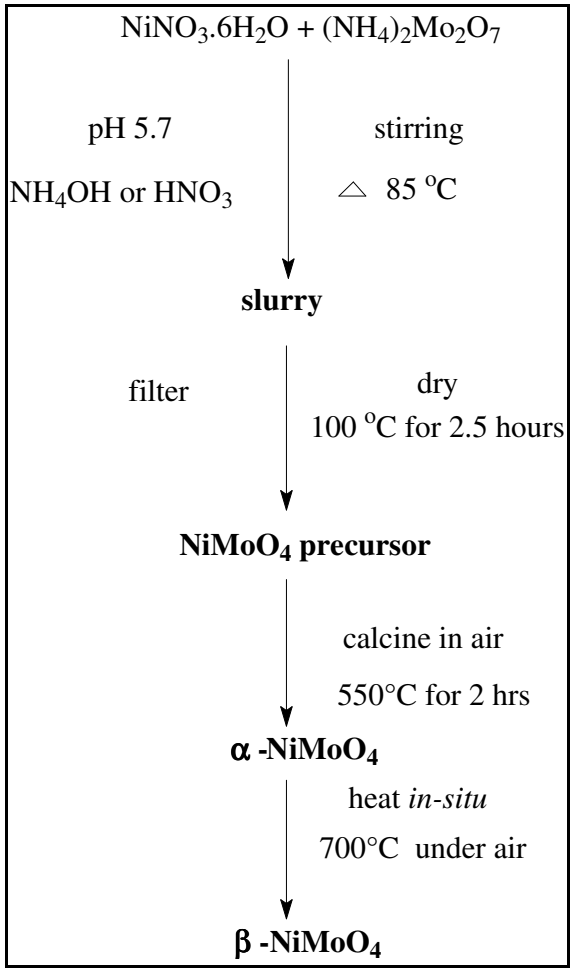

Fig. 3.7: Flow chart showing synthesis of catalysts.

3.2.2 Catalyst activation

α-$NiMoO_4$ catalysts were obtained after calcining the precursors in airflow at 550 °C for 2 hours. The calcined catalysts were pelletized and then sieved to particle size 300-600 μm.

The β-$NiMoO_4$ catalysts were prepared by heating the α-$NiMoO_4$ in the reactor to 700 °C under air, then maintaining the temperature for 5-15 minutes before cooling down to the reaction temperatures, which were always above 300 °C.

3.2.3 Preparation of pure MoO_3 and NiO catalysts

Reagents used:

- Molybdenum(VI)oxide, MoO_3, ACS reagent, Aldrich, 99.5% purity
- Nickel(II) oxide, NiO, 99%, Sigma Aldrich
- H1 Sasol Wax

Procedure

Catalytic powders that are too fine in nature may be mixed with substances known as binders and compressed into pellets or as a moist paste through a die and dried to give extrudate. The pellet may need to be calcined to oxidize the binder [3]. Due to the particles of the pure oxides being so fine, pure NiO powders were mixed with 5% Sasol wax and then pressed to form pellets, sieved to the appropriate particle size and finally calcined at 550 °C for 2 hours, as was done for the other catalysts.

MoO_3 had to be tested in powder form since attempts to pelletize, even in the presence of the binders, failed.

3.2.4 Preparation of caesium-promoted molybdates

Reagents used:

- caesium nitrate, 99% purity, Aldrich
- pure α-$NiMoO_4$ catalyst

Procedure

The wet impregnation technique was employed [4]. Pure $NiMoO_4$ (~3 g) was mixed with 30 mL deionized water containing the appropriate concentration of dissolved caesium nitrate, depending on the promoter loading required (atomic ratio of metal/ Mo). For instance, a 3% loading requires 4.12 mmol caesium (~80.22 mg caesium nitrate). The resulting slurry was then stirred at 80 °C overnight (15 hours), filtered and dried at 120 °C for 4 hours [4].

The impregnated catalysts were then calcined in air for 2 hours at 550 °C and also pelletized and sieved to a particle size of 300-600 μm.

All catalysts were pelletized with a KBr die set pelletizer.

3.3 Catalyst characterization

Brunauer-Emmet-Teller (BET) surface area measurements, inductively-coupled plasma optical emission spectroscopy (ICP-OES), powder X-ray diffraction (XRD), high temperature X-ray diffraction (HT-XRD), Fourier-transform infrared (FTIR) spectroscopy, attenuated total reflection (ATR), Raman spectroscopy, scanning electron microscopy (SEM), energy dispersive X-ray (EDX) analysis, X-ray photo-electron spectroscopy (XPS), temperature programmed reduction (TPR), temperature programmed oxidation-mass spectrometry (TPO-MS) and temperature programmed desorption (TPD) were employed to characterize the catalysts.

3.3.1 Brunauer-Emmet-Teller (BET) surface area measurements

The BET equation developed by Brunauer, Emmet and Teller [5] was used for determining the surface area of the catalysts using a Tristar (Micromeritics) instrument at Sasol Technology, Sasolburg, South Africa and using a Gemini Micromeritics instrument at the University of KwaZulu-Natal. The method is based on the non-specific physisorption of nitrogen onto the sample at -196 °C, the condensation temperature of the adsorbing nitrogen gas. A sample of catalyst was degassed overnight at 200 °C under nitrogen flow. The sample was then cooled to room temperature and re-weighed.

3.3.2 Inductively-coupled plasma optical emission spectroscopy (ICP-OES)

ICP-OES was used to determine the elemental composition of the bulk. The instruments used were a Jobin-Yvon (JY 24) and a Perkin Elmer DV 5000. Multi-element standards of nickel, molybdenum and caesium were prepared over the appropriate concentration range to obtain a good calibration which was used for quantification purposes. Samples were digested with a small amount of HCl. In most cases the samples were not very soluble and so they were heated before dilution.

Nickel ICP Standard Solution, Fluka, c (Ni) = 1.000 g/l; in 0.5 M HNO_3
Molybdenum ICP Standard Solution, Fluka, c (Mo) = 1.000 g/l; in 0.5 M HNO_3
Caesium ICP Standard Solution, Fluka, c (Cs) = 1.000 g/l; in 0.5 M HNO_3

3.3.3 X-ray diffraction (XRD)

Phase identification was done by comparing the sample XRD pattern to the library of data (JCPDS cards 33-948, 45-01142, 5-508 and 4-835). Spectra were recorded on a Philips PW

1730/10 diffractometer using cobalt Kα radiation source of wavelength 1.78897 Å at the School of Geology, University of KwaZulu-Natal.

3.3.3.1 High temperature X-ray diffraction (HT-XRD)

High temperature XRD experiments were performed to characterize the β-phase and to monitor any phase changes during catalytic testing. The samples of the synthesized catalyst were analyzed in air using a Panalytical X'Pert Pro powder diffractometer with X'Celerator detector with variable divergence and receiving slits with Fe filtered Co-Kα radiation and Anton Paar HTK16 heating chamber. The phases were identified using X'Pert Highscore plus software. The sample of the commercial molybdate was characterized using a Bruker AXS D8 X-ray diffractometer with a Vantec-1detector with an Anton Paar TCU 750 temeprature control unit. A Cu-Kα radiation source was used.

3.3.4 Fourier-transform infrared (FTIR) spectroscopy

FTIR was another diagnostic tool used for the identification of phases of the catalyst. IR spectra were recorded on a Nicolet 410 Impact Fourier-Transform Infrared spectrometer. The sample was introduced into a small quantity of KBr powder, a disc was pressed, and then analyzed from 370 – 1400 cm^{-1}. To prevent moisture from being absorbed by the sample, the preparation was done in the presence of an IR lamp. A background scan was done on a blank KBr pellet as a further precaution.

3.3.5 Attenuated total reflection (ATR)

IR spectra of catalysts were also recorded with a Perkin Elmer Spectrum 100 series on a diamond crystal using the attenuated total reflection technique. A powdered sample was placed to completely cover the crystal. Then pressure was applied to the sample by tightening a pressure plate to ensure intimate contact between the sample and crystal.

3.3.6 Raman spectroscopy

Laser Raman spectroscopy was further used to identify the phases of the catalyst. Raman spectra were recorded with a 180° configuration in a System 1000 Renishaw Raman spectrometer equipped with a microscope and a Renishaw CCD detector. The light source was an argon-ion laser giving incident radiation of 514 nm.

3.3.7 Scanning electron microscopy (SEM) and energy dispersive X-ray (EDX) analysis

Scanning electron microscopy contributed significantly to understanding the nature of the active form of the $NiMoO_4$ catalysts. The technique provided information about the morphological structure of the surface and about the elemental composition with the use of energy dispersive X-ray analysis.

Samples were stuck onto metal stubs with double sided carbon tape and coated with gold in the Polaron SEM coating unit E5100 to prevent charging by the incident electron beam. The analysis was performed using a Leo 1450 scanning electron microscope fitted with a Link ISIS energy dispersive X-ray analytical system and the software used to capture the images was a Leo-32 SEM UIF version 3.02.09.

3.3.8 X-ray photo-electron spectroscopy (XPS)

XPS measurements were carried out using a VG Escalab 200 MKII spectrometer. An aluminum anode (K_α = 1486.6 eV) was used to generate the X-ray radiation (240 W (20 mA; 12kV)). Measurements were carried out with a 0.1 s dwelling time; 0.1 eV step for the selected regions. To obtain sufficient signal-to-noise ratio, the Ni 2p region was scanned 50 times (i.e. making the total measurement time approximately 2 hours). Peak deconvolution (Gaussian-Lorentian mixture) was carried out with Casa XPS software and the spectra were charge corrected to the contaminant C 1s signal at 284.5 eV. XPS analysis was also carried out at an ambient temperature of 20 °C ± 5 °C and a relative humidity of a 50% RH ± 25% RH using a Physical Electronics Quantum 2000 Scanning ESCA microprobe. The X-rays were 20 W Al Kα monochromated radiation. The pass energy was set to 117.4 eV with a resolution of 1 eV for wide scans and 0.25 eV for narrow scans.

3.3.9 Gas chromatography-mass spectrometry (GC-MS)

Gaseous and liquid products (aqueous and organic products) were analyzed by GC-MS to determine the composition of products. Analysis was done with a Perkin Elmer Autosystem XL GC fitted with an Elite 5 ms column at the University of KwaZulu-Natal, Howard College campus and with a HP 6890 model GC-MS fitted with a PONA Column at Sasol Technology (Pty) Ltd. Standard compounds that were identified by GC-MS were then injected into the GC's linked to the reactor to verify the retention times of the products.

3.3.10 Temperature programmed reduction (TPR)

TPR determines the number of reducible species present in the catalyst and the temperature at which reduction occurs. This analysis was performed with an Autochem II 2920, automated catalyst characterization Micromeritics system.

The analysis starts by flowing the reducing gas (5% hydrogen in argon) though the sample (50 mg) at ambient temperature. While the gas flows, the temperature of the sample is raised linearly at a rate of 5 °C/min^{-1} to a temperature of 850 °C or 900 °C with time and the consumption of hydrogen by adsorption is monitored.

3.3.11 Temperature programmed oxidation-mass spectrometry (TPO-MS)

In each TPO-MS experiment a 100 mg sample of the catalyst was loaded into a quartz reactor (4 mm internal diameter) followed by purging in helium for 30 min. The reactor was heated under a 10% O_2/He flow of 20 ml/min to 900 ºC at 10ºC/min. The evolution of product was monitored with a Balzers QMA 400 quadrupole mass spectrometer.

3.3.12 Temperature programmed desorption (TPD)

TPD which determines the number of sites present in the catalyst was performed with an Autochem II 2920, automated Micromeritics system. The sample was saturated with ammonia basic probe molecule at 10 ml/min for 60 min. The sample was then purged with 75 ml/min helium for 60 min and the analysis was performed by heating the sample at 10 ºC/min from room temperature to 550 ºC.

3.4 Catalytic testing

Non-catalytic and catalytic reactions were carried out in the stainless steel reactor (32.5 cm) mentioned previously (**Fig. 3.8.**) For the catalytic testing, catalyst charge was made up of 1ml catalyst diluted with caborundum of 80 grit size (1:4). All void space in the reactor was filled with carborundum. The catalyst bed was separated from the carborundum with quartz wool plugs which also served to keep the catalyst bed in place.

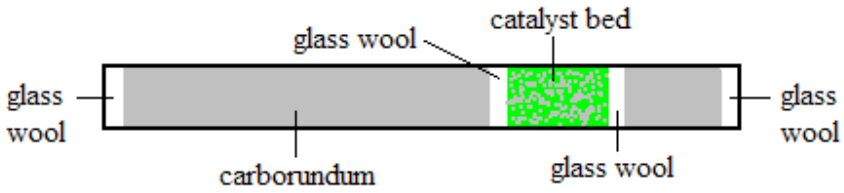

Fig. 3.8: Reactor packing for catalytic testing showing location of glass wool, carborundum and catalyst bed.

Non-catalytic testing comprised of blank experiments performed with an empty reactor and carborundum-packed reactors. For the carborundum-packed reactors, carborundum of varying sizes was used (24 grit, 80 grit and 300-600 μm (~30-50 grit)).

Testing was done in the temperature range 300-500 °C, with varying fuel/air ratios and flow rates for non-catalytic testing. For the catalytic testing varied contact times or gas hourly space velocities and dilution with nitrogen as well as varied fuel/air ratios were used. Steady state testing procedures used for evaluating the catalytic performance were defined by the equations given in the definitions and calculation section pp viii.

3.5 Startup procedure

Safe testing and operation of oxidation catalysts is of great importance and therefore a good knowledge of the flammability limits for combustible-oxidant mixtures is essential.

Homogeneous combustible gas-air mixtures are flammable i.e. they can propagate a flame freely, only within a limited range of compositions. The more dilute mixture is called the lower flammability limit (LFL) and the more concentrated mixture is called the upper flammability limit (UFL). Each combustible has its own flammability limit which is affected by temperature, pressure, direction of flame propagation and the surroundings.

Generally, the flammability limits widen as temperature and pressure are increased and become narrower as inert gases, such as carbon dioxide or nitrogen, are added. Oxidation of *n*-hexane was studied below the LFL and above the UFL.

Before experiments, the reactor was heated progressively from ambient temperature to the desired temperature under nitrogen and then the feed was introduced. Depending on whether the nitrogen was required (as diluent) the flow was maintained after which the air was introduced.

3.6 Materials used

3.6.1 The feed

Properties of n-hexane

Molecular formula: C_6H_{14}

Molecular weight: 86.18 g/mol^{-1}

Boiling point: 68.7 °C

Melting point: -95 °C - 100 °C

Density: 0.659

Flammability range: 1.7- 7.7% in air

3.6.2 Chemicals and reagents

Table 3.1 lists the chemicals and reagents used for compound identification and quantification

Table: 3.1: Chemicals and reagents used for compound identification and quantification.

Chemical:	Company:	Purity:
Cyclohexane	Lab-Scan	AR, 98%
Benzene	ACE	AR, > 89%
2-Hexene (*cis*)	Aldrich	AR, 85%
2-Hexene (*trans*)	Aldrich	AR, 85%
3-Hexene	Aldrich	AR, 99%
1-Hexene	Acros	AR, 97%
Hexane	Acros	99.99%
2,5-Dimethyltetrahydrofuran	Aldrich	GC, 99%
2,5-Hexandione	Aldrich	GC, 99%
Acetic acid	Associated Chemical Enterprises	AR, 99.5%
Acetaldehyde	Fluka	GC, 99%
Propanoic acid	Aldrich	99%

References

[1] J. C. Chetty, "ODH of *n*-Hexane and Octane over VMgO Catalysts", Department of Chemistry and Applied Chemistry, PhD Thesis, University of KwZulu-Natal, Durban, 2007.

[2] C. Mazzocchia, R. Del Rosso and P. Centola, An. Quim., 79 (1980) 108.

[3] G. C. Bond, "Heterogeneous Catalysis, Principles and Application", Oxford Science Publication, 1987.

[4] L. M. Madeira, R. M. Martin-Aranda, F. J. Maldonado-Hodar, J. L. G. Fierro and M. F. Portela, J. Catal., 169 (1997) 469.

[5] J. M. Thomas and W. J. Thomas, "Principles and Practice of Heterogeneous Catalysis", VCH Verlagsgesellsschaft mbh, Weinheim, 1996.

CHAPTER 4
CHARACTERIZATION: RESULTS AND DISCUSSION

4.1 Introduction

Catalytic behaviour is influenced by the crystalline structure and chemical nature of catalysts. In order to study the physicochemical properties of the catalyst system, which influence their activity and selectivity in oxidative dehydrogenation and partial oxidation processes, a detailed characterization of the catalyst needs to be done. This project considers a study of the structural and compositional properties in conjunction with the catalytic testing. In this chapter the focus is on one aspect of the project, namely the synthesis and characterization of $NiMoO_4$ catalysts.

4.2 Catalyst synthesis

A range of $NiMoO_4$ precursors were synthesized by the co-precipitation method. It was found that the pH of the reaction medium, as well as parameters such as precipitation temperature and temperature at filtration strongly affected the stoichiometry of the catalyst and purity of the phases. Although the reaction conditions were kept constant, there was difficulty in obtaining catalysts with a Ni:Mo ratio of 1. The precipitates obtained from the co-precipitation method that were used in the testing (catalysts A-C) are described in **Table 4.1**. The colour of the precipitates obtained varied from yellow to green and darkened after calcination. Catalyst D was β-$NiMoO_4$ which was prepared *in-situ* from its precursor α-$NiMoO_4$. Catalysts E and F were the pure oxides, NiO and MoO_3 respectively.

Table 4.1: Labelling of synthesized precursors.

Name of precursor	Colour of precursor	Colour of catalyst
Catalyst A	green	dark green
Catalyst B	yellow-green	light yellow
Catalyst C	green	brown
Catalyst E	green	dark green
Catalyst F	white	light blue

4.3 Catalyst characterization

4.3.1 Chemical composition: ICP and EDX

The bulk elemental composition of the catalysts was determined by ICP (**Table 4.2**). EDX was used in this project as a complementary technique to the ICP to compare metal composition results. EDX analysis, however, depends on depth of beam penetration, which is usually unknown, hence whether EDX results give the surface composition or bulk composition cannot be stated with confidence. Furthermore, EDX is a single point technique, which means there is higher degree of error in EDX analysis and these results are not shown. This technique however did confirm the elements present.

Table 4.2: Atomic ratios of catalysts synthesized (ICP).

	Uncalcined (precursor) Ni/Mo ratio	**Calcined (catalyst) Ni/Mo ratio**
Catalyst A	0.81	0.85
Catalyst B	0.99	1.00
Catalyst C	1.38	1.41

The ICP results have shown that there is slight increase in Ni/Mo ratio when comparing the precursor to the calcined catalyst (**Table 4.2**). This is possibly due to molybdenum loss due to MoO_3 sublimation that occurs during calcination.

4.3.2 BET surface area

Surface area measurements (**Table 4.3**) show that the chemical composition of the catalysts strongly affects the surface area and that there is a direct relationship between the two parameters. Surface areas of the catalysts were found to increase as the Ni:Mo ratios increased. The surface area of the catalyst with a Ni/Mo ratio of 1 was in agreement with that expected for a stoichiometric catalyst [1]. The catalyst with Ni:Mo < 1 had the lowest surface area of the molybdates, as was expected, due to the presence of excess molybdenum in the form of MoO_3 [1, 2].

The surface areas of the spent catalysts A, B and C were greater than those of the fresh catalysts (**Table 4.3**). This was attributed to the coking phenomena that were found to occur under the conditions at which these catalysts were tested. Coke particles act as cement between catalyst particles blocking the void spaces [3] between them and contribute their own surface area.

Table 4.3: BET surface areas of catalysts synthesized.

	***SA* BET (m^2/g) Fresh**	***SA* BET (m^2/g) Used**
Catalyst A (α-$NiMoO_4$, MoO_3)	16.8	30.0
Catalyst B (α-$NiMoO_4$)	35.3	40.9
Catalyst C (α-$NiMoO_4$, β-$NiMoO_4$, NiO)	50.8	68.2
Catalyst E (NiO)	4.79	4.5
Catalyst F (MoO_3)	3.89	3.8

4.3.3 XRD

X-ray diffraction patterns were used to determine the phase composition of the catalysts and the *d*-spacings of all six catalysts were compared to JCPDS cards 33-948, 45-01142, 5-508 and 4-835 for α-$NiMoO_4$, β-$NiMoO_4$, MoO_3 and NiO respectively (**Fig. 4.1**). For catalyst A peaks are assigned to both the α-$NiMoO_4$ (2θ = 16.86, 27.98, 38.07, 45.61 51.39, 57.91°) and the MoO_3 (2θ = 14.87, 27.26, 31.89, 39.43, 41.55, 65.98°) phases suggesting excess molybdenum due to the MoO_3 phase. For catalyst B, major peaks characteristic of α-$NiMoO_4$ at 2θ =16.62, 29.50, 33.60, 38.02, 38.29 and 51.42^o are observed.

The XRD pattern of catalyst C shows the presence of the peak at 2θ =33.61^o, characteristic of α-$NiMoO_4$, and overlapping peaks at 2θ = 31.01 and 31.16°, which correspond to β-$NiMoO_4$ [4]. NiO was also identified by the peak at 2θ = 51.26°. Although α-$NiMoO_4$ is stable at room temperature and the β-$NiMoO_4$ is stable only at higher temperatures (> 250 °C), it is possible for the β-$NiMoO_4$ to be stabilized at room temperature, if there is excess nickel relative to the stoichiometric $NiMoO_4$ requirement [5]. This is because a solid solution of the vacancy type is formed when dissolved Ni ions occupy the normal octahedral positions in the structure of the β-phase, while some tetrahedral positions of the Mo remain empty. The solubility limit for the solid solution formed with nickel is at Ni:Mo = 1.1-1.2. Since the ratio of Ni:Mo is 1.41 for catalyst C characteristic peaks of β-$NiMoO_4$ are observed in the XRD pattern of this catalyst.

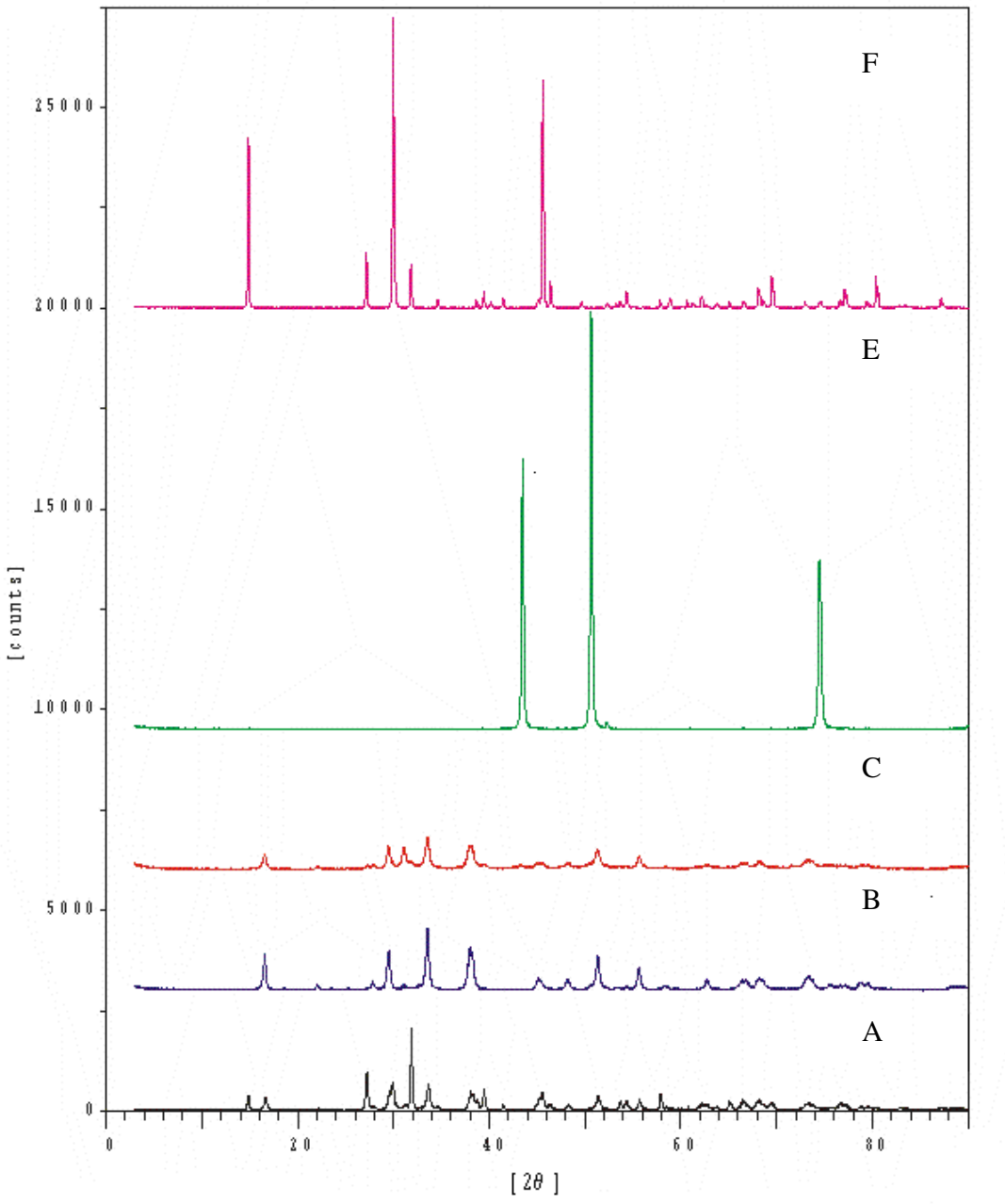

Fig. 4.1: XRD patterns for catalyst A, catalyst B, catalyst C, catalyst E and catalyst F at room temperature.

The distinct differences in the XRD patterns between the uncalcined catalyst (precursor) and α-$NiMoO_4$ were observed as reported in literature (**Fig. 4.2**) [6]. The intensity and resolution of the peaks improve after calcination due to increased crystallinity of the catalyst.

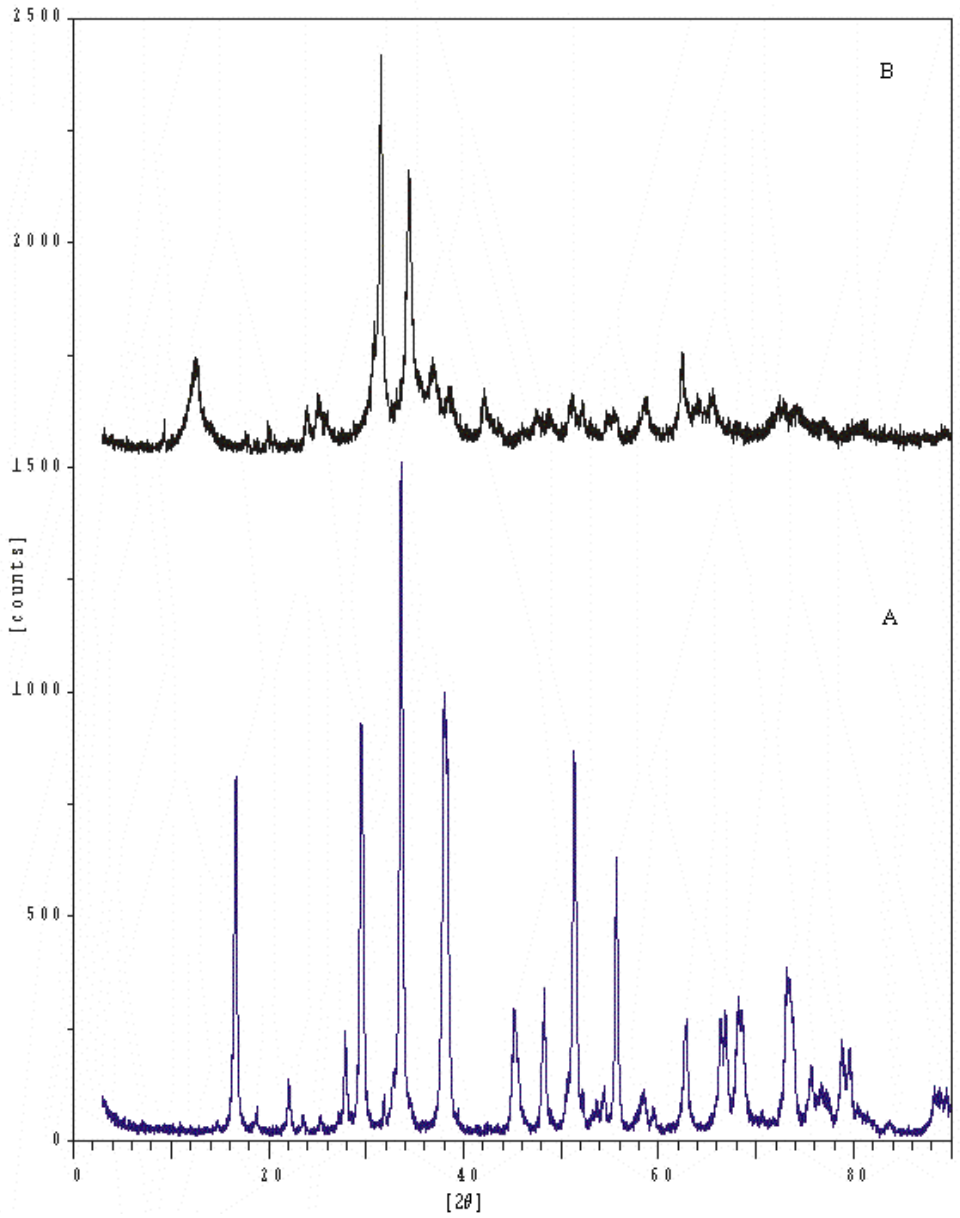

Fig. 4.2: X-ray diffraction pattern for catalyst B calcined (A) and uncalcined (B).

4.3.4 FTIR

FTIR spectra were used to confirm the phases of the catalysts. The bands at 820 and 880 cm^{-1} are due to MoO_3 phases, whereas the bands at 970, 930 and 580 cm^{-1} are due to the α-$NiMoO_4$ phase for catalyst A (**Fig 4.3A**). Catalyst B (**Fig.4.3B**) only showed bands due to the α-$NiMoO_4$ phase.

The IR spectrum of catalyst C (**Fig. 4.3C**) shows two peaks at 597 and 963 cm^{-1}, which are similar to those of catalyst B, but it has two more peaks at 881 and 807 cm^{-1}, which correspond to the β-$NiMoO_4$ phase. These peaks are used to distinguish between the two phases as a result of the structural change from six coordinate molybdenum in the α-phase, to four coordinate molybdenum in the β-phase [7].

Thus analysis by FTIR and XRD shows that the catalysts examined were of three different types: catalyst A was $NiMoO_4$ with excess MoO_3, catalyst B was the pure α-$NiMoO_4$, and catalyst C was the β-$NiMoO_4$ stabilized with excess NiO.

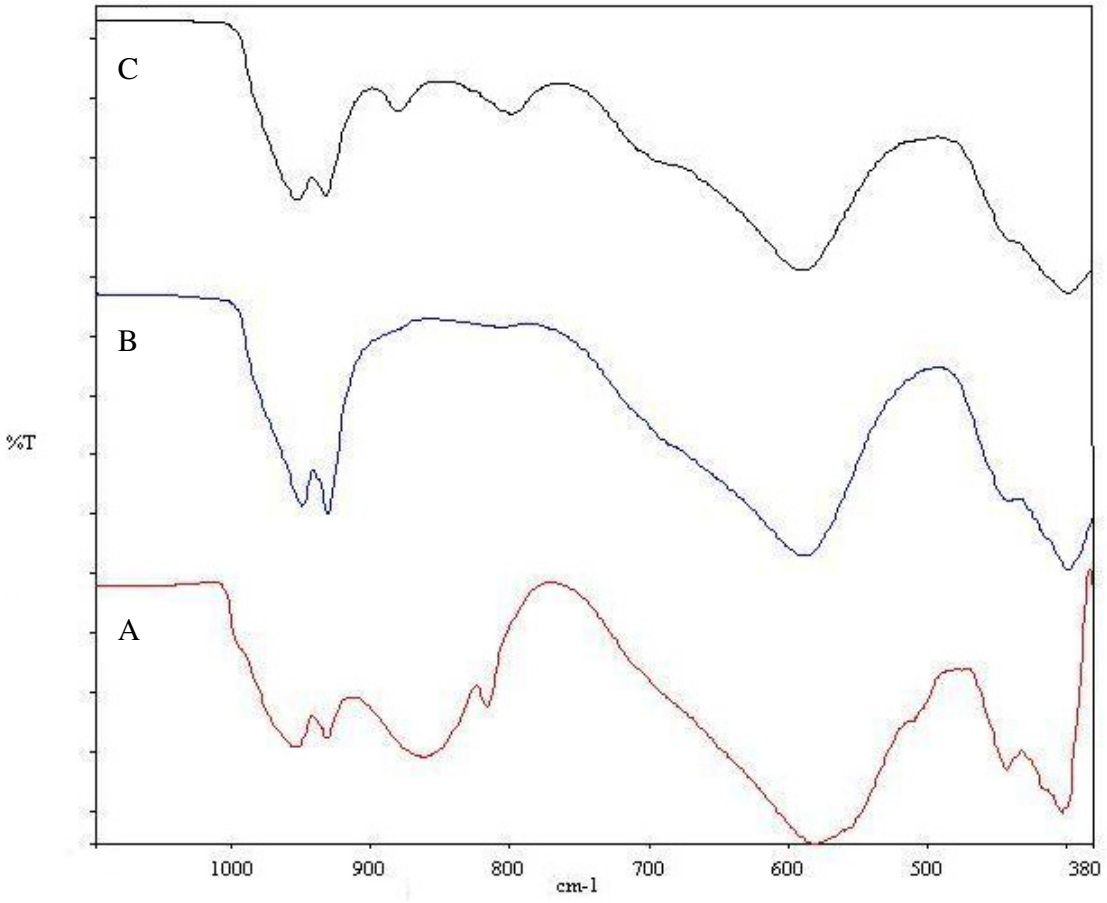

Fig. 4.3: FTIR spectra of catalyst A, catalyst B and catalyst C.

4.3.5 HT-XRD

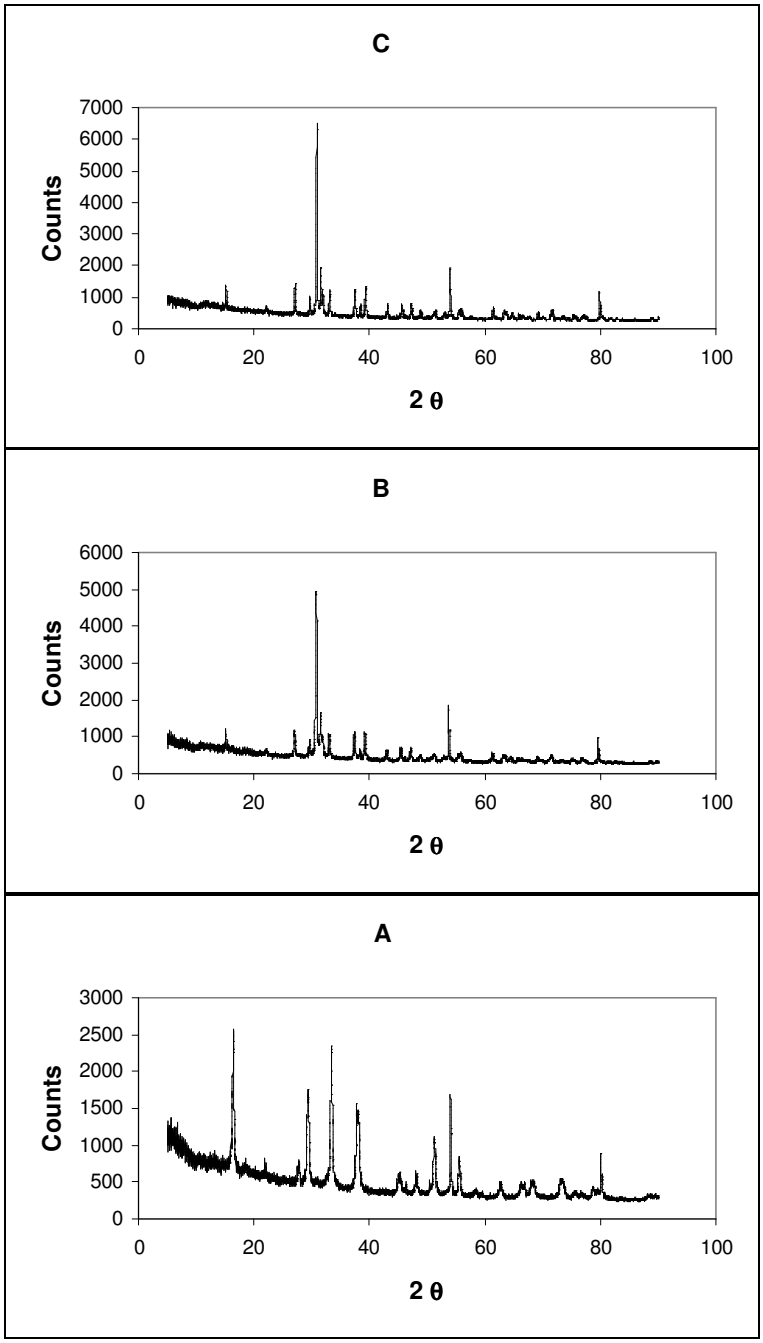

Fig. 4.4: XRD patterns for the precursor to catalyst D at 25 °C (A), catalyst D at 650 °C (B) and catalyst D at 300 °C (C).

Catalyst D, the pure β-$NiMoO_4$ phase which was prepared *in-situ*, was characterized with high temperature XRD experiments. High temperature scans were compared to JCPDS card 45-01142. As seen in **Fig. 4.4**, the precursor to catalyst D has the α-phase at room temperature and when heated to 650 °C it transforms to the β-phase. This phase was stable when cooled down to 300 °C and at the temperature range 300-500 °C at which the catalytic testing was performed, as shown by the overlapped XRD patterns (**Fig 4.5**).

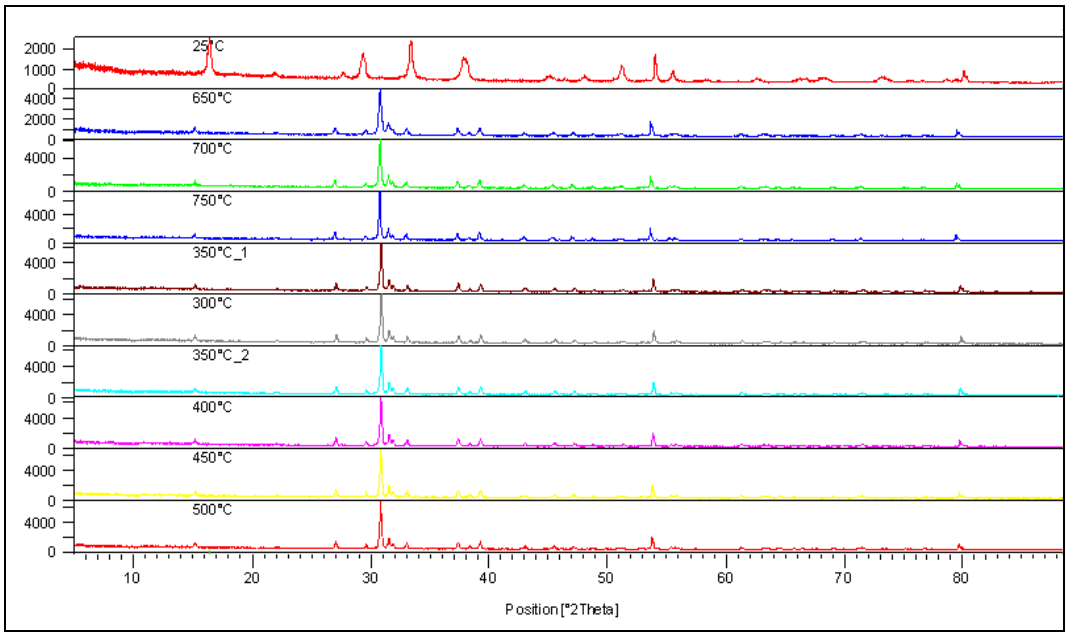

Fig 4.5: XRD patterns for catalyst D prior to activation (25 °C) and in-situ activation under air.

High temperature XRD was also performed on a sample of commercially obtained molybdate. The α-$NiMoO_4$ phase is evident at room temperature at 2θ = 27.2° and 29.7° as evidenced by the XRD of the uncalcined sample (**Appendix, Bavani [001]**). The phase transition to the β-phase occurs at 650 °C (**Appendix, Bavani [009]**) as shown by overlapping peaks at θ = 27.2°. This structure is maintained at the testing temperature, 300-500 °C (refer to the chromatogram at 300 °C in the **Appendix, Bavani [013]**).

4.3.6 SEM

Scanning electron micrographs showed that the stoichiometric catalyst was homogeneous with respect to the distribution of α-$NiMoO_4$ particles, having a sponge-like appearance (**Fig. 4.6a**). Metal clusters were observed for the non-stoichiometric catalysts (Ni:Mo ratios lesser or greater

than one), since there are free metal oxides that are not part of the Ni-Mo-O system. A cluster of well defined crystallites attributed to MoO_3 distinctly different from that of the pure α-$NiMoO_4$ particles is seen in **Fig. 4.6b** [1]. The higher magnified image of catalyst A shows the distinct particle identities of the two phases (**Fig 4.6d**).

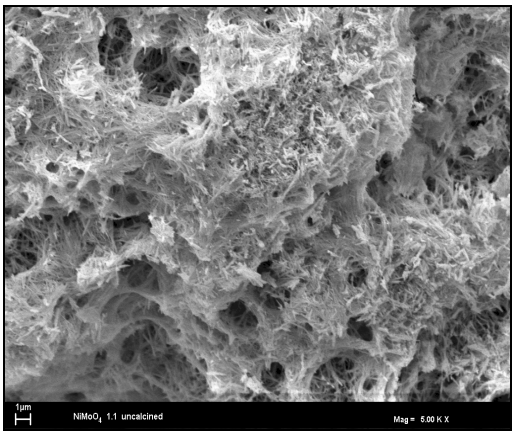

Fig. 4.6a: SEM image of catalyst with Ni:Mo = 1.

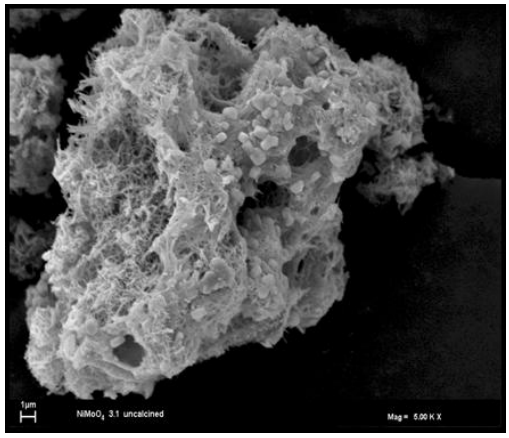

Fig. 4.6b: SEM image of catalyst with Ni:Mo < 1.

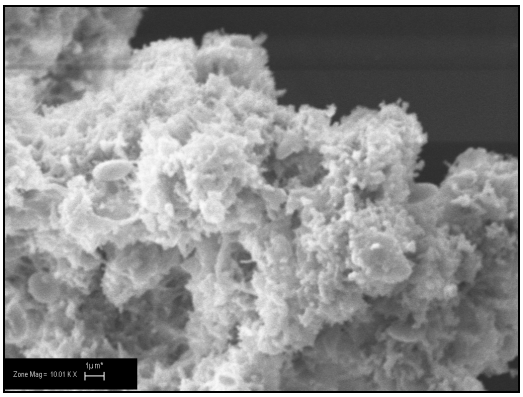

Fig. 4.6c: SEM image of catalyst with: Ni:Mo > 1.

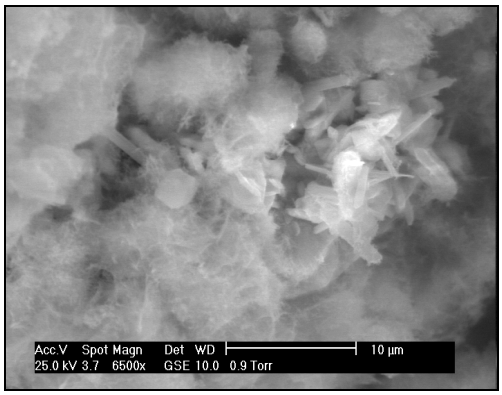

Fig.4.6d: SEM image of catalyst with Ni:Mo < 1 at higher magnification.

4.3.7 XPS

XPS was performed on catalysts A, B and C to evaluate the possible variation in oxidation states and environments of the metals**.** The samples have binding energies (**Table 4.4**) characteristic of Ni-Mo-O bonds as previously reported [8]. The results indicated that the Mo 3d binding energies for the $NiMoO_4$ catalysts are identical to the MoO_3 and the Ni 2p binding energies are similar for

the Ni-Mo-O catalysts and different to those of NiO. It can be concluded from this that the oxidation states of Mo and Ni do not change in samples with different Ni:Mo ratios (catalysts A and B). The Mo3$d_{5/2}$ and Ni2$p_{3/2}$ binding energies (**Table 4.4**) are typical of Mo^{6+} and Ni^{2+} oxidation states. Hence in samples containing excess MoO_3 exclusion of entirely new compounds being formed can be confirmed. Used catalyst A showed no nickel or molybdenum, only a strong carbon signal as expected due to the large amount of carbon. It is evident from the binding energies of the used catalyst B (**Table 4.4**, **Fig 4.7c** and **Fig 4.7d**) that the oxidation states of the metals do not change after testing. The Ni/Mo atomic ratios were in agreement to those obtained from ICP analysis.

Table 4.4: XPS data for $NiMoO_4$ samples used in catalytic testing (eV) [8].

Sample	Mo3d $_{5/2}$	Mo3d $_{3/2}$	Ni 2p $_{3/2}$	Ni 2p $_{1/2}$
MoO_3	*232.7*	*235.8*		
$NiMoO_4$	*232.6*	*235.7*	*855.7*	*873.3*
NiO			*853.3*	*871.3*
Catalyst A	232.2	235.5	855.6	873.2
Catalyst B	232.1	235.3	855.4	873.2
Catalyst C	231.5	234.7	855.0	872.5
used cat A	-	-	-	-
used cat B	232.6	235.8	855.8	873.5

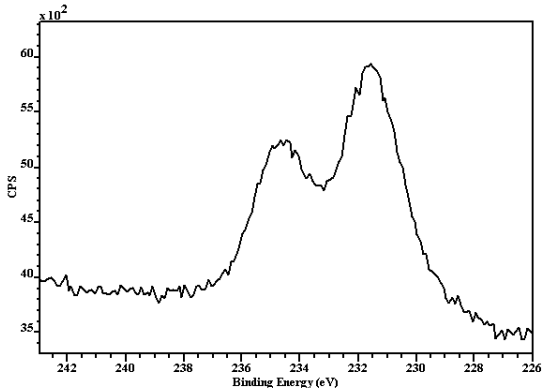

Fig. 4.7a: XPS of cat B Mo 3d region.

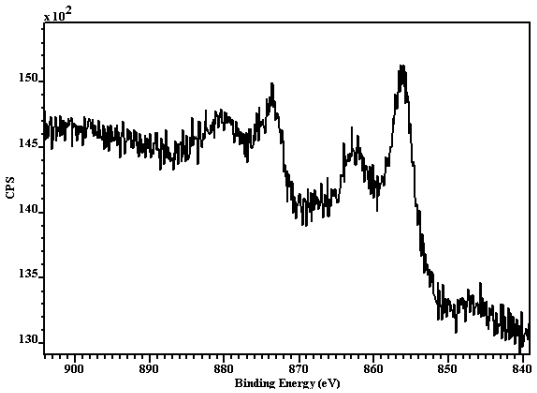

Fig. 4.7b: XPS of cat B Ni 2p region.

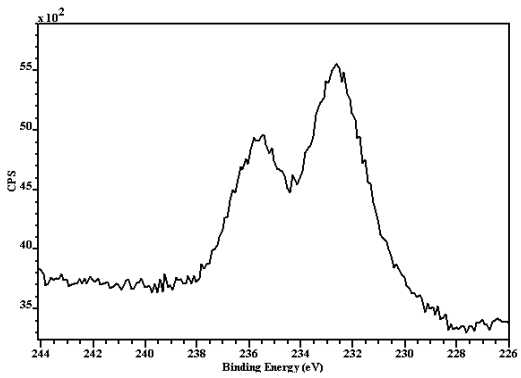

Fig. 4.7c: XPS of used cat B Mo 3d region.

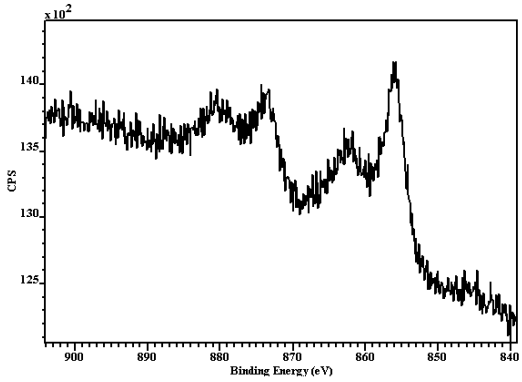

Fig. 4.7d: XPS of used cat B Ni 2p region.

4.3.8 TPR

TPR was performed to get some information on the reactivity of the catalyst's surface and adsorption properties. It is of particular importance to understand the behaviour of this phase under reduction conditions, since this catalyst is known to operate *via* a redox mechanism.

The TPR profile for α-$NiMoO_4$ is clearly similar to that reported previously [9]. There are two reduction peaks for the synthesized pure nickel molybdate catalyst. These occur at 613.7 °C and 815.0 °C (**Fig. 4.8**). The positions of the peaks differ, however, from the catalyst prepared from a commercially obtained molybdate sample which has maxima at 699.7 °C and 829.7 °C (**Fig. 4.8**). The positions of the maxima for both these catalysts differ from literature, and this is possibly due to different reaction conditions used in the TPR analysis and/ or synthesis.

The first step in the mechanism involves the low temperature reduction of $NiMoO_4$ to a number of possible products (metallic nickel and possibly Ni_4Mo, and amorphous MoO_2). The second peak is due to the high temperature reduction of Mo^{4+} leading to metallic molybdenum, intermetallic Ni_3Mo and a Ni-Mo alloy [9].

For the mixed phase catalyst, C, three maxima are observed. These are at 504.6 °C, 569.3 °C and 761.6 °C (**Fig. 4.9**). Catalyst E, NiO, showed a reduction peak at about 457.4 °C (**Fig. 4.9**) due to the reduction of NiO to metallic nickel. For MoO_3 two reduction peaks are observed, one at 695.2 °C and the other at 836.8 °C (**Fig. 4.9**). The first peak is assigned to MoO_3 reduction to MoO_2 which begins at low temperature and the second peak is due to MoO_2 reduction to metallic molybdenum [10].

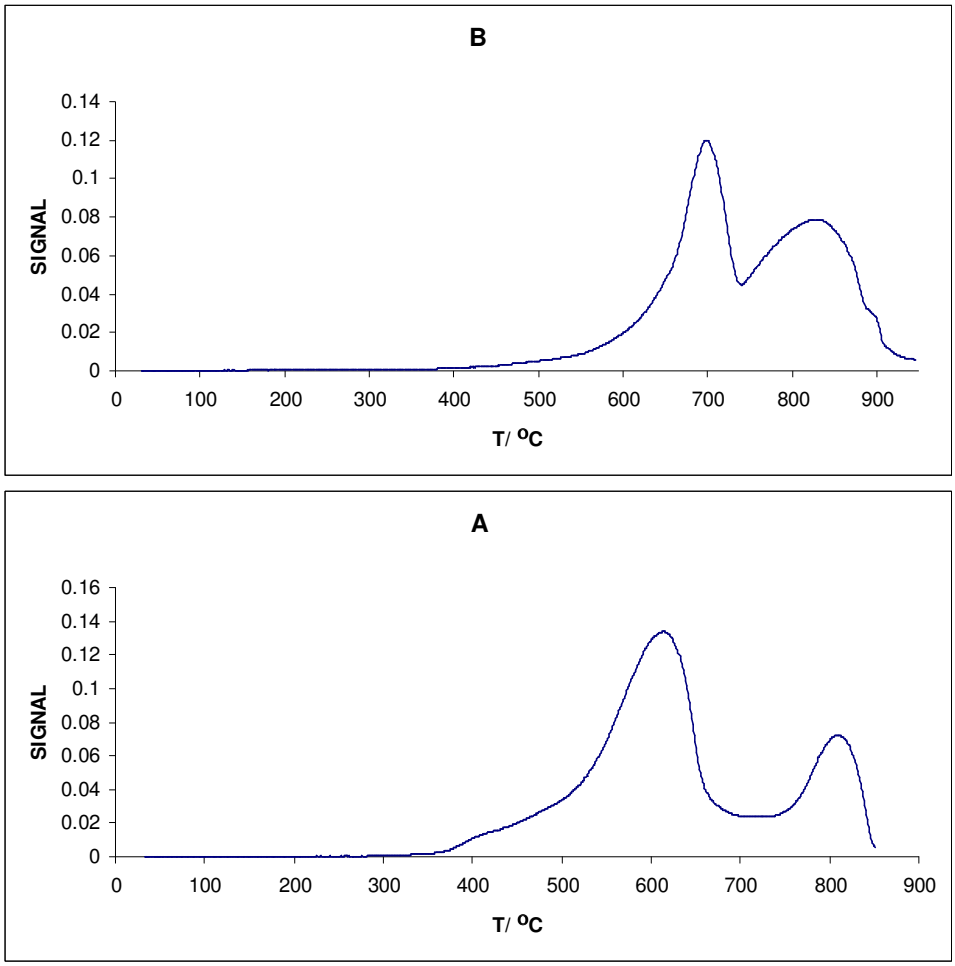

Fig. 4.8: TPR profiles of A) synthesized α-$NiMoO_4$ catalyst B) α-$NiMoO_4$ commercial catalyst with 5% H_2 in Argon.

4.3.9 Raman spectroscopy

$NiMoO_4$ catalysts are suitably characterized by Raman spectroscopy and this technique can be used to detect small amounts of segregated phases, such as MoO_3, in the Ni-Mo-O system. For catalysts with Ni:Mo < 1, catalyst A, the Raman spectrum (**Fig. 4.10b**, **Table 4.5**) showed bands due to the α-$NiMoO_4$ phase and additional bands typical of MoO_3 were found. The stoichiometric catalyst B only showed characteristic Raman peaks due to the α-$NiMoO_4$ phase (**Fig. 4.10a**, **Table 4.5**).

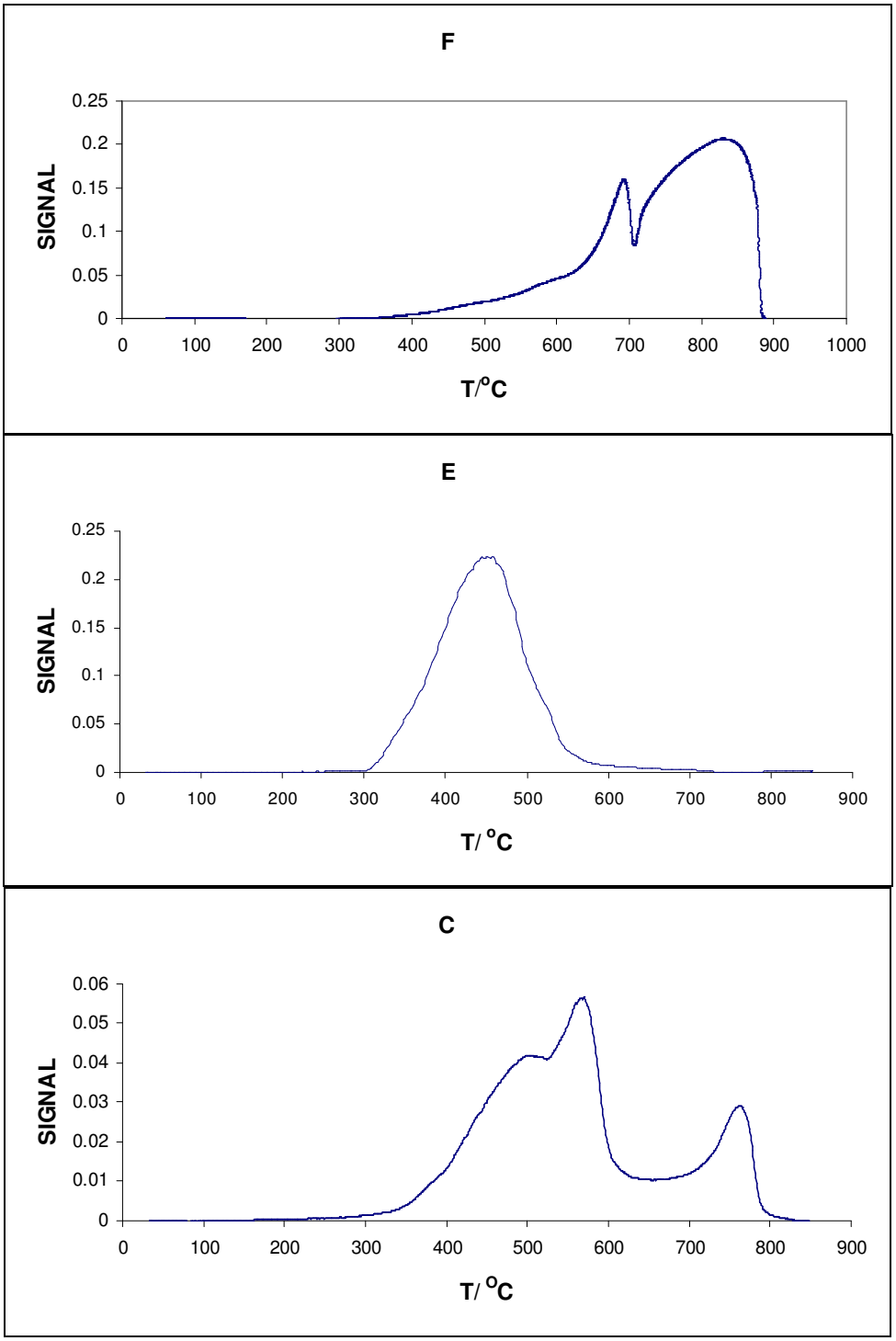

Fig. 4.9: TPR profile of catalyst C, catalyst E and catalyst F with MoO_3.

Table 4.5: Assignment of Raman bands (cm^{-1}) for catalyst A and B.

Catalyst B		**Catalyst A**	
Raman bands (cm^{-1})	**Phases**	**Raman bands (cm^{-1})**	**Phases**
962 vs	$NiMoO_4$	996 s	MoO_3
914 s	$NiMoO_4$	962 s	$NiMoO_4$
707 s	$NiMoO_4$	915 s	$NiMoO_4$
491 m	$NiMoO_4$	819 vs	MoO_3
418 m	$NiMoO_4$	708 s	$NiMoO_4$
387 m	$NiMoO_4$	666 s	MoO_3
370 m	$NiMoO_4$	469 m	MoO_3
329 m	$NiMoO_4$	420 m	$NiMoO_4$
		416 w	$NiMoO_4$
		337m	MoO_3

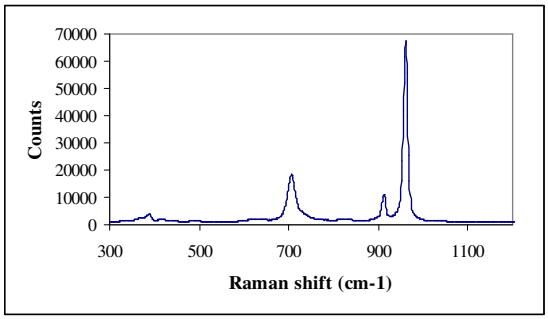

Fig. 4.10a: Raman spectrum of catalyst B.

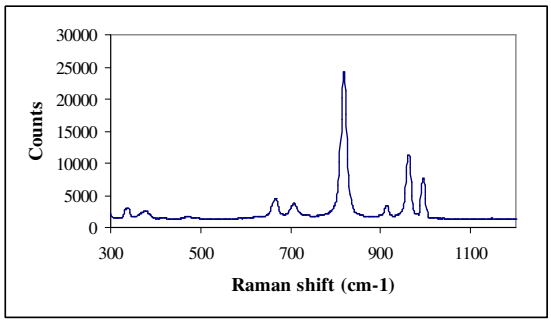

Fig. 4.10b: Raman spectrum of catalyst A.

4.4 TPO-MS

Coke is a carbonaceous deposit that has the ability to deactivate a catalyst. This may occur due to an impurity in the reactant or may be generated as a reaction by-product, such as carbon deposition during a reaction of a hydrocarbon. Its effect may be either of a temporary or permanent nature. Metallic catalysts are particularly sensitive to poisons such as coke. Some of the used catalysts tested above the UFL were hard and black in appearance, such as used catalyst D. When a sample of this catalyst was monitored with TPO-MS the evolution of CO_2 (m/z = 44), which is a gasification product of carbon ($C + O_2 \rightarrow CO_2$) was found. This confirmed carbon in the form of coke. The carbon weight % determined by TPO was 0.7%. **Fig. 4.11** shows the TPO profile of used catalyst D which suggests carbon deposits of different reactivity were present.

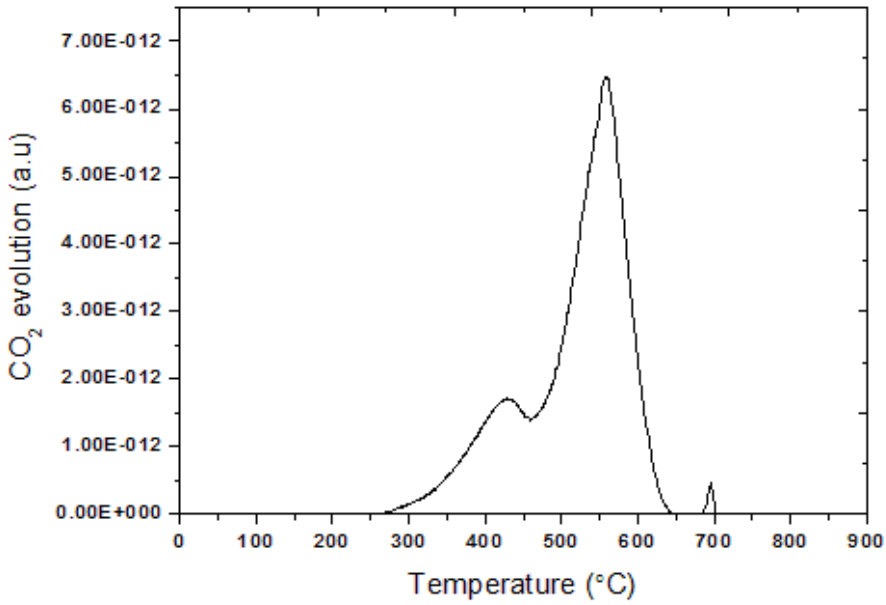

Fig. 4.11: TPO profile of used catalyst D.

The surface area was found to be 48.9 m^2/g, much greater that that of the fresh catalyst.

4.5 Promoted catalysts

The $NiMoO_4$ precursors were doped with different loadings of the alkaline metal caesium. These catalysts were characterized with ICP to check the metal/Mo molar ratios, which are shown in **Table 4.6**.

Table 4.6: Chemical composition and surface of areas of Cs-promoted catalysts.

	ICP (Cs/Mo)	***SA* BET (m^2/g)**
Catalyst unpromoted	-	35.3
Catalyst 3.5% Cs promoted	0.035	30.2
Catalyst 5.7% Cs promoted	0.057	28.4

Differences in the surface areas for the promoted and unpromoted catalysts were observed with BET analysis. The surface area of the Cs-promoted catalyst was found to be lower with respect to the unpromoted catalyst. Alkali promoters such as caesium block active sites which reduces their surface area. It was found that higher promoter loadings lead to a greater decrease in S_{BET} (**Table 4.6**). The decrease in surface area of the $NiMoO_4$ catalysts suggests a change in surface properties [11].

There are no significant shifts in the ATR bands of the Cs-promoted catalysts relative to the unpromoted catalysts (**Fig. 4.12**) and neither is there any significant difference in the XRD patterns of the alkali promoted catalysts when compared to the unpromoted catalysts (**Fig. 4.13**). The XRD patterns are for the unsintered catalysts. This was also observed previously [11].

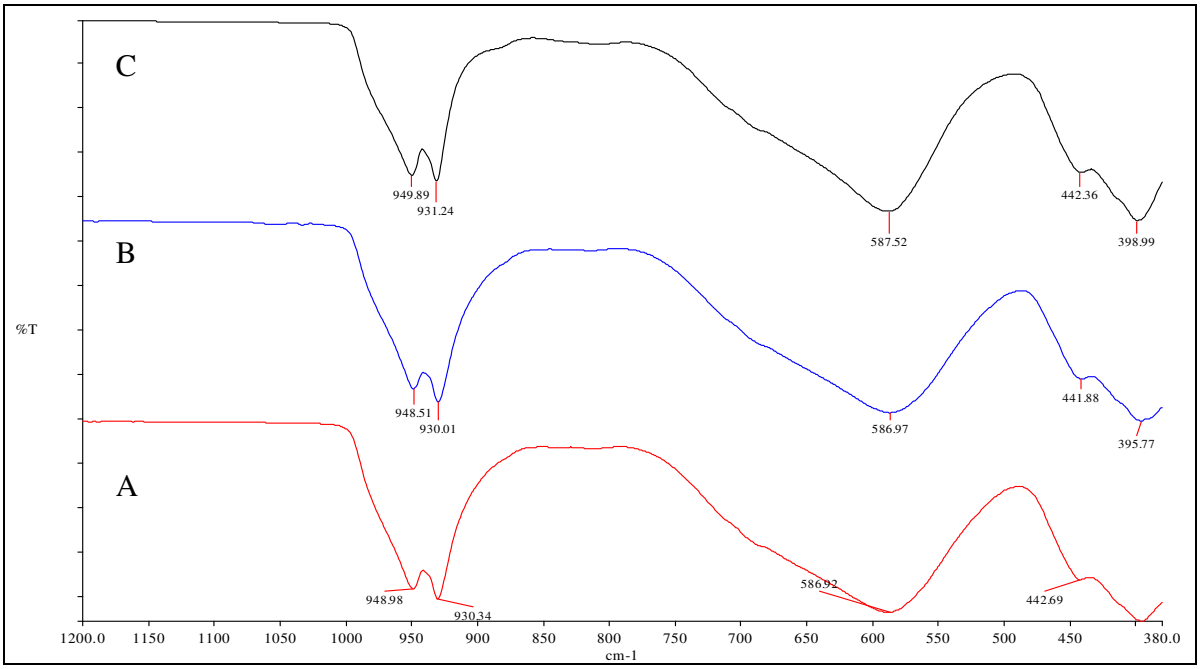

Fig. 4.12: ATR FTIR spectra of unpromoted (A), 3.5% Cs-promoted (B) and 5.7% Cs-promoted (C) catalysts.

The binding energies for Ni 2p and Mo 3d shown from XPS measurements (**Table 4.7**) are indicative of nickel and molybdenum atoms in their regular environments. However, the promoters have shifted the Mo 3d band to lower frequencies which would increase the average electron density of the molybdenum ions with respect to the nucleophilicity of their oxygens.

Table 4.7: XPS data for unpromoted and promoted $NiMoO_4$ samples.

Sample	**Mo3d $_{5/2}$ (ev)**	**Ni 2p $_{3/2}$ (ev)**	**Cs 3d (ev)**
unpromoted	232.5	855.9	
3.5% Cs-$NiMoO_4$	231.9	855.6	724.1

All these techniques suggest that the promoter does not alter the structure of the catalyst and no segregation of phases occurs. The influence of the promoter changes the surface characteristics only [11].

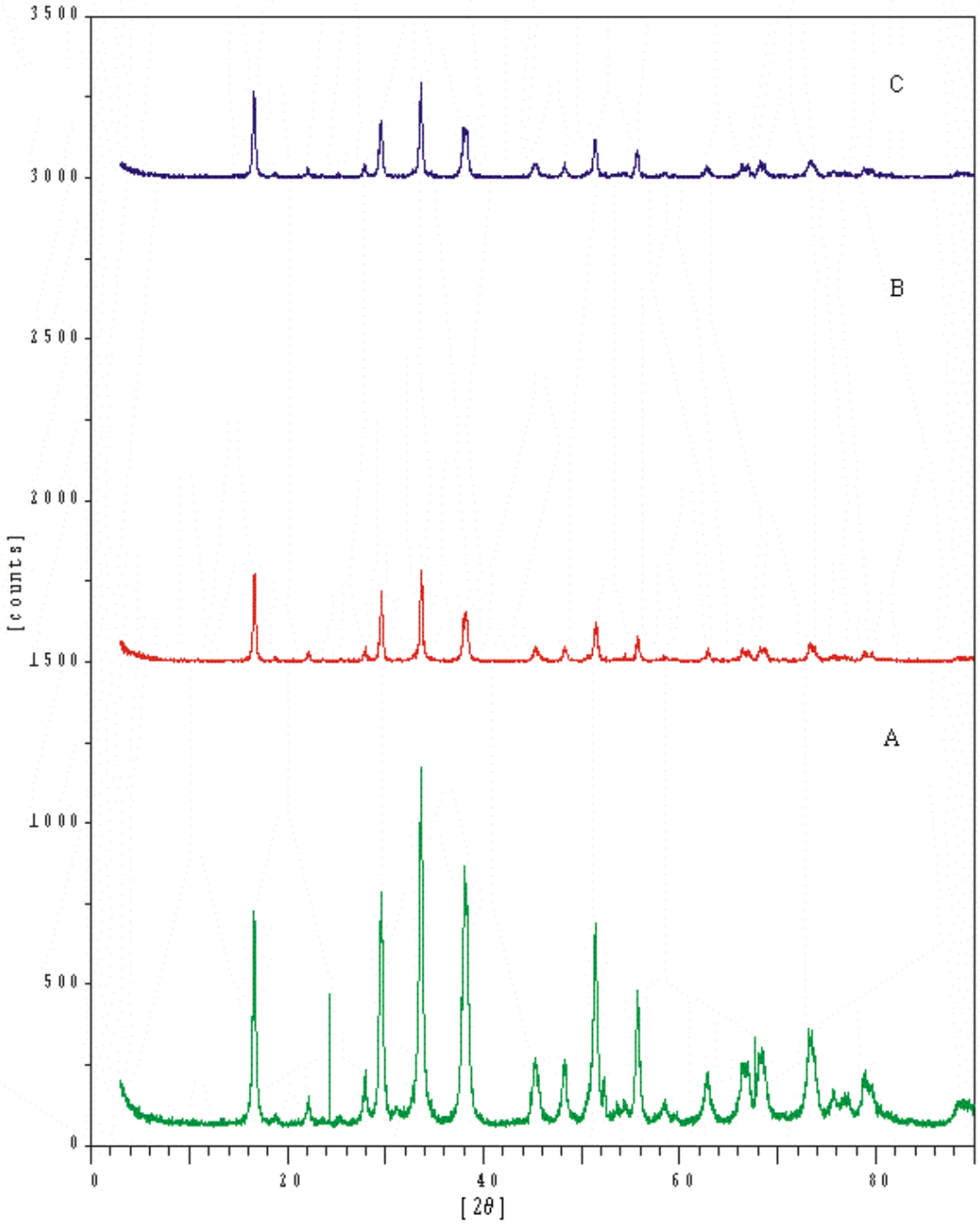

Fig. 4.13: XRD patterns of unpromoted catalyst (A) and 3.5% Cs-promoted (B) and 5.7% Cs-promoted catalysts (C).

4.6 NH_3-TPD

To investigate the acid-base nature of nickel molybdate NH_3-TPD was performed. **Fig. 4.14** shows the NH_3-TPD profile. A maximum is shown around 209.3 ºC with a shoulder peak at 239.2 ºC which decreases very quickly. A second maximum forms at 593.6 ºC but could not completely be determined because the experiments were performed only up to 600 °C to avoid the α to β transition. These results suggest that the catalyst exhibits some acidity involving possibly 2 or 3 types of sites [12]. The colour of the catalyst had changed from the original light-green to purple-black suggesting a nitrogenated compound was formed. Hence, using a different adsorbate to estimate the acidity or alternatively using CO_2 as a probe for TPD is necessary. This experiment, however, could not be performed due to the lack of expertise and access to this facility. The effect of Cs doping on surface basicity of nickel molybdate was proven by this method [6, 12, 13].

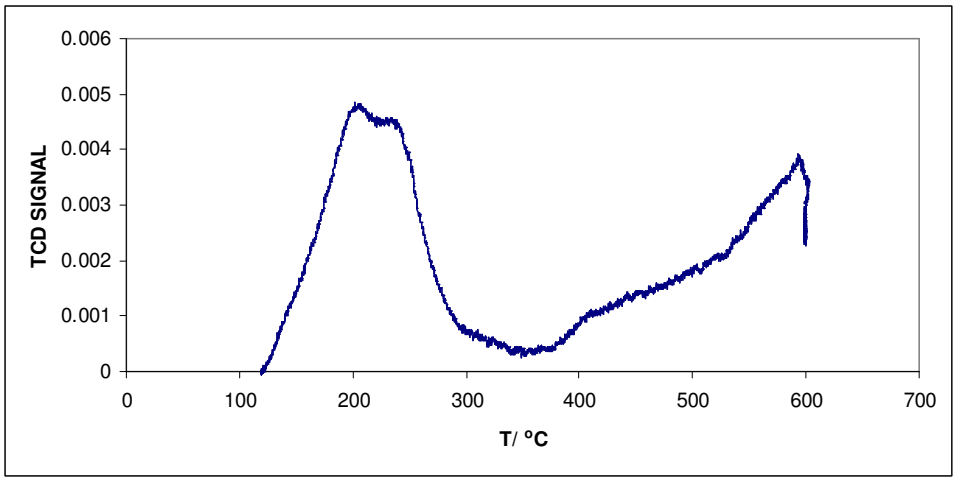

Fig. 4.14: NH_3-TPD profile for catalyst B.

4.7 Conclusion

$NiMoO_4$ precursors were synthesized by the co-precipitation method (catalysts A-C). These catalysts before and after calcination varied in chemical composition as determined from ICP. XRD and IR spectroscopy showed that these catalysts also varied in phase composition: catalyst A (MoO_3 and α-$NiMoO_4$), catalyst B (pure α-$NiMoO_4$) and catalyst C (α-$NiMoO_4$, β-$NiMoO_4$ and NiO). High temperature XRD showed that catalyst D, after *in-situ* activation, was composed of pure β-$NiMoO_4$. Raman spectroscopy was further used to show the phase composition of catalysts A and B. XPS was further used to confirm the chemical composition of the catalyst B and also showed that the Mo3$d_{5/2}$ and Ni2$p_{3/2}$ binding energy are typical of Mo^{6+} and Ni^{2+} oxidation states. BET surface areas were found to be influenced by the chemical and phase

composition of the catalysts. TPR showed the reduction potential for all catalysts. The used catalysts that had coked were analyzed by BET surface area measurements, XPS and TPO-MS.

Caesium-doped $NiMoO_4$ catalysts showed a reduction in surface area as measured by BET. No significant changes in the ATR FTIR spectra and XRD pattern were noted for these catalysts.

The NH_3-TPD profile suggested that the catalyst exhibits some acidity involving possibly 2 or 3 types of sites. However, due to the formation of nitrogenated compounds an alternative method for analysis of acidity is required.

References

[1] U. Ozkan and G. L. Schrader, J. Catal., 95 (1985) 120.

[2] N. Fujikawa, K. Wakui and K. Tomita, Catal. Today, 71 (2001) 83.

[3] F. J. Maldonado-Hodar, L. M. Madeira and M. F. Portela, J. Catal., 164 (1996) 399.

[4] F. J. Maldonado-Hodar, L. M. Madeira, M. F. Portela, R. M. Martin-Aranda and F. Freire, J. Mol. Catal. A: Chem., 111 (1996) 313.

[5] L. M. Plyasova, I. Ivanchenko, M. M. Andrushkevich, R. A. Buyanov, I. S. Itenberg, G. A. Khramova, L. G. Karakchiev, G. N. Kustova, G. A. Stepanov, A. L. Tsailingol'd and F. S. Philipenko, Kinet. Catal., 14 (1973) 882.

[6] L. M. Madeira, R. M. Martin-Aranda, F. J. Maldonado-Hodar, J. L. G. Fierro and M. F. Portela, J. Catal., 169 (1997) 469.

[7] C. Mazzocchia, C. Aboumrad, C. Diagne, E. Tempesti, J. M. Herrmann and G. Thomas, Catal. Lett., 10 (1991) 181.

[8] U. Ozkan and G. L, Shrader, J. Catal., 95 (1985) 120.

[9] L. M. Madeira, M. F. Portela, C. Mazzocchia, A. Kaddouri and R. Anouchinsky, Catal. Today, 40 (1998) 229.

[10] J. L. Brito, J. Laine and K. C. Pratt, J. Mater. Sci., 24 (1989) 425.

[11] R. M. Martin-Aranda, M. F. Portela, L. M. Madeira, F. Freire and M. Oliveira, Appl. Catal. A, 127 (1995) 201.

[12] F. J. Maldonado-Hodar, L. M. Madeira, M. F. Portela, R. M Martin-Aranda and F. Freire, J. Mol. Catal. A: Chem., 111 (1996) 313.

[13] L. M. Madeira, J. M. Herrmann, F. G. Freire, M. F. Portela and F.J. Maldonado, Appl. Catal. A, 158 (1997) 243.

CHAPTER 5
NON-CATALYTIC STUDIES ON *n*-HEXANE

Alkane activation in the presence of oxygen proceeds at relatively high temperatures because of the stability of paraffins. Metal surfaces when hot can generate heat necessary to initiate reactions and form active intermediates which promote partial oxidation *via* homogeneous reactions [1] as in the case of the stainless steel reactors used in this study. Apart from experimental parameters such as temperature, reactor design, gas composition and flow rates affecting the conversion of hexane and product selectivity in catalytic systems, it is recognized that gas phase radical reactions affect the product distribution. Homogeneous pathways may form a major route in the production of desired products [2] or they may result in non-selective oxidation. A comparison of catalytic and non-catalytic oxidative dehydrogenation of hexane has been made to determine contributions from heterogeneous versus homogeneous reaction systems.

Some comparisons of homogeneous and heterogeneous systems have been reported previously [1, 3-10].

In studies involving the non-catalytic and catalytic conversion of ethane over VMgO catalysts, non-catalytic ODH of ethane gave higher activity and selectivity at high temperatures than at low temperatures especially when a large fraction of the reactor was occupied by inert silica granules. It was postulated that the activation mechanism of ethane over the catalysts is dependent on temperature. Heterogeneous processes occur at low temperatures, whereas heterogeneous-homogeneous ones account for the behaviour of catalysts at higher temperatures [3].

An investigation of contributions of both homogeneous and heterogeneous systems for propane ODH with oxide catalysts showed that selectivity to propene was higher in the absence of the catalyst. With a purely heterogeneous catalysed reaction there was a limit for the yield of propene but in combination with a homogeneous system the yield of the desired product could be further improved [4].

The significance of gas phase chemistry in catalyst systems was further suggested with noble metal gauze reactors tested with short contact times for the oxidative dehydrogenation of ethane and propane. At low conversions, homogeneous reactions gave better selectivity to olefins due to

lower O_2 consumption. Higher conversions were obtained with the catalyst due to combustion. The Pt gauze increased reaction rates compared to the empty reactor [5].

It was further proposed, in the partial oxidation of linear C_1-C_5 alkanes in a single gauze reactor under fuel rich conditions at short contact times, that coupled heterogeneous initiated homogeneous systems exists with total combustion primarily catalysed by the Pt surface and oxygenates and olefins are formed by gas-phase reactions [6]. With butane ODH using the Pt gauze reactor, the study showed that the gauze does not play an important role, since reactions occur in the void space of the catalyst possibly *via* an alkylperoxy intermediate [1].

The reported study on *n*-hexane oxidation in a single gauze reactor also proceeded *via* free radical mechanisms [11]. In the partial oxidation of *n*-hexane over Pt-coated alumina foam monoliths homogeneous reactions contributed to cracked product and C_6 olefins formation [12] depending on the fuel/air ratios. A further investigation on the effect of voids and dilution on *n*-hexane has been reported [13]. Voids in the catalyst packing and dilution of catalysts effect the conversion of feed as well as selectivity towards thermodynamically favored products. Voids contribute to cracked-product formation [14].

Detailed homogeneous reaction mechanisms were simulated to support the hypothesis that olefins were made through gas phase chemistry for the partial oxidation of octane isomers and mixtures on rhodium coated foams [10].

5.1 Testing above the upper flammability limit (UFL)

Homogeneous gas-phase reactions were monitored in blank experiments with empty reactors and reactors packed with carborundum. It was shown that the presence of quartz chips in the reactor tube reduces conversion. This is due to the high surface area to volume ratio being reduced which terminates chain reactions of free radicals [15]. To interpret the contributions made by homogeneous gas phase reactions, reactor tubes were packed with inert SiC (carborundum). The particle size of the carborundum affects the conversion of feed under non-catalytic conditions, because the smaller the particle size, the higher the surface/volume ratio which results in even lower homogeneous reaction contribution. Size 80 grit carborundum was used. This resulted in a small pressure differential across the reactor (~5 kPa). Comparisons were done using the same feed/air ratios to investigate the effect of this packing on homogeneous reactions.

Table 5.1 shows the % fuel/air and fuel/O_2 ratios used for the non-catalytic testing performed.

Table 5.1: Actual % fuel/air and fuel/O_2 ratios used in experiments.

% Hexane/Air	13.7	31.8	56.8
Hexane/O_2 ratio	0.76	2.22	6.25

The product profile for both the empty and carborundum-packed reactor was, more or less the same, comprising of cracked products (propane, propene, butane, butene, ethanal), benzene, cyclohexene, hexenes and CO_x. This of course depended entirely on the parameters that were used in the investigation. Water was also produced from the ODH process or the combustion.

5.1.1 The effect of flow rates on *n*-hexane above the UFL

The rate at which the gas flows through the reactor affects residence time of the feed. For this reason experiments were conducted at different flow rates using a fuel/O_2 ratio of 2.2 and a temperature of 300 °C to monitor the effect of the flow rate on the conversion of the feed as well as the selectivity to the various products in an empty as well as a carborundum-packed reactor.

5.1.1.1 *Empty reactor above the UFL*

In an empty reactor, increasing the flow rate decreases the conversion of the feed. This is expected because shorter residence time reduces the number of free radical reactions that occurs in the void space of the reactor. In terms of product selectivity, CO_x and cracked products are favoured at all flow rates. This is due to hexane contacting onto the walls of the reactor and forming free radicals which promotes cracking mechanisms and allows the complete decomposition to CO_x. As the flow rate is increased a decrease in CO_x is clearly seen because of insufficient time for the combustion reaction to occur. With the cracked products, a less distinct pattern is observed. The decreased flow rate from 99 ml/min to 66 ml/min resulted in a decrease in cracked product selectivity, possibly due to the increase in the hexene and cyclic C_6 product selectivity.

Hexene formation is only seen at 33 ml/min and 66 ml/min because the mechanism supporting the formation of this product is only possible at longer residence times. Cyclic C_6 products production decreases with increasing flow rate suggesting that its formation can be non-catalytic. These results are shown in **Fig. 5.1**.

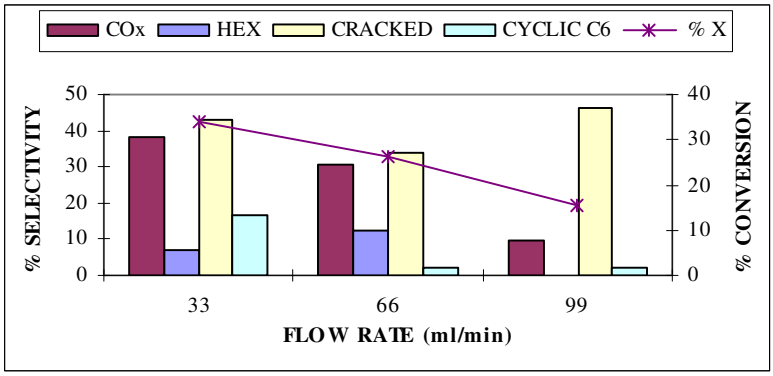

Fig. 5.1: Effect of flow rate on n-hexane conversion and selectivity to products in an empty reactor for fuel/O_2 ratio 2.2 at 300 °C.

5.1.1.2 *Carborundum-packed reactor above the UFL*

Fig. 5.2 shows the effect of flow rate on *n*-hexane conversion and selectivity to products in a carborundum-packed reactor at a fuel/O_2 ratio of 2.2 at 300 °C. In the carborundum-packed reactor conversion seems to increase with increasing flow rate but it must be noted that margin of error is large since overall the conversion is small (< 0.5%) so this may not be an external mass transfer control effect. Conversion in the carborundum-packed reactor was lower than in the empty reactor at lower flow rates because the gas phase reaction is rapidly quenched. By the time the void space is of the same dimensions (volume) as found for a typical catalyst bed, then conversion has been typically reduced by two orders of magnitude and no hexene is detected at the slower flow rates.

CO_x formation decreases with increasing flow rate due to decreased residence time and while cracking seems to increase with increasing flow rate. Hexene formation is only observed at the fastest flow since the faster the flow rate the better that chance of the hexene being removed from the reactor preventing further reactions.

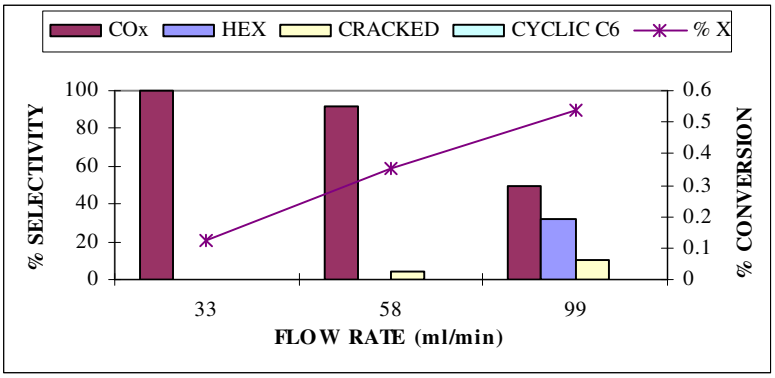

Fig. 5.2: Effect of flow rate on n-hexane conversion and selectivity to products in a carborundum-packed reactor for fuel/O_2 ratio 2.2 at 300 °C.

5.1.2 The effect of fuel/air ratio on *n*-hexane in an empty reactor above the UFL

The paraffin in air mixture can be introduced to the reactor in three different ways:(i) high alkane to oxygen ratio, (ii) stoichiometric ratio of alkane to oxygen and (iii) low alkane to oxygen ratio.

The low paraffin to oxygen ratio is not usually favoured because it gives high paraffin conversion, low selectivity to desired products and high selectivity to carbon oxides because of the oxygen rich environment.

Operating at high paraffin to oxygen ratios has the main advantage in that it favours high selectivities. However, due to oxygen starvation catalyst deactivation is highly probable. For a stoichiometric ratio of paraffin to oxygen, the alkane is in excess when the oxygen is consumed in side reactions such as combustion. After these considerations it is more appropriate to work above the flammability range, *i.e.* in a hydrocarbon rich environment. Hydrocarbon conversion is low and better selectivity to desired products can be achieved. Also carbon oxide production is lowered due to less oxygen being available [16].

Both catalytic and non-catalytic testing was then carried out mostly below the stoichiometric value of *n*-hexane to oxygen in this thesis. Usually for processes like this it is desirable to use pure oxygen as the oxidant [16], however air replaced oxygen as a source of the oxidant since it is cheaper than a pure oxygen source for both laboratory scale and industrial scale processes.

5.1.2.1 *Empty reactor above the UFL*

Oxygen limitation is another variable that may affect the mechanism supporting gas phase reactions in an empty reactor. From **Fig. 5.3,** which shows the effect of % fuel/air in an empty reactor at 33 ml/min at 300 °C, conversion decreases with increasing % fuel/air [2]. This is because the higher the fuel/oxygen ratio the lower the oxygen availability which reduces the number of oxygen radicals forming and hence one expects a decrease in conversion. By increasing the oxygen content in the reaction mixture a greater number of gas phase reactions can occur [4].

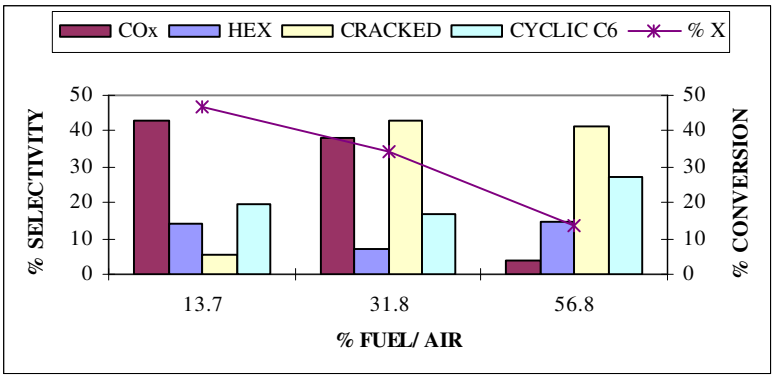

Fig. 5.3: Effect of % fuel/air on n-hexane conversion and selectivity to products in an empty reactor at 33 ml/min at 300 °C.

Cracking increased with increased fuel/O_2 ratios, which suggests that an oxygen-deficient environment promotes this type of mechanism. Combustion, however, increases with decreased fuel/air % as expected, due to more oxygen forming radicals. Provided that there is sufficient oxygen available CO_x's will dominate. The cyclic C_6 products seem to increase or decrease relative to the hexenes suggesting that these types of products may arise from the same mechanism non-catalytically. The amount of cyclic C_6 products produced is quite significant.

5.1.2.2 *Carborundum-packed reactor above the UFL*

By varying the fuel/O_2 % (**Fig. 5.4**) in a carborundum-packed reactor operated at 33 ml/min at 300 °C, only significant conversion (2.8%) is observed for 56.8% fuel/O_2 %. At lower feed ratios, the feed may be the limiting reactant hence almost no conversion is observed. The only products observed in the carborundum-packed reactor are the CO_x's.

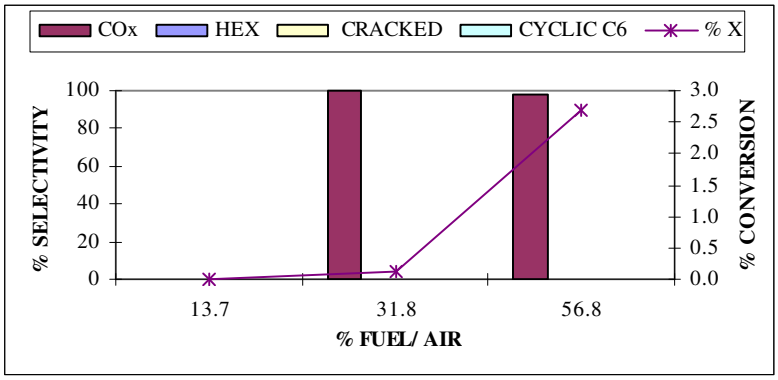

Fig. 5.4: Effect of % fuel/ air on n-hexane conversion and selectivity to products in a carborundum-packed reactor at 33 ml/min at 300 °C.

5.1.3 The effect of temperature on *n*-hexane above the UFL

5.1.3.1 *The effect of temperature on n-hexane in an empty reactor above the UFL*

Fig. 5.5 shows the effect of temperature on non-catalytic conversion of *n*-hexane in an empty reactor for different fuel/air ratios at 33 ml/min. Non-catalytic conversion increases with temperature for all fuel/air % except for 13.7% where there is a leveling off after 375 °C. For all feed/air % there is a leveling off for conversion due to the oxygen limiting conditions [4, 13].

Below ~ 400 °C conversion is higher for the fuel/air % in the order 13.7% > 31.8% > 56.8%. This can be predicted due to more oxygen being available that will promote free radical formation. Above this temperature, however, the trend is reversed for the different fuel/air ratios. It can be assumed that above this critical temperature the feed becomes the limiting reactant due to the thermodynamics. Due to larger exotherms being generated at the higher temperatures, and less free radicals being available, the demand is not met to the same degree as when there is more feed available for consumption in these homogeneous gas phase reactions [10].

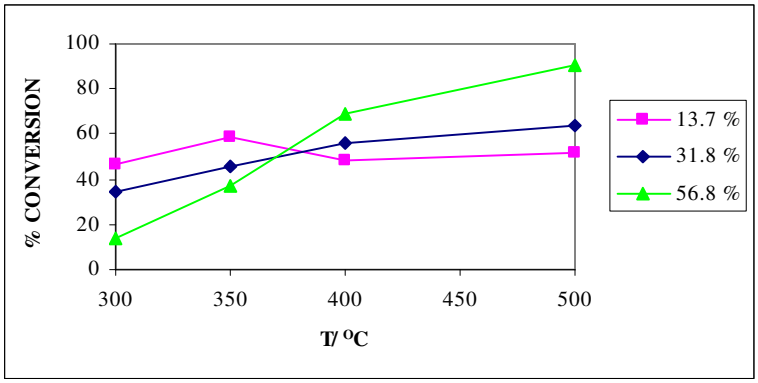

Fig. 5.5: Effect of temperature on non-catalytic conversion of n-hexane in an empty reactor for different fuel/air % at 33 ml/min above the UFL.

Mainly 2-hexene was produced in an empty reactor suggesting that its formation is non-catalytic (**Fig. 5.6**). A drop in *trans*-2-hexene selectivity from 400°C to 500 °C is due to possible decomposition.

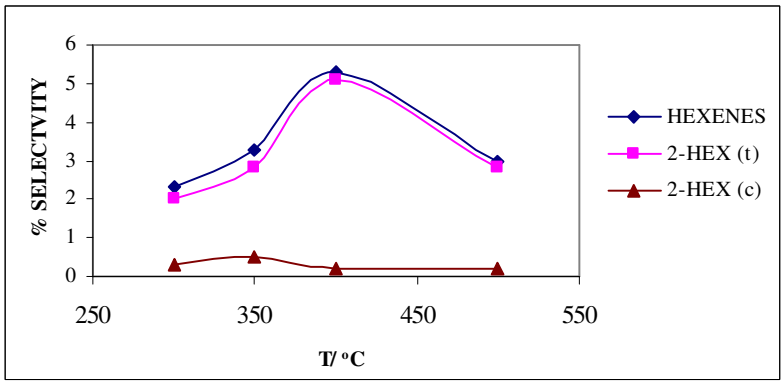

Fig. 5.6: Effect of temperature on the selectivity to hexenes for the non-catalytic conversion of n-hexane at flow rate 33 ml/min for fuel/O_2 ratio 2.2.

The selectivity to CO appears to be higher than that of CO_2 (**Fig. 5.7**) at all temperatures and this is characteristic of homogeneous oxidation processes that proceed *via* peroxy-type radicals [2, 9]. It must also be noted that CO selectivity increases from 400 °C to 500 °C confirming the decomposition of *trans*-2-hexene.

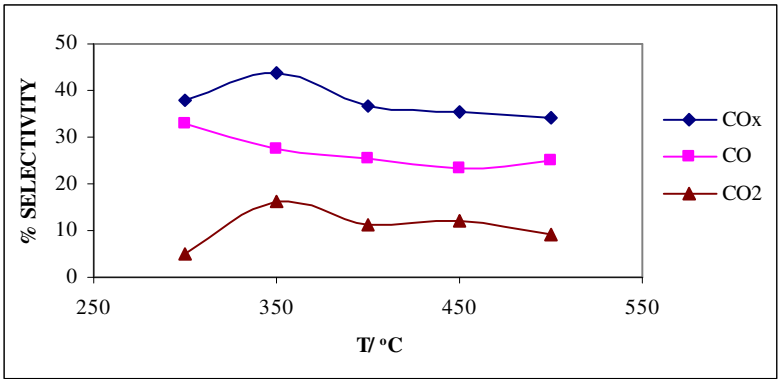

Fig. 5.7: Effect of temperature on CO_x selectivity for non-catalytic conversion of n-hexane at flow rate 33 ml/min for fuel/O_2 ratio 2.2.

High selectivity to cracked products is observed in an empty reactor (**Fig 5.8**) and these products dominate over dehydrogenation products [2]. It is also further suggested from the increase in cracked alkane selectivity from 400°C to 500°C that at the higher temperatures *trans*-2-hexene decomposes to either CO or cracked alkanes.

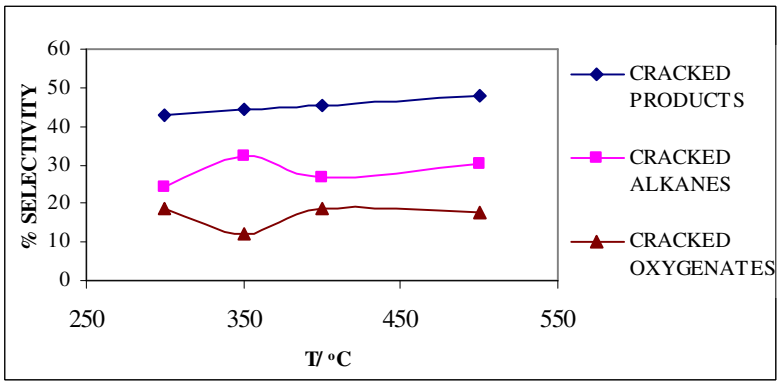

Fig. 5.8: Effect of temperature on the selectivity to cracked products for non-catalytic conversion of n-hexane at flow rate 33 ml/min for fuel/O_2 ratio 2.2.

Considerable amounts of cyclic C_6 products were produced at 400 °C though gas-phase chemistry (**Fig. 5.9**). This suggests that void spaces in the reactor propagate free radicals in the reactor for the formation of aromatics but increased temperatures favour cracking and complete combustion, as a result a decrease in benzene selectivity is observed at temperatures above 400 °C.

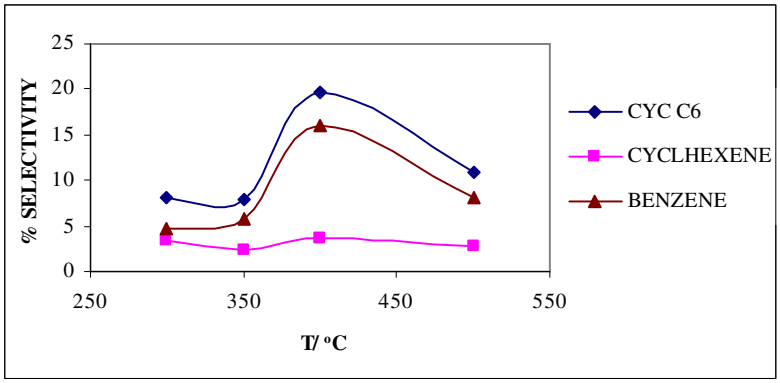

Fig. 5.9: Effect of temperature on the selectivity to cyclic C_6 products for non-catalytic conversion of n-hexane at flow rate 33 ml/min for fuel/O_2 ratio 2.2.

5.1.3.2 *The effect of temperature on n-hexane in a carborundum-packed reactor above the UFL*

Below 400 °C (**Fig. 5.10**) the conversion for all three fuel/air ratios are more or less the same *i.e.* less than 5%. Above this temperature the conversion increases sharply. The amount of feed converted decreases for the fuel/air % in the order 13.7% < 31.8% < 56.8%. Thermodynamic factors influence bond homolysis of the feed to generate free radicals. Hence, at the lower temperatures the carborundum (SiC) manages to quench the free radical propagation resulting in lower activity, however, the sudden increase in conversion from 400 °C implies that beyond this temperature greater numbers of free radicals are generated due to the thermodynamics and the effect of the caborundum is less effective.

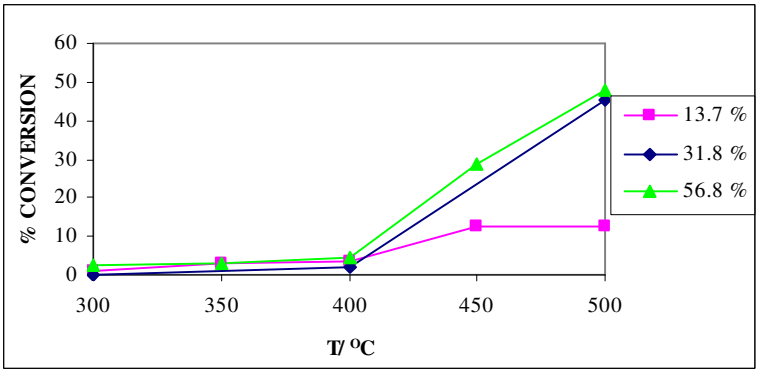

Fig. 5.10: Effect of temperature on non-catalytic conversion of n-hexane in a carborundum-packed reactor for different fuel/air % at 33 ml/min above the UFL.

Since an empty stainless steel tube leads to conversion of hexane to products and that a carborundum-packed tube favours CO_x formation, it implies that the stainless steel tube provides a reactive surface for hexane conversion. Whereas previous work on the effect of reactor material on hexane conversion has shown that higher conversions were obtained in a stainless steel tube than a pure quartz tube (SiO_2), at temperatures above 400 °C the products from both types of tubes were the same [13]. These findings showed that carborundum packed stainless steel and quartz reactors do indeed provide reactive surfaces for hydrocarbon conversion, but conversions for both were low.

5.2 Mechanism of homogeneous reactions

Stainless steel reactors are composed of Co, Mn, Fe and Cu. These metals have the ability to initiate free radicals in oxidation reactions by their involvement in a redox cycle [17].

The formation of free radicals begins with the abstraction of hydrogen from the paraffin to form an alkyl radical. Addition of O_2 directly to the paraffin results in an alkyl radical and a hydroperoxy radical or else a radical such as the hydroxyl radical may desorb from the catalyst/metal surface and abstract a hydrogen atom from the paraffin [11]. The alkyl radical can either dehydrogenate oxidatively to form an olefin (**Fig. 5.11**) or directly add an oxygen molecule to produce an alkylperoxy radical. This radical rearranges by internal H-atom abstraction proceeding *via* a cyclic peroxide intermediate. Loss of the hydroxyl radical accounts for the formation of oxygenates.

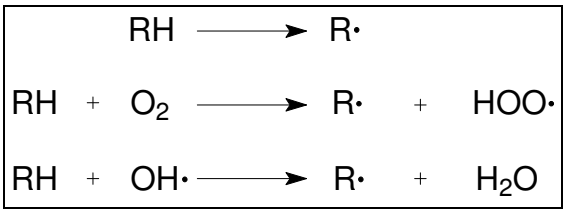

Fig. 5.11: Formation of the alkyl radical.

The other products that were observed from the non-catalytic reactions were the carbon oxides and aldehydes. Carbon oxides observed in stainless steel reactors may arise from two sources, benzene and aldehydes as previously reported. The mechanism involves hydroxylation of

benzene to a dihydoxy-derivative, rupture of the ring and then rapid decomposition to CO and CO_2 [18]. Carbon monoxide is favoured over carbon dioxide [19].
Aldehydes were reported to be the first stable products from hydrocarbon oxidation with one less carbon than the initial hydrocarbon. Further oxidation of the aldehyde results in degradation into shorter chain aldehydes and carbon monoxide or carbon dioxide [20].

5.3 Conclusion

Blank reactor studies on *n*-hexane have shown that non-catalytic reactions are quite significant in stainless steel reactors. Filling the reactor tubes with carborundum greatly reduces homogeneous gas phase reactions and therefore helps in studying the effect of the catalyst.
Parameters such as flow rate, fuel/air % and temperature play a significant role in the conversion and product distribution for both the empty and carborundum-packed reactor.

Since homogeneous gas phase reactions still exist, although to a small degree with the carborundum-packed reactor, a homogeneous-heterogeneous system must be considered in this study for the oxidative dehydrogenation of *n*-hexane over nickel-molybdenum oxide catalysts.

References

[1] S. Marengo, P. Comotti and G. Galli, Catal. Today, 81 (2003) 205.

[2] V. P. Vislovskiy, T. E. Suleimanov, M. Y. Sinev, Y. P. Tulenin, L. Y. Margolis and V. C. Corberan, Catal. Today, 61 (2000) 287.

[3] Z. Chao and E. Ruckenstein, J. Catal., 222 (2004) 17.

[4] R. Burch and E. Crabb, Appl. Catal. A, 100 (1993) 111.

[5] R. Lodeng, O. A. Lindvag, S. Kvisle, H. Reier-Nielsen and A. Holmen, Appl. Catal. A, 187 (1999) 25.

[6] D. I. Iordanolglou, A. S. Bodke and L. D. Schmidt, J. Catal., 187 (1999) 400.

[7] J. A Barbero, M. A Banares, M. A Pena and J. L. G. Fierro, Catal. Today, 71 (2001) 11.

[8] R. P. O'Connor and L. D. Schmidt, J. Catal., 191 (2000) 245.

[9] C. Resini, M. Panizza, F. Raccoli, M. Fadda, M. M. Carnascali, G. Busca, E. Fernandez Lopez and V. S. Escribano, Appl. Catal. A, 251 (2003) 29.

[10] G. J. Pannancio, K. A. Williams and L. D. Schmidt, Chem. Eng. Sci., 61 (2006) 4207.

[11] R. P. O' Connor and L. D. Schmidt, Chem. Eng. Sci., 55 (2000) 5693.

[12] A. G. Dietz III, A. F. Carlsson and L. D. Schmidt, J. Catal., 176 (1996) 459.

[13] H. B. Friedrich, N. Govender and M. R. Mathebula, Appl. Catal. A, 297 (2006) 81.

[14] L. D. Schmidt, E. J. Klein, C. A. S. Leclerc, J. J. Krummenarcher and L. N. West, Chem. Eng. Sci., 58 (2003) 1037.

[15] A. A. Lemonidou and A. E. Stambouli, Appl. Catal. A, 171 (1998) 325.

[16] G. Centi, F. Cavani and F. Trifiro, "Selective Oxidation by Heterogeneous Catalysis", Kluwer Academic/ Plenum Publishers, New York, 2001.

[17] R. A. Sheldon and J. K. Kochi, "Metal Catalysed Oxidations of Organic Compounds", New York, 1981.

[18] R. G. W. Norrish and G. W. Taylor, Proc. Roy. Soc., A 234 (1956) 160.

[19] V. A. Shtern, "The Gas Phase Oxidation of Hydrocarbons", London, 1964.

[20] J. C. Pope, F. J. Dykstra and E. Graham, J. Am. Chem. Soc., 51 (1929) 2203.

CHAPTER 6
TESTING NiO-MoO_3 CATALYSTS ON *n*-HEXANE

Nickel molybdenum oxide catalysts with different chemical compositions that were synthesized and characterized (**Chapter 4**) were investigated for the oxidative dehydrogenation of *n*-hexane. Previous work on this catalyst system showed promise for the lower hydrocarbons C_2, C_3 and C_4 and to date no work was reported on *n*-hexane. The influence of phase composition of $NiMoO_4$ catalysts on their catalytic activity and selectivity to dehydrogenation products was studied. The optimum phase was then further investigated with changing reaction conditions such contact time variation, fuel/O_2 ratios, nitrogen dilutions. This chapter reflects the catalyst tests performed on *n*-hexane feed with a fixed bed continuous flow reactor with feed/air ratios above and below the flammability limit using air as the oxidant. The optimum phase was then promoted and tested. Finally a plausible reaction pathway was proposed based on the experimental findings.

6.1 Testing above the upper flammability limit (UFL)

6.1.1 The effect of phase composition of NiO-MoO_3 catalysts on *n*-hexane oxidation

The oxidative dehydrogenation of *n*-hexane was investigated with the six catalysts, catalyst A: α-$NiMoO_4$ with excess MoO_3; catalyst B: α-$NiMoO_4$; catalyst C: α-$NiMoO_4$ with β-$NiMoO_4$ and NiO; catalyst D: pure β-$NiMoO_4$; catalyst E: NiO and catalyst F: MoO_3. Products observed for all six catalysts were the carbon oxides (CO and CO_2), isomers of hexene (1-hexene, 2-hexene and 3-hexene), cyclic C_6 products (cyclohexene and benzene), cracked products: alkanes/alkenes (propane/ene, butane/ene) and oxygenates (ethanal, acetic acid and propanoic acid). Considerable amounts of 2,5-dimethyltetrahydrofuran and 2,5-hexanedione were observed for catalysts A and C. As expected for the ODH reaction, water was also produced as a by-product for all reactions and it is also a product of combustion. These products were similar to those obtained in studies involving gas phase and catalytic reactions of *n*-hexane with VMgO catalysts and also in a single gauze reactor [1, 2].

The experiments were performed in the temperature range 300-500 ºC using the fixed bed reactor setup as described in **Chapter 3**.

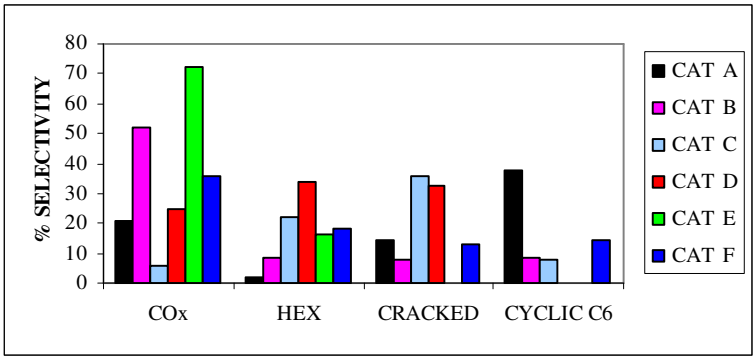

Fig. 6.1: Product distribution at equal conversion levels (13%) below 400 °C for NiO-MoO_3 catalysts.

A comparison of all six catalysts at constant conversion (13%) showed that catalyst D gives the highest selectivity to the hexenes, 32%, of which greater than 50% is due to the 1-hexene isomer. Catalyst E gives the highest selectivity to CO_x, catalyst C the highest total cracked product selectivity, and for the cyclic C_6 products, catalyst A is the best (**Fig. 6.1**).

The selectivity to CO_x is much higher for catalyst B than for catalyst D, and catalyst D is much more selective towards the hexenes than catalyst B. A correlation between CO_x and butenes selectivity was also observed between the two phases, α-$NiMoO_4$ and β-$NiMoO_4$, in propane and *n*-butane oxidation [3, 4]. The difference in hexene selectivity for the two phases may be related to the difference in the reactivity of lattice O^{2-} anions with the hydrocarbon present on the surface of both phases. The different oxygen environments (octahedral versus tetrahedral) on the active catalytic site *i.e.* the metal-oxygen bond strength, is responsible for this, as seen in the shift in frequencies of the Mo-O absorptions band in the IR spectra (**Section 4.3.4,** [3]).

Catalyst A contains the two phases: α-$NiMoO_4$ and MoO_3. Separately these catalysts, catalyst B and catalyst F respectively, showed lower selectivity to cyclic C_6 products and higher selectivity to CO_x. In combination (catalyst A), these two phases favour cyclic C_6 formation and seem to inhibit decomposition to CO_x. If catalyst F produces hexenes which are possible intermediates to benzene, then the formation of benzene and CO_x will take place at different catalytic sites and the purpose of catalyst B will be to selectively block the complete oxidation sites promoting the formation of cyclic compounds. A known synergetic effect, further discussed later, that exists between the two oxide phases is responsible for the better catalytic activity of catalyst C. The MoO_3 can act as an oxygen source for $NiMoO_4$ preventing the irreversible deep reduction of the

pure phase to NiO and MoO_2. Mo^{5+} produced from Mo^{6+} by reduction with hydrocarbons was reported as the active oxidation state for dehydrogenation by metal molybdates. If this species were preserved then better catalytic performance would result [5, 6].

Catalyst C contains the three phases: α-$NiMoO_4$, β-$NiMoO_4$ and NiO. When these phases were tested separately, they showed a high selectivity to the CO_x's and lower or no selectivity to the cracked products and the combination of these phases results in reduced selectivity to the CO_x's and increased selectivity to the cracked products, suggesting inhibition of combustion products. This mixed phase catalyst shows low selectivity to the dehydrogenation products. This suggests no beneficial synergetic effects between the three phases.

The effect of temperature on conversion and selectivity to the various products was investigated for catalysts A-F and the results for three temperatures 300 °C, 350 °C and 400 °C are given in **Table 6.1** for all catalysts.

When expressing the results in terms of hexane conversion and hexene selectivity the β-phase should be better because its active surface area is lower compared to the α-phase (**Table 4.3**, **Section 4.3.2**) and this is what is observed (**Table 6.1**). The increased hexene selectivity for the β-phase is accounted for by the lower CO_x selectivity which is related to the structural oxygen-molydenum co-ordination but it also has a higher reduction rate (the rate at which lattice oxygen is consumed) relative to the α-phase [7]. Consistent with the ODH of other alkanes, lattice oxygen plays a crucial role in the ODH of hexane and is governed by a redox or Mars-van Krevelen mechanism [8]. Based on isothermal reduction data for the β-phase small amounts of oxygen can be removed from the catalyst and restored in less time compared to the α-phase. This gives a better redox cycle than the α-phase and a more effective catalyst [7].

Catalyst A appeared to show the highest activity (47.1% conversion at 400 ºC) as seen in **Table 6.1** and **Fig. 6.2**. This may be attributed to a synergetic effect between the MoO_3 and α-$NiMoO_4$ phases [9]. For the synergetic effect the important condition is that the interface between the two crystalline phases in contact must be coherent [9]. Both catalyst B and F are crystalline phases as inferred by XRD. If the crystallographic lattice misfit is small, the surface energy barriers are lowered and the electrons and oxygen ions cross the interface more easily. In this way a redox co-couple modifies the active redox couple in $NiMoO_4$ and explains why a mixed oxide is better than a single oxide [9]. The higher conversion results in increased selectivity to secondary products

(CO_x and cracked products) characteristic in the oxidation of light alkanes [10]. However, the selectivity to the cyclic C_6 products is high. When MoO_3 is present the irreversible reduction of the $NiMoO_4$ to MoO_4 and Ni is inhibited as discussed above.

Table 6.1: Catalytic results for hexane oxidation over NiO-MoO_3 catalysts at CT = 1.8 s.

	T/ ^{o} C	X (%)	Selectivity				
			CO_x	Hexenes	T-cracked	Cyc C_6	Others
CAT A	300	26.9	24.7	1.5	26.3	20.0	27.5
	350	45.8	37.8	7.8	30.7	15.1	8.6
	400	47.1	43.7	7.9	10.5	22.4	15.5
CAT B	300	4.0	35.7	5.3	29.0	0.0	30.0
	350	9.3	40.6	6.2	23.9	0.0	29.3
	400	13.0	51.1	7.8	7.4	8.6	25.1
CAT C	300	8.3	15.1	15.8	28.5	5.0	35.6
	350	14.5	4.0	22.2	37.9	8.3	27.6
	400	19.1	6.7	20.4	39.3	12.4	21.2
CAT D	300	9.0	24.5	35.3	22.3	0.0	17.9
	350	13.9	28.7	32.8	21.1	2.5	5.8
	400	15.4	38.0	31.6	19.7	4.3	5.5
CAT E	300	4.4	87.9	5.2	0.0	0.0	6.9
	350	14.6	69.1	16.5	0.0	0.0	14.4
	400	22.3	42.8	33.2	0.0	8.4	15.6
CAT F	300	0.0	0.0	0.0	0.0	0.0	0.0
	350	1.5	0.0	26.3	0.0	0.0	73.7
	400	13.1	35.9	17.7	11.7	14.2	20.5

Feed: 31.9% hexane, 14.3% O_2, 53.9% N_2, atmospheric pressure, 1 ml catalyst

Although the pure NiO phase is active it gives the highest selectivity to the carbon oxides at comparable conversions relative to the other catalysts (**Fig. 6.1**). NiO has a high reduction rate and therefore higher production of carbon oxides is expected [7]. However with increasing temperature hexene selectivity increases but this due to mostly the 2- and 3-hexenes. Although this catalyst became discoloured during the testing, coking was less evident as seen from the BET data of the spent catalyst (**Chapter 4**, **Table 4.3**). It is possible that NiO is not completely reduced to metallic nickel at 400 °C so the thermodynamics at increased temperatures favour these products over combustion products.

2,5-Dimethyltetrahydrofuran and 2,5-hexanedione were significantly produced with catalyst A and catalyst C and it can be assumed that the combination of phases was responsible for their formation due to the synergetic effect [9]. For catalyst F the dominant product was methylcyclopentane, ~55%, falls under "others" in **Table 6.1**. The selectivity profiles for all catalysts appear to be different; therefore we can assume that the phase composition of these catalysts is responsible for their behaviour.

According to the mechanism for the selective ODH of alkanes the hydrocarbon is activated by abstraction of an H atom to form an adsorbed alkyl radical and a surface OH group [5]. The oxidation reaction is initiated by highly reactive surface oxygen species. The hydrocarbon adsorption bond strength to the surface is influenced by the metal oxygen bond and hence the product distribution would differ for the catalysts. From all products formed over all the catalysts studied it can be proposed that the ODH process exists because abstraction of a C_2 hydrogen atom from hexane occurs.

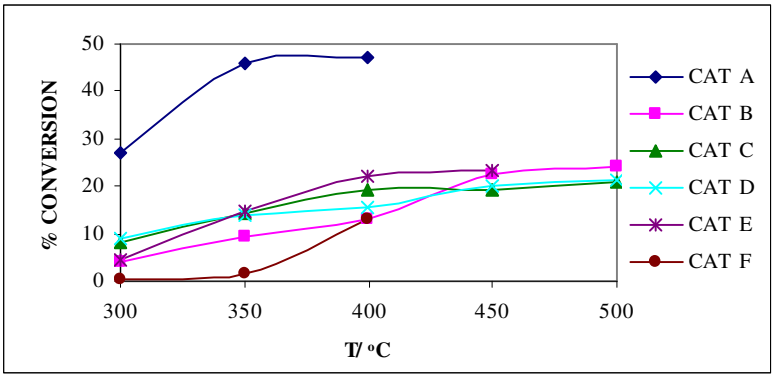

Fig. 6.2: The influence of temperature on n-hexane conversion with NiO-MoO_3 catalysts at CT = 1.8 s.

As was expected, for all six catalysts, conversion increased with temperature then remained constant (**Fig. 6.2**). This can be explained by the reaction being conducted under fuel-rich conditions. The O_2:hydrocarbon ratio requirement for total combustion is 9.5 and only a 0.45 ratio was supplied. Thus at higher temperatures the limiting reactant, oxygen, is exhausted and, because the demand is more rapid, conversion remains constant [1, 11]. All catalysts remained stable up to 500 °C, except catalyst A which deactivated at 400 °C. Deactivation was due to coking which is common for catalysts when no oxygen is available [12]. This was evidenced by the catalysts becoming hard and black. When this occurred the feed no longer passed freely and

there was a build up of back pressure in the reactor. The coke was confirmed with BET (**Chapter 4**, **Table 4.3**), TPO (**Chapter 4**, **Fig. 4.11**) and XPS (**Chapter 4**, **Table 4.4**) analysis of the used catalysts.

The highest selectivity to total hexenes was obtained with catalyst D, namely 35.3% at 300 °C (**Table 6.1, Fig. 6.3**). Of this, 24.8% was due to the 1-hexene isomer, and the remaining 10.5% was due to 2-hexenes and 3-hexenes. Since 1-hexene is favoured at the lowest temperature and the internal isomers are favoured at the higher temperatures one can conclude that increasing the temperature favours isomerization (**Fig. 6.3**). Based on the thermodynamic data [13] the ratio of the internal isomers favoured is in the order *trans*-2-hexene > *cis*-2-hexene > *cis*-3-hexene > 1-hexene. It is therefore possible that an isomerization equilibrium among the three linear isomers is established: which limits the isomers at each temperature.

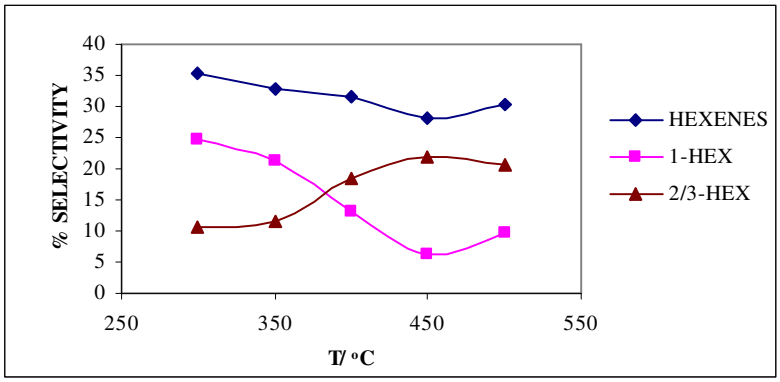

Fig. 6.3: Effect of temperature on the selectivity of hexenes for catalyst D at CT = 1.8 s.

A comparison of carbon oxides selectivity of catalyst D with temperature shows that CO_2 was dominant over CO at all temperatures (**Fig. 6.4**). It is known that CO_2 is produced as a result of heterogeneous combustion [2]. The opposite trends shown by carbon oxides and hexene selectivity with temperature indicate that these products may be produced by competing mechanisms or that hexene is decomposed to carbon oxides. Hence there are two different pathways to CO_x.

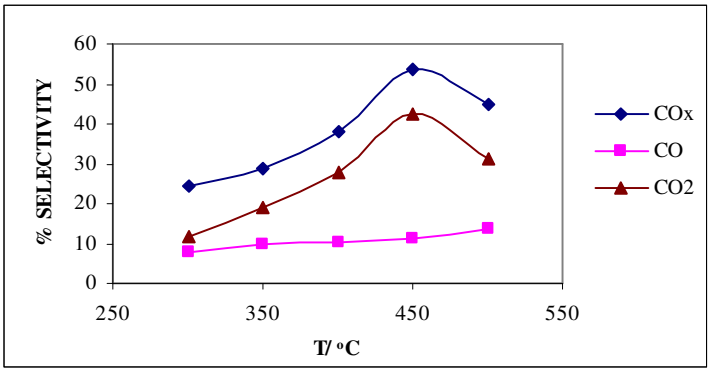

Fig. 6.4: Effect of temperature on CO_x selectivity for catalyst D at CT = 1.8 s.

Cracked oxygenates are favoured over the cracked alkanes/alkenes. Overall, however, the selectivity to the cracked alkanes/alkenes is low. From the oxygenates, ethanal is dominant (**Fig. 6.5**).

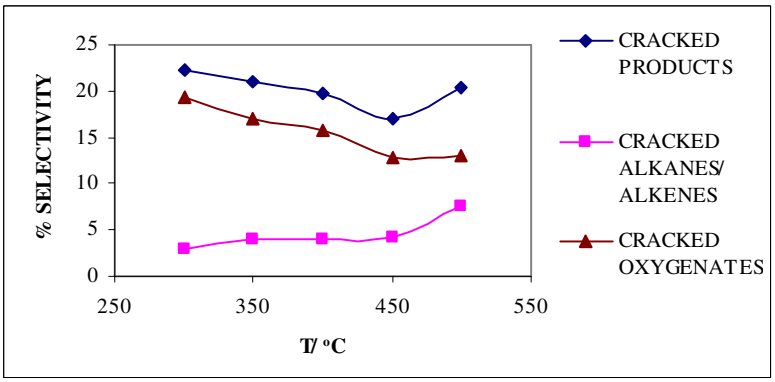

Fig. 6.5: Effect of temperature on the selectivity of cracked products for catalyst D at CT = 1.8 s.

The overall trend for cyclic C_6 products changes with temperature. The selectivity to benzene increases with temperature up to 400 °C, then drops, whilst cyclohexene selectivity decreases with increasing temperature to 400 °C and then increases. This trend indicates that cyclohexene and benzene are competing products (**Fig. 6.6**). The thermal stability of benzene decreases from 400 °C because it is subsequently oxidized to CO_x (**Fig. 6.4**). Cyclohexene selectivity is possibly observed to increase because it is slightly more resistant to further oxidation than benzene.

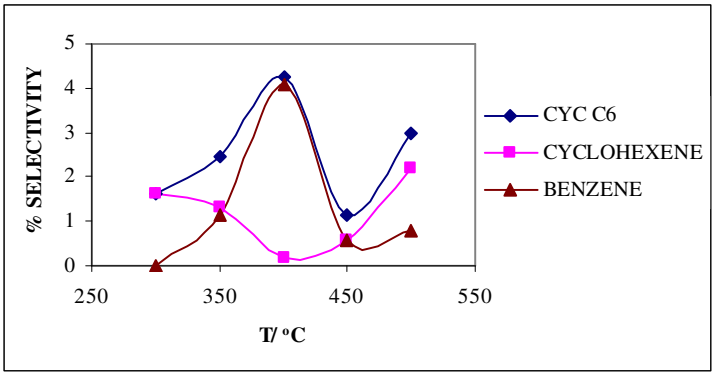

Fig. 6.6: Effect of temperature on the selectivity of cyclic C_6 products for catalyst D at CT = 1.8 s.

Comparison of the $NiMoO_4$ catalysts with different nickel-molybdenum ratios has shown that their chemical composition and structure affects their catalytic activity in the oxidative dehydrogenation of *n*-hexane. Catalyst D showed that the pure β-$NiMoO_4$ phase, at a contact time of 1.8 s, gave a total hexene selectivity of 35.3% at 300 °C and a 1-hexene selectivity of 24.8%.

It was clear from the comparison of the different phases of the nickel molybdate catalysts that the two different modifications of $NiMoO_4$, which differ in the molybdenum coordination, show different activity and selectivity. The pure β-phase appears to be more active and significantly more selective toward the hexenes than the α-phase. However, the α-phase with MoO_3 was more active than both the pure phases. This suggests that the synergetic effect plays an important role in modifying catalytic activity and the β-$NiMoO_4$ form is significantly more selective to hexenes than the α-phase.

Based on results from the effects of $NiMoO_4$ catalysts on *n*-hexane oxidation, β-$NiMoO_4$ shows good potential for high value hexenes. Hence further investigations were focused on testing the β-$NiMoO_4$ phase to optimize selectivity to hexenes. To improve selectivity to dehydrogenation products, reaction conditions were optimized and the following parameters were investigated: the effect of contact time over β-$NiMoO_4$, the effect of *n*-hexane dilution with nitrogen over β-$NiMoO_4$ and the effect of the fuel/air ratio over β-$NiMoO_4$.

Since alkanes are far less active when compared to the desired products (e.g. alkenes and aldehydes), the conditions under which paraffin activation can occur is important. One of the main challenges in paraffin oxidation is to carefully control the temperature and oxygen content

so that it is adequate to convert alkanes to desired products but not lead to complete combustion of these products.

The flammability range for hexane in air is 1.7- 7.7 v/v % at room temperature and the range widens with temperature and pressure [14]. All the experiments mentioned were done above the upper flammability range since high fuel/air ratios result in an oxygen deficient environment which reduces the possible over-oxidation of alkanes.

6.1.2 The effect of contact time on β-$NiMoO_4$ above the UFL

Experimental data are shown in **Fig. 6.7** for β-$NiMoO_4$ tested above the upper flammability limit using *n*-C_6H_{14}/O_2 = 2.2 at 300°C. The contact time was varied by changing the flow rate of feed while keeping the volume (1 ml) of catalyst constant. The range of contact times tested was 0.61-2.4 s.

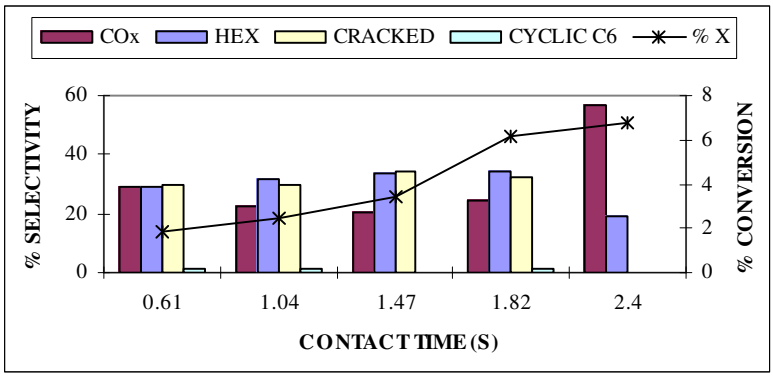

Fig. 6.7: Effect of contact time on n-hexane conversion and selectivity to products (fuel/O_2 ratio 2.2, T = 300 °C).

As expected, the amount of *n*-hexane converted increases with increasing contact time due to increasing residence time of the feed over the surface of the catalyst (**Fig. 6.7**). The maximum conversion is 6.8%. The selective oxidation of hydrocarbons over $NiMoO_4$ catalysts involves the dynamic interaction of the gas-phase with the surface of the catalyst (redox mechanism of Mars-van Krevelen) [15, 16]. Under fuel-rich conditions the gas phase has a low oxidizing potential and will influence the oxidation state of the active species of the catalyst. A less oxidized catalytic surface is expected to give less active catalysts when operating above the UFL [15]. This may explain why β-$NiMoO_4$ shows low activity.

Very little or no selectivity to the cyclic C_6 products (< 1.5%) was observed at all contact times. It is possible that these products are not thermodynamically favoured at this low temperature.

The selectivity to hexenes increases with increasing contact time until 1.82 seconds and then decreases. The drop in hexene selectivity at contact time 2.4 seconds can be accounted for by the rapid increase in carbon oxides produced, since a longer residence time of hexenes on the catalyst surface would favour consecutive oxidation, hence over oxidation. The highest selectivity to total hexenes is 34.4%.

At the longest contact time (2.4 seconds) carbon oxides are the dominant products. At the shortest contact time (0.61 seconds) there are almost equal selectivities to both the cracked and carbon oxide products suggesting that the reaction time is too short for the cracked products to totally oxidise to carbon oxides. The trend for the selectivity to total decomposition products appears to be the inverse to the selectivity to hexenes. It is suspected that the amount and type of decomposition product formed depends on the stability of the hexenes at the different contact times.

Tables 6.2- 6.6 shows selectivity, yield and conversion values for the β-$NiMoO_4$ catalyst above the UFL for different contact times.

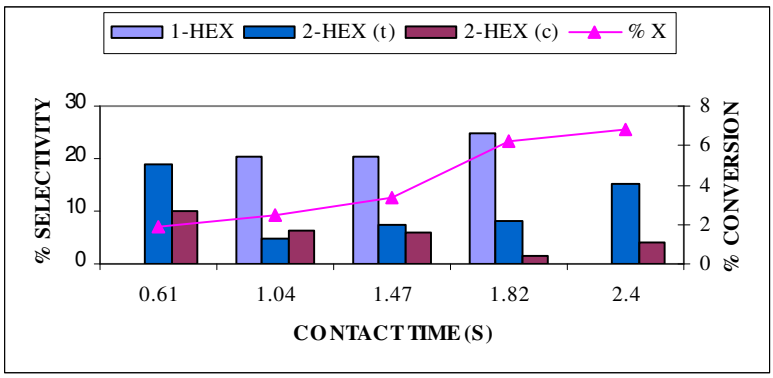

Fig. 6.8: Effect of contact time on hexene selectivity (fuel/O_2 ratio 2.2, T = 300 °C).

1-hexene is only formed at the intermediate contact times between 1.04 and 1.82 seconds (**Fig. 6.8**). The highest selectivity to 1-hexene is 24.8% at the longer contact time. Usually 2-hexene is preferred over 1-hexene because the rate of hydrogen abstraction from a 2° carbon is twice as fast as from a 1° carbon, but in paraffin ODH the activation and rate determining step is the irreversible abstraction of hydrogen from a secondary carbon to give an adsorbed alkyl radical.

The removal of another hydrogen from either carbon one or three results in olefin formation. At this contact time it is possible that 1-hexene forms over the catalyst and is stabilised under these conditions and does not undergo isomerization to the 2-hexenes on the catalyst. No selectivity to 1-hexene is observed at a contact time 0.61 seconds since the residence time of the feed in the reactor is too short. Since the operation is above the UFL, the surface of the catalyst is saturated with adsorbed species [15] and there is a possibility that intermediate olefinic species, probably 1-hexene that has been desorbed into the gas phase, transform to the 2-hexene isomers. At a contact time of 2.4 s the 1-hexene has possibly isomerized.

6.1.3 The effect of nitrogen dilution

A diluent such as nitrogen is reported to have a 'simple' or inert diluent effect on catalytic cracking [17]. This diluent lowers the concentration of reactant in the gas phase, hence there is a lower population of carbenium ions on the surface of the catalyst and lower gas-phase concentrations of reactants. As a result both initiation and propagation reactions are slowed down. This effect may change the conversion and selectivity of products obtained from *n*-hexane oxidation since this system probably endures some free radical initiation on the catalyst surface and propagation due to the reaction mixture being in the gas-phase [17]. Dilution of the feed with nitrogen also promotes thermal quenching and suppresses the rate of gas-phase reactions [2].

From the contact time study, a contact time of 1.82 seconds gave the highest selectivity to total hexenes (*i.e.* 34.4% of which 24.8% was due to 1-hexene and 9.5% was due to the 2-hexenes at a 6.2% conversion. When this feed was diluted with 43% nitrogen only a slight improvement in hexene selectivity was obtained. However, when the catalyst was tested at a contact time of 1.04 seconds, the dilution with 43% nitrogen showed great improvement compared to the undiluted feed. Hence, using the same n-C_6H_{14}/O_2 ratio of 2.2 at 300 °C and a contact time of 1.0 seconds, the feed was diluted with nitrogen using dilutions between 31 and 60% (diluted portion of feed). **Fig. 6.9** compares the results from these nitrogen dilution experiments. There was a small improvement in conversion ~ 1.5% when the undiluted (0%) and diluted (31%) feed was compared. Carbon oxide selectivity was reduced from 52.6% to 21.7% and hexene selectivity improved from 32.0% to 49.9%. Nitrogen dilution, however, also caused cracked product formation up to dilutions of 43%.

Table 6.2: The effect of temperature on conversion, selectivity and yield of products for the ODH of n-hexane over β-$NiMoO_4$ above the UFL for a CT of 0.61 s.

		% SELECTIVITY					% YIELD				
T/ °C	**% X**	**CRACKED ALKANES**	**CRACKED OXYGENATES**	**HEXENES**	**CYCLIC C_6**	**CO_x**	**CRACKED ALKANES**	**CRACKED OXYGENATES**	**HEXENES**	**CYCLIC C_6**	**CO_x**
300	1.9	29.9	0.0	28.9	1.2	28.8	0.6	0.0	0.5	0.0	1.5
350	4.5	19.9	2.2	23.6	2.9	29.9	0.9	0.1	1.1	0.0	1.5
400	10.6	11.8	2.3	20.4	10.9	35.4	1.3	0.2	2.2	0.0	3.6
450	13.7	7.6	4.8	20.1	2.7	43.6	1.1	0.7	2.8	0.2	9.8
500	15.9	6.9	4.6	19.3	5.3	46.7	1.2	0.8	3.3	0.5	8.1

Table 6.3: The effect of temperature on conversion, selectivity and yield of products for the ODH of n-hexane over β-$NiMoO_4$ above the UFL for a CT of 1.04 s.

		% SELECTIVITY					% YIELD				
T/ °C	**% X**	**CRACKED ALKANES**	**CRACKED OXYGENATES**	**HEXENES**	**CYCLIC C_6**	**CO_x**	**CRACKED ALKANES**	**CRACKED OXYGENATES**	**HEXENES**	**CYCLIC C_6**	**CO_x**
300	2.5	0.0	0.0	32.0	1.0	52.2	0.0	0.0	0.8	0.0	1.4
350	6.5	0.0	0.0	32.5	0.5	62.7	0.0	0.0	1.5	0.0	4.0
400	8.0	0.0	0.0	33.6	0.7	67.4	0.0	0.0	2.7	0.1	5.4
450	11.6	0.0	0.0	31.0	19.8	32.2	0.0	0.0	3.6	2.3	3.7
500	25.6	48.2	2.6	16.9	4.0	24.8	12.3	0.7	4.3	1.0	6.3

Table 6.4: The effect of temperature on conversion, selectivity and yield of products for the ODH of n-hexane over β-$NiMoO_4$ above the UFL for a CT of 1.47 s.

		% SELECTIVITY					% YIELD				
T/ °C	**% X**	**CRACKED ALKANES**	**CRACKED OXYGENATES**	**HEXENES**	**CYCLIC C_6**	**CO_x**	**CRACKED ALKANES**	**CRACKED OXYGENATES**	**HEXENES**	**CYCLIC C_6**	**CO_x**
300	3.4	13.5	20.8	33.9	0.0	20.6	0.5	0.7	1.2	0.0	0.7
350	5.2	10.6	18.0	29.8	3.1	29.3	0.6	0.9	1.6	0.2	1.5
400	16.8	11.5	9.1	27.1	3.2	34.0	1.9	1.5	4.6	0.5	5.7
450	20.4	20.7	5.6	15.8	3.9	45.1	4.2	1.2	3.2	0.8	9.2

Table 6.5: The effect of temperature on conversion, selectivity and yield of products for the ODH of n-hexane over β-$NiMoO_4$ above the UFL for a CT of 1.82 s.

		% SELECTIVITY					% YIELD				
T/ °C	**% X**	**CRACKED ALKANES**	**CRACKED OXYGENATES**	**HEXENES**	**CYCLIC C_6**	**CO_x**	**CRACKED ALKANES**	**CRACKED OXYGENATES**	**HEXENES**	**CYCLIC C_6**	**CO_x**
300	9.0	2.9	19.4	35.3	0.0	24.5	0.3	1.8	3.2	0.0	2.2
350	13.9	4.0	17.1	32.8	2.5	28.7	0.6	2.4	4.6	0.4	4.0
400	15.4	4.0	15.7	31.6	4.3	38.0	0.6	2.4	4.9	0.7	5.9
450	19.9	4.2	12.8	28.1	1.2	53.6	0.8	2.5	5.6	0.2	10.7
500	21.4	7.5	12.9	20.4	3.0	54.7	1.6	2.8	6.5	0.6	9.6

Table 6.6: The effect of temperature on conversion, selectivity and yield of products for the ODH of n-hexane over β-$NiMoO_4$ above the UFL for a CT of 2.40 s.

T/ °C	% X	% SELECTIVITY					% YIELD				
		CRACKED ALKANES	**CRACKED OXYGENATES**	**HEXENES**	**CYCLIC C_6**	**CO_x**	**CRACKED ALKANES**	**CRACKED OXYGENATES**	**HEXENES**	**CYCLIC C_6**	**CO_x**
300	6.8	0.0	0.0	19.3	0.0	56.9	0.0	0.0	1.3	0.0	3.9
350	7.8	0.0	0.0	19.7	0.1	60.0	0.0	0.0	1.5	0.0	4.7
400	12.3	0.0	0.0	9.1	0.5	74.5	0.0	0.0	1.1	0.1	9.1
450	32.8	0.0	0.4	5.7	13.5	60.2	0.0	0.1	1.9	4.4	19.7
500	37.5	16.0	0.0	5.3	3.0	58.0	6.0	0.0	3.9	1.1	2.2

Conversion increased with increasing nitrogen dilution up to 43% then dropped and this trend was observed previously. Dilution of the feed with too much nitrogen uses more energy for heating up the nitrogen molecules than overcoming thermodynamic barriers [2]. The maximum conversion at this dilution (**Fig. 6.9**) was 7.1%. Hexene selectivity also improved with nitrogen dilution up to 43% and then dropped. The highest selectivity to hexenes was 54.7%. The drop in hexene selectivity was matched by the concurrent increase in carbon oxide selectivity. These results suggest that nitrogen dilution much beyond 43% is not advantageous, possibly due to there being too few reactant molecules in the gas phase and the probability of reaching an active site is correspondingly small, causing a drop in activity. Since there are no competing reactants, there is a greater chance of adsorbed molecules undergoing further oxidation. With increasing nitrogen dilution beyond 43% there is a reduction in cracked products and a corresponding increase in carbon oxide production.

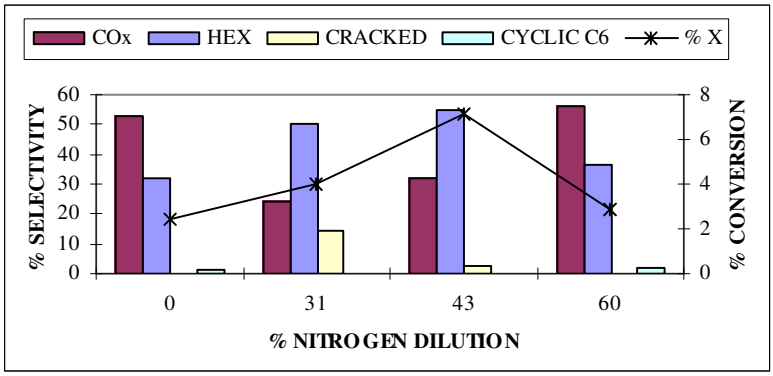

Fig. 6.9: Effect of nitrogen dilution on n-hexane conversion and selectivity of products (fuel/O_2 ratio 2.2, T = 300 °C).

Looking at the separate hexene isomers (**Fig. 6.10**), there was an increase in the selectivity of the *trans*-2-hexene isomer with increasing dilution. The difference in selectivity to *trans*-2-hexene between the undiluted and 60% diluted feed was 22%. 1-hexene also improved in selectivity but only up to 43% dilution and then disappeared completely. This was probably due to isomerization to the internal isomers (2-hexene) at the highest dilution and consecutive decomposition. The highest selectivity to 1-hexene was 27.4%. *Cis*-2-hexene selectivity showed a less regular trend. Very little 3-hexene was produced which co-eluted with *trans*-2-hexene. The ratio between the two isomers was ~ 3:1.

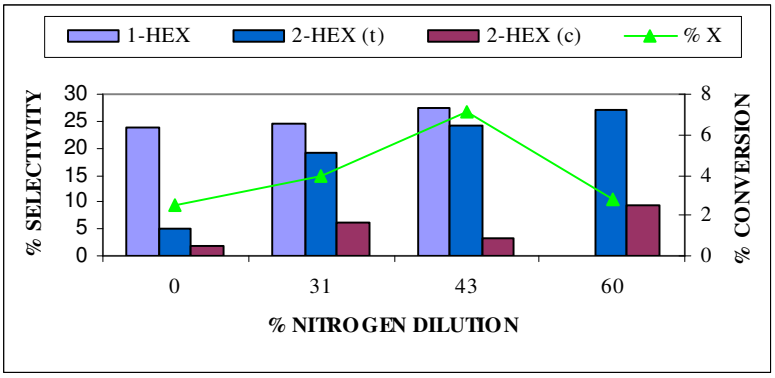

Fig. 6.10: Effect of nitrogen dilution on hexene selectivity (fuel/ O_2 ratio 2.2, T = 300 °C).

With increasing temperature, the overall selectivity to hexenes decreases and 1-hexene decreases relative to the 2-hexenes which further suggest an isomerization pathway for these isomers.

6.1.3.1 Comparison of the α- and β-$NiMoO_4$ catalysts after nitrogen dilution

From the data obtained from dilution experiments conducted on β-$NiMoO_4$, the best conditions to obtain good selectivity to hexenes were a fuel/O_2 ratio of 2.2, a contact time of 1.04 s and dilution with 43% nitrogen operating above the UFL. The other polymorph was then tested under these conditions and **Fig. 6.11** shows a comparison of the α- and β-phases of nickel molybdate at equal conversions. Catalyst B (α-$NiMoO_4$) gives the higher selectivity to carbon oxides and catalyst D (β-$NiMoO_4$) gives the higher selectivity to hexenes. This observation was also made when the two catalysts were compared under different conditions (without dilution) mentioned earlier in **Section 6.1.1**.

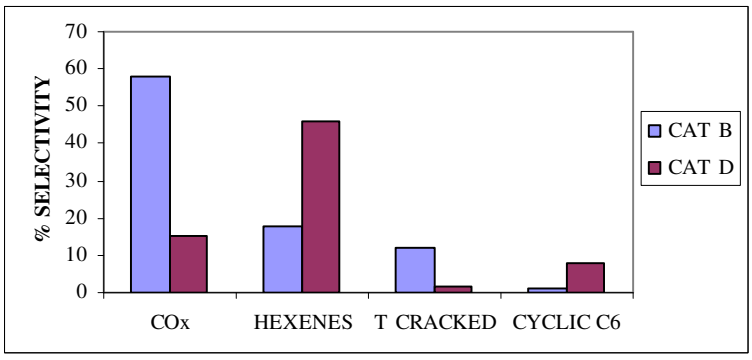

Fig. 6.11: Comparison of α- and β-$NiMoO_4$ catalysts at equal conversion levels (25%) at 385 °C, CT 1.04 s and 43% nitrogen dilution.

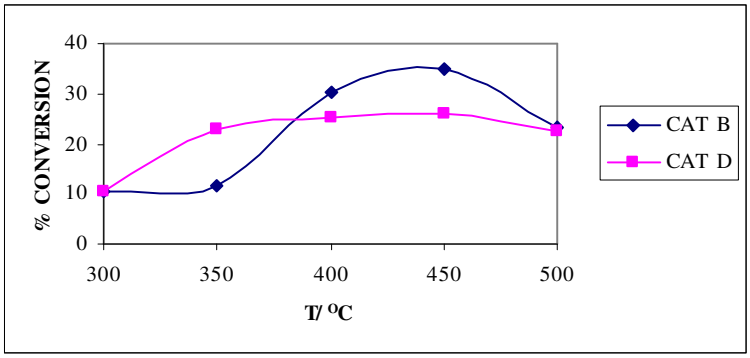

Fig. 6.12: Effect of temperature on conversion for α- and β-$NiMoO_4$ catalysts at CT 1.04 s, 43% nitrogen dilution.

Comparison of the conversion profiles (**Fig. 6.12**) for both catalysts indicate that above 385 °C, catalyst B is more active than catalyst D. These results may suggest that, although it was earlier found that a difference in molybdenum co-ordination was responsible for differences in the catalysts activity, temperature also plays an important role. At T = 500 °C the activity catalyst B is more or less equivalent to catalyst D because the activity of catalyst B has decreased. This is possibly due to the coking of α-$NiMoO_4$.

6.1.4 The effect of fuel/O_2 ratio on β-$NiMoO_4$

Selective oxidation of hydrocarbons depends on the availability of oxygen species on the surface of the catalyst. These are either oxide ions (O^{2-}) or oxygen atoms doubly bonded to the metal atoms/ ions. Since gaseous oxygen supplied to a catalytic system affects the oxidizing potential of the catalyst, the effect of fuel/O_2 ratio for *n*-hexane oxidation over β-$NiMoO_4$ was investigated. Using the conditions that gave best selectivity to hexenes from the contact time and nitrogen dilution experiments *i.e.* contact time 1.0 seconds, nitrogen dilution of 43% and temperature 300 °C, the fuel/O_2 ratio was varied. Fuel/O_2 ratios of 0.76, 2.22 and 6.25 *n*-C_6H_{14}/O_2 were investigated (**Fig. 6.13**).

At a fuel/O_2 ratio of 6.3 no conversion occurred. As this ratio was reduced an increase in conversion was observed as expected due to increased oxygen availability. The best conversion was achieved at the lowest fuel/O_2 ratio (0.8). As expected, the feed with the lowest fuel/O_2 ratio is more oxidizing and would be more active but less selective.

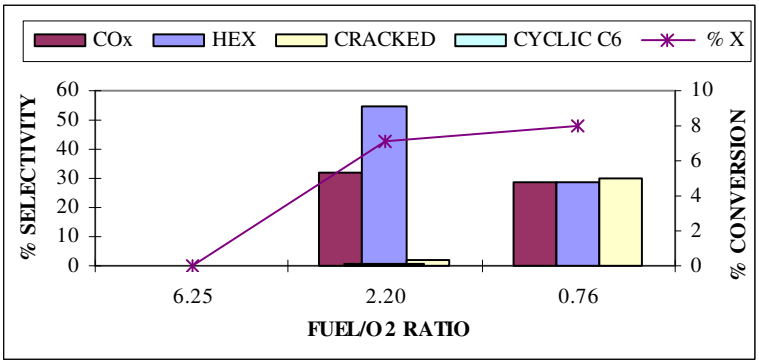

Fig. 6.13: Effect of fuel/O_2 ratio on n-hexane conversion and selectivity to products at 300 ℃, CT 1.04 s and 43% nitrogen dilution.

There was a decrease in selectivity to the hexenes from 54.7% to 28.9% when the supply of oxygen relative to the fuel was increased, *i.e.* ratios from 2.2 to 0.8 (**Fig. 6.13**). CO_x selectivity was similar for both a fuel/O_2 ratio of 2.2 and 0.8 and the cracked product selectivity was significantly higher for a fuel/O_2 ratio of 0.8 than a fuel/O_2 ratio of 2.2. Changing the paraffin/oxidant ratio would result in a restructuring of the catalyst surface [18] and different products selectivity may be expected.

6.1.5 Comparison of the commercially obtained $NiMoO_4$ with the synthesized β-$NiMoO_4$ catalysts at CT 1.8 s

Since $NiMoO_4$ can be obtained commercially, it was decided to compare the synthesized catalyst to the commercially obtained $NiMoO_4$. Thus the commonly obtained molybdate was calcined and thermally activated to form the β-phase using the same procedure as that of the synthesized catalyst (catalyst D). A 31.8% hexane/air feed and a contact time of 1.8 seconds was used. **Fig. 6.14** compares the conversion with temperature for both catalysts. Below 400 °C the commercial catalyst (catalyst G) has low activity, thereafter conversion reaches 25% but the catalysts cokes. The synthesized catalyst shows much higher activity and was stable up to 500 °C.

Comparison of the product selectivity for the two catalysts at equal conversion at 438 °C showed that the commercial catalyst had higher cracked product selectivity, lower carbon oxide selectivity, lower hexene selectivity and higher cyclic C_6 product selectivity than the synthesized catalyst (**Fig. 6.15**). The difference in performance may be due to different methods of preparation of the nickel molybdate catalysts, which affects the catalytic performance.

The difference in catalytic behaviour observed for the two catalysts was reflected in the characterization results such as the TPR profiles (**Chapter 4**, **Section 4.3.8**). The BET surface area for the two catalyst precursors also differed. The precursor to catalyst D had a surface area of 35.3 m^2/ g and for the precursor to catalyst G it was 30.0 m^2/ g. Since catalyst surface area is related to activity this may contribute to the poorer activity of the catalyst derived from the commercially obtained molybdate. Also, although the XRD's of the synthesized (**Chapter 4, Section 3.4.5**) and commercial molybdates (refer to the **Appendix**) are similar, there are small differences in the shifts and relative intensities of the relevant peaks characteristic of the β-phase for both these catalysts.

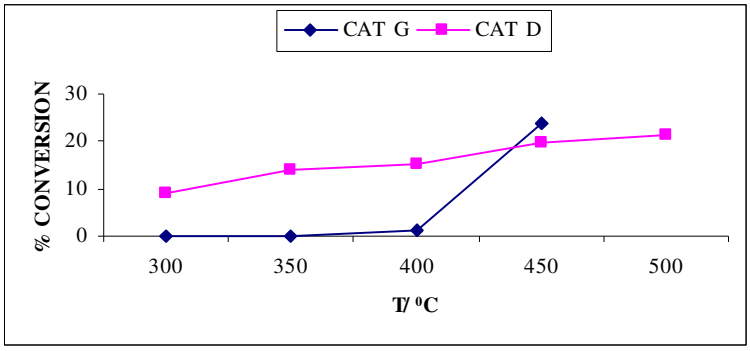

Fig. 6.14: Comparison of n-hexane conversion with temperature for the β-phase of the commercial catalyst and synthesized catalyst at CT 1.8 s and a fuel/O_2 ratio of 2.2.

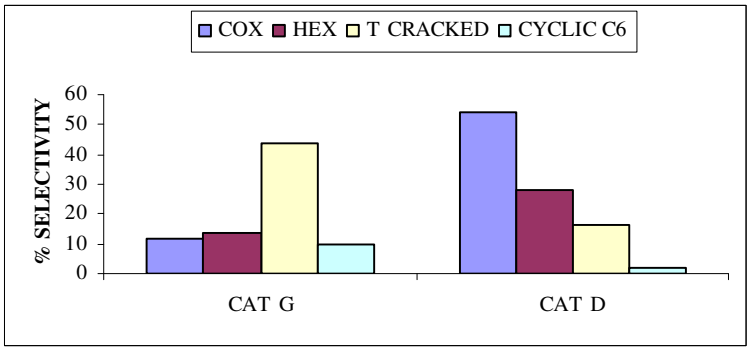

Fig. 6.15: Comparison of selectivity for the activated β-phase commercial catalyst and the synthesized catalyst at equal conversion (19%) at 438 °C, CT 1.8 s and a fuel/O_2 ratio of 2.2.

6.2 Testing below the lower flammability limit (LFL)

Most catalytic testing was done above the upper flammability limit (UFL), because the over-oxidation of products can be reduced by restricting the availability of oxygen. To confirm the

validity of the assumption experiments below the LFL to determine what happens in an oxygen rich environment were conducted. For these tests a *n*-C_6H_{14}/O_2 ratio of 0.02 was chosen.

6.2.1 Effect of contact time on β-$NiMoO_4$ below the LFL

To investigate the effect of contact time on the β-$NiMoO_4$ catalyst below the LFL, the flow rate of the feed (33, 49, 66 and 150 ml/min) was changed and the volume of catalyst was kept constant. This gave contact times of 1.8, 1.2, 0.9 and 0.4 seconds.

The products observed were the carbon oxides (carbon monoxide and carbon dioxide), the cyclic C_6 products (cyclohexane, cyclohexene and benzene), cracked products (propa/ene and buta/ene) and the hexenes (2- and 3-hexenes). No 1-hexene was found under these conditions.

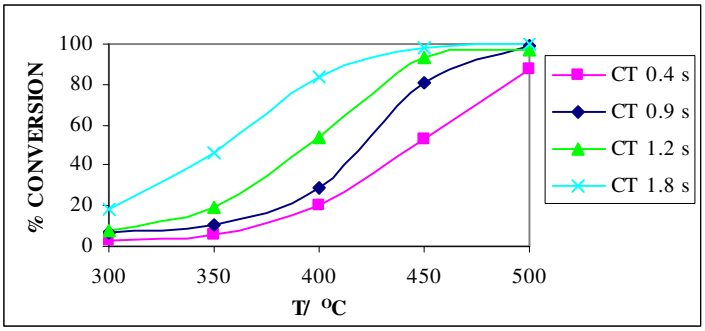

Fig. 6.16: The influence of temperature on n-hexane conversion for β-$NiMoO_4$ catalysts tested at different contact times below the LFL (n-C_6H_{14}/O_2 ratio of 0.02).

The data obtained for the effect of temperature on conversion for β-$NiMoO_4$ at different contact times below the LFL (**Fig. 6.16**) showed a similar trend to those obtained above the UFL, which was an increase in conversion with temperature and then stabilization. An increase in conversion with increased contact time was also observed at all temperatures. Very high conversions are observed below the LFL. In fact at the longest contact time (CT 1.8 s) 100% conversion was achieved at 500ºC.

Tables 6.7- 6.10 show the full data for the results obtained below the LFL in terms of product selectivity and yields at different contact times for β-$NiMoO_4$. These also reflect the high yields obtained for CO_x (due to high conversions and selectivities) at the highest temperatures.

Table 6.7: The effect of temperature on conversion, selectivity and yield of products for the ODH of n-hexane over β-$NiMoO_4$ below the LFL for a CT of 0.40 s.

		% SELECTIVITY					% YIELD				
T/ °C	**% X**	**CRACKED ALKANES**	**CRACKED OXYGENATES**	**HEXENES**	**CYCLIC C_6**	**CO_x**	**CRACKED ALKANES**	**CRACKED OXYGENATES**	**HEXENES**	**CYCLIC C_6**	**CO_x**
300	3.0	0.2	0.0	68.6	10.2	0.0	0.0	0.7	2.7	0.4	0.0
350	5.3	2.8	0.0	68.0	10.4	0.0	0.0	1.3	3.7	0.6	0.0
400	20.2	3.0	0.0	11.7	5.2	63.8	0.0	2.6	2.4	1.0	8.6
450	53.0	3.4	0.0	3.1	2.9	67.4	0.0	7.9	1.7	1.5	22.2
500	87.6	3.8	0.0	0.5	1.9	69.3	0.0	21.1	0.5	1.9	40.1

Table 6.8: The effect of temperature on conversion, selectivity and yield of products for the ODH of n-hexane over β-$NiMoO_4$ below the LFL for a CT of 0.91 s.

		% SELECTIVITY					% YIELD				
T/ °C	**% X**	**CRACKED ALKANES**	**CRACKED OXYGENATES**	**HEXENES**	**CYCLIC C_6**	**CO_x**	**CRACKED ALKANES**	**CRACKED OXYGENATES**	**HEXENES**	**CYCLIC C_6**	**CO_x**
300	6.6	0.0	5.5	68.0	12.4	0.0	0.0	0.3	3.6	0.7	0.0
350	10.2	0.6	0.0	28.0	6.0	57.7	0.0	0.0	0.0	0.0	5.2
400	28.7	1.2	0.3	12.2	3.0	81.3	0.0	0.1	3.4	0.0	22.5
450	81.2	3.0	5.2	3.3	2.1	79.4	0.6	3.8	2.6	1.9	57.0
500	99.4	3.3	4.7	0.0	2.4	84.9	0.2	5.6	0.2	2.5	84.9

Table 6.9: The effect of temperature on conversion, selectivity and yield of products for the ODH of n-hexane over β-$NiMoO_4$ below the LFL for a CT of 1.2 s.

		% SELECTIVITY					% YIELD				
T/ °C	**% X**	**CRACKED ALKANES**	**CRACKED OXYGENATES**	**HEXENES**	**CYCLIC C_6**	**CO_x**	**CRACKED ALKANES**	**CRACKED OXYGENATES**	**HEXENES**	**CYCLIC C_6**	**CO_x**
300	18.1	1.9	24.3	2.1	3.1	67.1	0.3	4.4	0.4	0.6	12.1
350	46.0	5.7	13.1	0.0	5.9	74.6	2.6	6.0	0.0	2.7	34.3
400	83.8	2.6	0.0	0.0	2.3	95.9	2.2	0.0	0.0	1.9	80.4
450	97.7	1.8	0.0	0.0	0.0	95.3	1.7	0.0	0.0	0.0	93.1
500	99.9	0.8	0.0	0.0	0.0	98.3	0.8	0.0	0.0	0.0	98.3

Table 6.10: The effect of temperature on conversion, selectivity and yield of products for the ODH of n-hexane over β-$NiMoO_4$ below the LFL for a CT of 1.8 s.

		% SELECTIVITY					% YIELD				
T/ °C	**% X**	**CRACKED ALKANES**	**CRACKED OXYGENATES**	**HEXENES**	**CYCLIC C_6**	**CO_x**	**CRACKED ALKANES**	**CRACKED OXYGENATES**	**HEXENES**	**CYCLIC C_6**	**CO_x**
300	8.0	5.6	35.8	16.6	16.9	0.0	0.4	2.9	1.3	1.7	0.0
350	19.4	29.4	16.4	11.0	14.4	18.0	5.7	3.2	1.3	2.8	3.5
400	53.5	46.6	0.0	0.6	3.3	40.8	25.0	0.0	0.3	1.8	21.9
450	93.6	49.4	0.0	0.0	1.9	47.5	46.2	0.0	0.0	1.8	44.5
500	97.6	45.8	0.0	0.0	0.9	51.8	44.7	0.0	0.0	0.8	50.6

A comparison of the effect of contact time on conversion and selectivity for β-$NiMoO_4$ at 300 °C (**Fig. 6.17**) clearly shows the increase in conversion with increasing contact time, due to the increased residence time of the feed. At this temperature the highest conversion is 18.1%.

Regarding the selectivity to the various products, hexenes selectivity decreases with increasing contact time. The highest selectivity to the hexenes is 68.6%. No 1-hexene is observed as previously mentioned. Cracked product formation increases up to a contact time of 1.22 seconds then drops due to carbon oxide formation. A long contact time is thus required for complete combustion to occur. The cyclic C_6 product selectivity initially increases with increased contact time but also drops after a contact time of 1.22 seconds due, possibly, to decomposition.

At this low fuel/O_2 ratio, the number of adsorbed species on the surface of the catalyst is low, chances of the adsorbed intermediates desorbing into the gas phase are low [18] and fewer products should be observed if the contact time is short and this is as observed here. Also, the temperature is low enough to not allow other products to form thermodynamically.

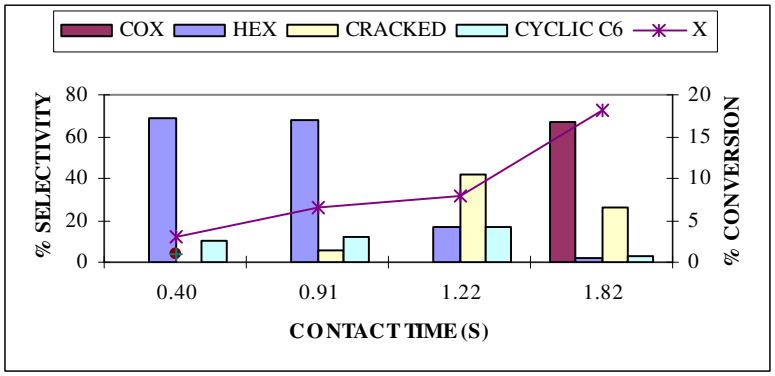

Fig. 6.17: Effect of contact time on conversion and selectivity with β-$NiMoO_4$ for n-C_6H_{14}/O_2 = 0.02, T = 300 °C.

6.2.2 Comparison between the α- and β-$NiMoO_4$ catalysts below the lower flammability limit

The two phases of $NiMoO_4$ (α- and β-) were compared below the LFL as was done above the UFL. In terms of conversion, catalyst D was slightly more active than catalyst B only above 400ºC (**Fig. 6.18**). These results showed an opposite trend to what was observed above the UFL

(**Fig. 6.2** and **Fig. 6.12**). This suggests that operating conditions for the catalyst may affect the activity of the different forms of nickel molybdate. Both catalysts showed very high conversions. At temperatures above 400ºC over 83% conversion is observed for both catalysts.

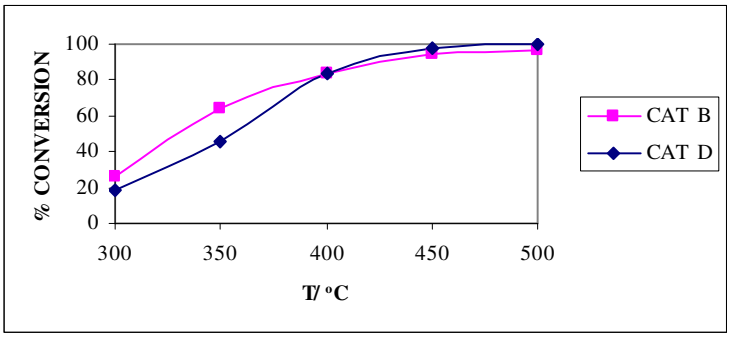

Fig. 6.18: The influence of temperature on n-hexane conversion for catalyst B and catalyst D below the LFL at CT 1.8 s.

In terms of product selectivity (**Fig. 6.19**), catalyst D showed a greater selectivity to CO_x but lower selectivity to the cracked products than catalyst B at comparable conversion. At this high conversion (83%) no hexene is observed, reflecting its instability at elevated temperatures. Thermodynamically, cyclic C_6 products are favoured and are more stable at 400 °C than the 2- and 3-hexene isomers.

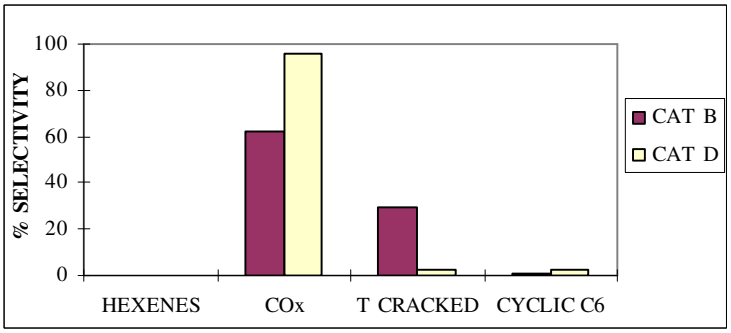

Fig. 6.19: Product distribution at equal conversion levels (83%) at 400 °C for catalyst B and catalyst D.

6.3 Comparison of β-$NiMoO_4$ above the UFL and below the LFL

Here the catalytic results reported for β-$NiMoO_4$ below the lower flammability limit (LFL) are compared to the results of an experiment above the UFL under the same conditions to determine whether operation above and below the flammability range affects the catalytic results.

Comparison of conversion for β-$NiMoO_4$ above the UFL (31.79% hexane/air) and below the LFL (0.52% hexane/air) at the same contact time (**Figs. 6.20-6.23**) showed that the catalysts had different activity under these conditions at all temperatures. Below the LFL the feed is much more oxidizing and, since the catalyst surface is in dynamic equilibrium with the gas phase (*i.e.* operating with the Mars -van Krevelen mechanism) [15, 18], much higher activity is expected and observed.

Comparing CO_x selectivity (**Fig. 6.20**) for β-$NiMoO_4$ above the UFL and below the LFL at all temperatures, total oxidation is favoured below the LFL as expected due to high oxygen availability. Except at 300ºC, higher cracked product selectivity (**Fig. 6.21**) is obtained above the UFL than below the LFL. Thus one may assume that operating the catalyst above and below the flammability limit results in two different pathways of decomposition, one in which a cracking mechanisms dominates, while the other favours a combustion mechanism. Operating below the LFL, catalytic sites are accessible and adsorbed species do not readily desorb into the gas phase, so over-oxidation of intermediate products is high. However, above the UFL cracking is more likely to occur due to the surface of the catalyst being over saturated with adsorbed intermediates.

Hexene production is highly favoured above the UFL at this contact time of 1.8 s and is produced at all temperatures, unlike below the LFL, where hexene production is only favoured at 300 °C (**Fig. 6.22**) and with no 1-hexene found.

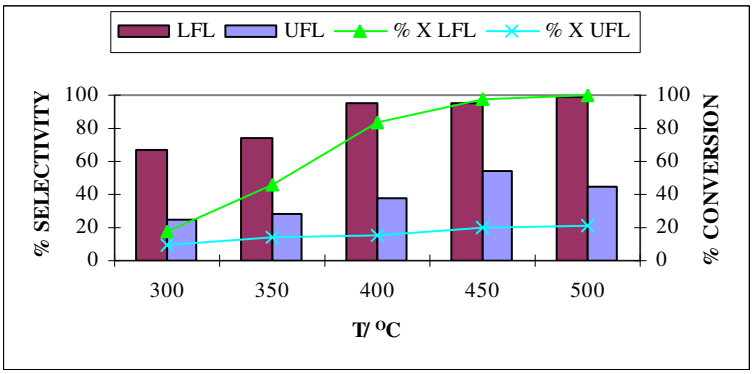

Fig. 6.20: Comparison of CO_x selectivity with temperature over β-$NiMoO_4$ above the UFL and below the LFL at CT 1.8 s.

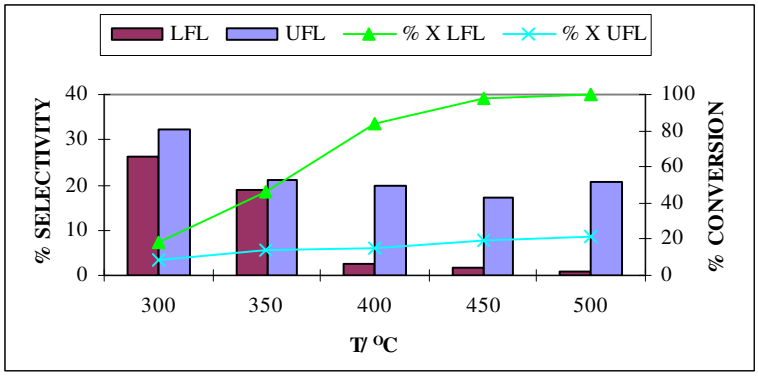

Fig. 6.21: Comparison of cracked product selectivity with temperature for β-$NiMoO_4$ above the UFL and below the LFL at CT 1.8 s.

Under these conditions, benzene is the only cyclic C_6 product produced below the LFL (**Fig. 6.23**). Its selectivity increases from 300 to 350 °C, then drops at 400 °C due to the thermal instability of benzene at elevated temperatures [1]. The trend for cyclic C_6 products above the UFL was discussed previously (**Fig. 6.6**).

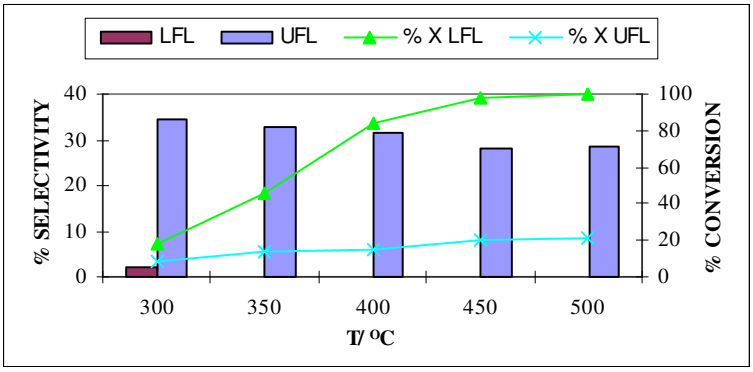

Fig. 6.22: Comparison of hexene selectivity with temperature for β-$NiMoO_4$ above the UFL and below the LFL at CT 1.8 s.

When operating under fuel lean conditions it was observed that the catalysts did not deactivate as was the case using fuel rich conditions although nitrogen dilution delayed the onset of coking. It seems that the availability of gaseous oxygen plays an important role in catalyst lifetime and the operating conditions definitely influence this.

Due to the risk involved in operating with feed compositions in the flammability range, especially with oxidation processes, no reactions were performed under these conditions.

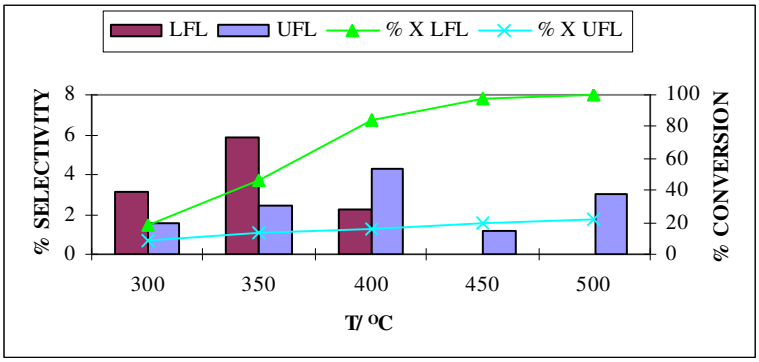

Fig. 6.23: Comparison of cyclic C_6 product selectivity with temperature for β-$NiMoO_4$ above the UFL and below the LFL at CT 1.8 s.

6.4 Effect of promoters on β-$NiMoO_4$

Promoters are substances which are not catalytically active on their own but are added to an active phase to allow it to function at its maximum capacity. They are added in small quantities to enhance the activity, selectivity or stability of the catalyst. These promoters may function differently and they have been divided into four classes [19, 20]. Textural promoters inhibit the growth of small particles of the active phase during use. Electronic promoters alter the electronic character by changing the chemical binding strength of catalysts. Structural promoters change the active metal surface, thereby altering specific reaction pathways. Promoters that protect the active phase against poisoning by impurities in the reactants and side-reactions are known as poison-resistant promoters. A promoted catalyst must comprise at least 75% active phase [19, 20].

Alkali and alkaline-earth metals were successfully employed [4, 21] as promoters to significantly improve the selectivity of butenes and butadienes of both the α and β phases of $NiMoO_4$ catalysts. A more detailed discussion on how these promoters' function is given in **Chapter 2.7.2.2**.

$NiMoO_4$ catalysts were promoted with different loadings of caesium. Preparation of these catalysts is given in **Chapter 3.2.4** and their characterization is given in **Chapter 4.5**. These promoted catalysts were tested using the optimized conditions that were used for best hexene selectivity obtained with the unpromoted β-$NiMoO_4$ catalysts *i.e.* fuel/O_2 ratio of 2.2, dilution with 43% nitrogen and a contact time of 1.04 seconds. The temperature range investigated was 300-500 °C.

6.4.1 Caesium doped catalysts

From the alkali metals used, caesium promoted β-$NiMoO_4$ catalysts gave the highest selectivity to butenes [4] when tested on *n*-butane and the same pattern for testing on *n*-hexane was expected. The precursors to β-$NiMoO_4$ with 3.5% and 5.7% caesium loadings were prepared and activated *in-situ* as for the unpromoted catalysts. **Tables 6.11-6.13** show the catalytic data obtained for the undoped and doped catalysts.

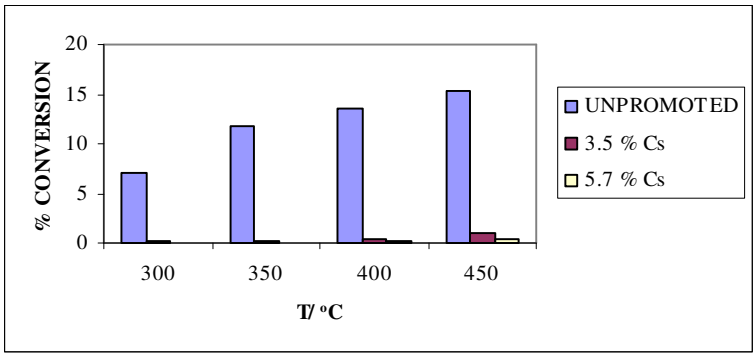

Fig. 6.24: Effect of temperature on n-hexane conversion with undoped and doped $NiMoO_4$ catalysts.

The incorporation of caesium reduced the activity of β-$NiMoO_4$ which is observed from the drop in conversion between the unpromoted and promoted catalysts (**Fig 6.24**). This may be accounted for by the decreased BET surface area of the catalysts due to doping [4, 21] suggesting that the dopant affects surface properties. Higher loadings of the alkali metal resulted in lower conversions correlated to further decreases in the surface areas. The decreased activity occurs because active sites that bind hexane are blocked by the caesium. If this is the case then limited catalysis can occur which reduces the activity of the catalysts.

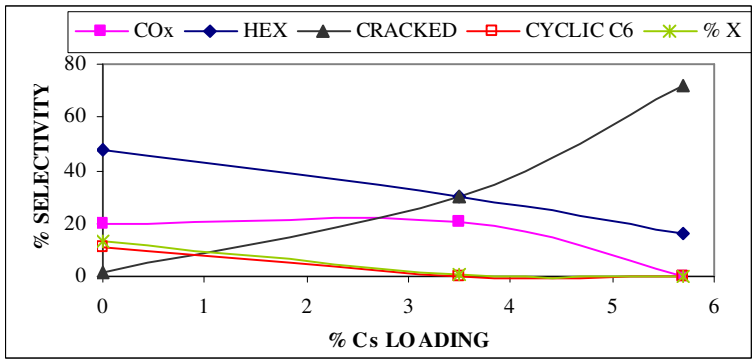

Fig 6.25: Effect of Cs loading on n-hexane conversion and selectivity to products at 400 °C.

Table 6.11: The effect of temperature on conversion, selectivity and yield of products for the ODH of n-hexane over undoped β-$NiMoO_4$ for CT 1.04 s.

T/ °C	% X	% SELECTIVITY				% YIELD			
		CRACKED PRODUCTS	HEXENES	CYCLIC C_6	CO_x	CRACKED PRODUCTS	HEXENES	CYCLIC C_6	CO_x
300	7.1	2.3	54.7	0.1	31.7	0.2	3.9	0.0	2.3
350	11.7	16.3	52.0	10.8	10.3	0.2	6.1	1.3	1.2
400	13.5	1.7	48.1	11.3	19.9	0.2	6.5	1.5	2.7
450	15.3	1.8	40.3	3.8	29.7	0.3	6.2	0.6	4.5

Table 6.12: The effect of temperature on conversion, selectivity and yield of products for the ODH of n-hexane over 3.5% Cs doped β-$NiMoO_4$ for CT 1.04 s.

T/ °C	% X	% SELECTIVITY				% YIELD			
		CRACKED PRODUCTS	HEXENES	CYCLIC C_6	CO_x	CRACKED PRODUCTS	HEXENES	CYCLIC C_6	CO_x
300	0.2	46.5	39.6	0.0	0.0	0.1	0.1	0.0	0.0
350	0.2	41.7	40.1	0.0	0.0	0.1	0.1	0.0	0.0
400	0.5	30.0	29.9	0.0	20.5	0.2	0.2	0.0	0.1
450	0.9	25.9	28.3	0.5	26.9	0.2	0.2	0.0	0.2

Table 6.13: The effect of temperature on conversion, selectivity and yield of products for the ODH of n-hexane over 5.7% Cs doped β-$NiMoO_4$ for CT 1.04 s.

T/ °C	% X	% SELECTIVITY				% YIELD			
		CRACKED PRODUCTS	HEXENES	CYCLIC C_6	CO_x	CRACKED PRODUCTS	HEXENES	CYCLIC C_6	CO_x
300	0.0	0.0	0.0	0.0	0.0	0.0	0.0	0.0	0.0
350	0.0	0.0	0.0	0.0	0.0	0.0	0.0	0.0	0.0
400	0.2	71.9	16.4	0.0	0.0	14.4	0.0	0.0	0.0
450	0.3	57.9	16.6	0.0	28.1	0.2	0.2	0.0	0.1

Comparison of the unpromoted catalyst to the promoted catalyst shows that the promoter also affected the selectivity of dehydrogenation products (**Fig. 6.25**), particularly selectivity to the hexenes. The selectivity to this desired product decreased with doping. The purpose of the alkali metal, however, was to increase the basicity of the catalyst surface to favour desorption of olefins which are more basic than the paraffin itself, which should reduce deep oxidation *i.e*. carbon oxide formation [22]. Since hexenes are considered to be nucleophilic, due to having high electron densities in their pi bonds, they should have weak interactions at the catalyst active site and be less reactive and increase in selectivity [4]. This was not the case in this study. NH_3-TPD showed that the catalyst is slightly acidic involving possibly two or three active sites. CO_2-TPD shows that the number of sites increases and they become more basic with doping. Alkali metal loading becomes disadvantageous beyond an optimum loading because the overdoping effect occurs [23]. Hence an explanation of these results is that, apart from the acid-base character, the concentration of the promoter ion also plays a significant role in the catalyst behaviour [24, 25].

In butane ODH selectivity to butenes improved up to 3% caesium loading only. This was correlated to increased electrical conductivity of the n-type semiconductor $NiMoO_4$ due to contribution of additional surface ionic conductivity from mobile Cs^+ which is associated with labile O^{2-} species. Beyond this metal loading the increase in caesium oxide particles leads to a loss in dispersion and a decrease in selectivity. Hence basicity, electrical conductivity and selectivity to dehydrogenation products are related [26].

TPR studies for *n*-butane showed that the reducibility of the catalyst decreases with increasing Cs loading [27]. If an oxide is difficult to reduce it will have low activity as is the case here and this suggests that the reaction occurs *via* the Mars -van Krevelen mechanism [8, 28, 29].

It is interesting to note that CO_x selectivity decreased as the selectivity to the cracked products increased with increasing promoter loading. This suggests that total decomposition is hindered by increasing surface basicity. The selectivity may also be related to its reducibility because if the metal-oxygen bond is strong (high reduction potential) it would be more difficult to remove oxygen to form oxygen containing compounds because it is more difficult for the catalyst to undergo redox cycles.

Cracked product selectivity is much higher for 5.7% caesium loading than for the 3.5% loading, which was compensated for by the decreased CO_x selectivity. Carbon oxides are products of deep

oxidation of hexane. The interaction of hexane with the catalytic surface is weaker for a more basic surface which reduces over-oxidation. This is true for the comparison of the promoted and unpromoted catalyst and increased promoter loading.

6.5 Reaction mechanism

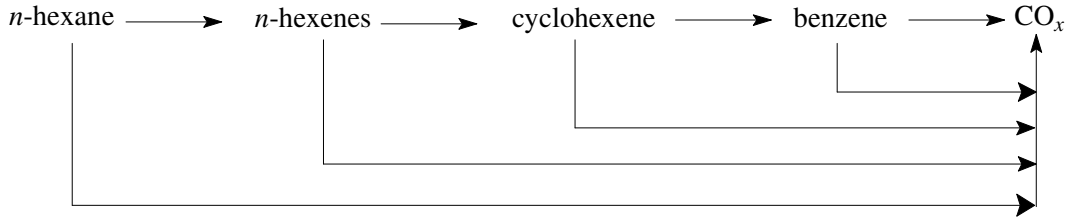

Scheme 6.1: Reaction pathway for the products from n-hexane.

Scheme 6.1 shows the pathways for the various products formed ending with the final decomposition products CO_x. Since the $NiMoO_4$ catalyst is only slightly basic, the surface of the catalyst favours a limited desorption of olefins and there is some interaction of the desorbed olefin and the catalyst surface. Depending on the residence time of the olefins on the surface, oxygen insertion is also possible. As mentioned in Chapter 2, the oxidative dehydrogenation of paraffins and $NiMoO_4$ in particular operates *via* the Mars -van Krevelen mechanism.

6.5.1 The pathway of 1, 2 and 3-hexene formation

n-Hexane is symmetric with one primary and two secondary carbon sites. In paraffin ODH it is well known that the activation and rate-determining step is the irreversible abstraction of hydrogen from a secondary carbon to give adsorbed radicals [29-32]. This adsorbed radical is very reactive and after removal of a second hydrogen from carbon 1 or 3 leads to 1- or 2-hexene, respectively. Isomerization of 2-hexene will lead to 3-hexene (**Scheme 6.2**).

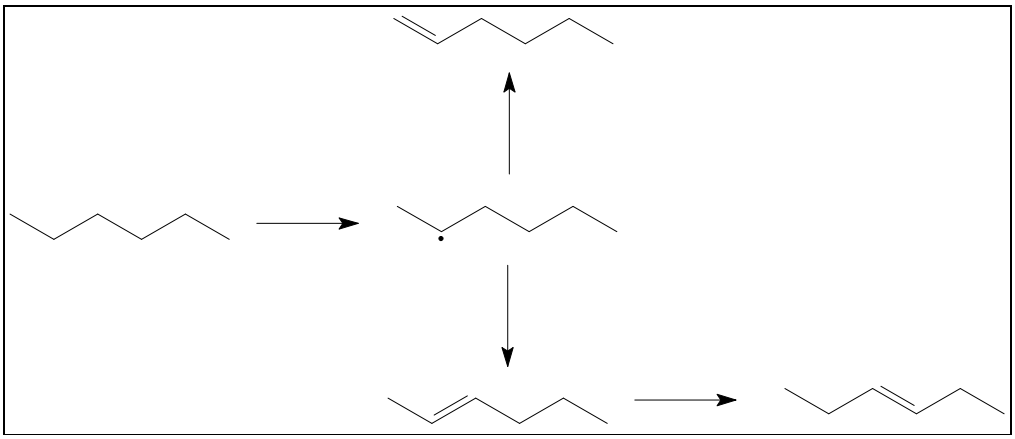

Scheme 6.2: Pathway of hexene formation.

6.6 Proposed reaction pathway for the ODH of *n*-hexane

Scheme: 6.3 shows the possible reaction mechanism for the ODH of hexane. Based on the data (**Chapter 6**, **Figs. 6.3-6.6**), 1-hexene selectivity decreases as the 2- and 3-hexenes selectivity increases. This is due to the possible isomerization equilibrium that exists between these isomers. Also as 1-hexene decreases there was an increase in benzene production. It can not be assumed however, that 1-hexene is the origin of benzene only because cyclohexene is already present initially. Three possible reaction mechanisms may exist for benzene formation, I) from 1-hexene *via* ring closure and ODH to benzene [33], II) 1,6 ring closure to cyclohexane followed by ODH to benzene and III) 1,5 ring closure followed by ring expansion to cyclohexane and ODH to benzene [34]. Since no cyclohexane was observed under these conditions, I is the most likely pathway with $NiMoO_4$. CO_x may arise from any intermediate since it increases with temperature.

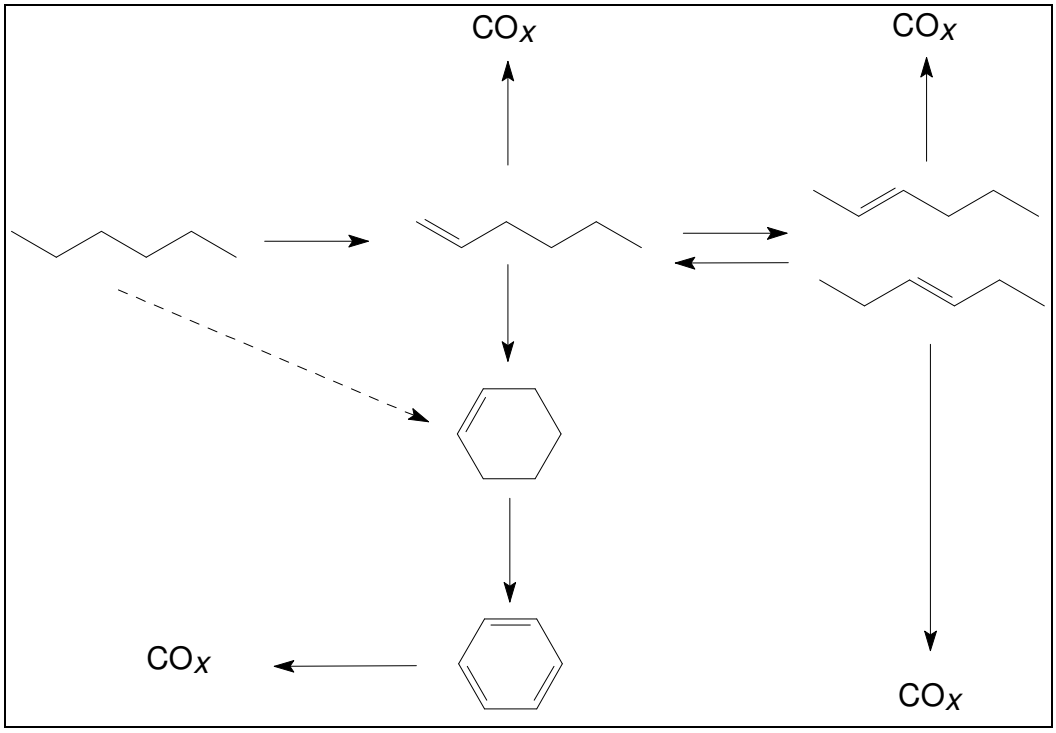

Scheme: 6.3: Possible reaction pathway for the ODH of n-hexane.

6.7 Summary and conclusion

Nickel molybdate catalysts of different phase composition were tested for the ODH of *n*-hexane above the UFL and all were found to be active. The product profile included CO_x, 1-hexene, 2-hexene, cyclohexene, benzene, propane/ene, butane/ene, ethanal, acetic acid, propanoic acid, 2,5-dimethyltetrahydrofuran, 2,5-hexanedione and water.

The six catalysts tested were catalyst A: α-$NiMoO_4$ with excess MoO_3; catalyst B: α-$NiMoO_4$; catalyst C: α-$NiMoO_4$ with β-$NiMoO_4$ and NiO; catalyst D: pure β-$NiMoO_4$; catalyst E: NiO and catalyst F: MoO_3. At equal conversion, it was found that catalyst A gave the highest selectivity to cyclic C_6 products, catalyst E gave the highest CO_x selectivity, catalyst C gave the highest total cracked product selectivity and catalyst D gave the highest hexenes selectivity. The most favoured product for MoO_3 was methylcyclopentane.

The catalyst with excess molybdenum in the form of MoO_3 showed the highest activity at 400 °C (31.9% hexane/air, at a contact time of 1.8 s), giving a conversion of 47.1%; however, selectivity to hexenes was poor. Catalyst D, the pure β-$NiMoO_4$ phase, at a contact time of 1.8 seconds gave a total hexene selectivity of 35.3% at 300°C and a 1-hexene selectivity of 24.8%.

Further testing of the β-$NiMoO_4$ phase to optimize selectivity to hexenes was performed above the UFL by varying the reaction conditions to improve the selectivity to dehydrogenation products. Changing the contact time at a constant temperature of 300 °C resulted in an increase in conversion. The highest conversion though was 6.8% at a contact time of 2.4 seconds. Hexene selectivity increased with increasing contact time, the highest being 34.4% of which 24.8% was due to 1-hexene. Above this contact time the CO_x's dominated.

When the feed was diluted with nitrogen there was an improvement in conversion up until 43% dilution. After this dilution the nitrogen uses more energy for heating than overcoming thermodynamic barriers. The hexene selectivity increased to 54.7%, while there was a drop in CO_x selectivity with the 43% dilution. The highest 1-hexene selectivity was 27.4%.

Changing the fuel/air ratio does affect hexene selectivity. The optimum condition in terms of hexene selectivity (particularly 1-hexene) was a fuel/O_2 ratio of 2.2, dilution with 43% nitrogen and a contact time of 1.04 seconds at 300 °C.

When the other polymorph, α-$NiMoO_4$ was compared to the β-$NiMoO_4$ above the UFL under the optimum conditions for hexene selectivity, at equal conversions, the β-phase again gave better selectivity to hexenes than the α-phase. The α-phase was shown to be more active above 385 °C. Hence it can be assumed that both the molybdenum coordination as well as temperature plays a role in terms of molybdate catalyst activity.

Comparison of the commercially obtained molybdate with the synthesized catalyst shows that both catalysts perform differently, due to the different methods of preparation. This was further confirmed by the different characterization data obtained for both catalysts.

When the hexane contact time was varied for β-$NiMoO_4$ below the LFL, the same product profile was observed as that when the catalyst was tested above the UFL except that no 1-hexene was observed. Conversion increased with temperature, then stabilized. Very high conversions were observed, up to 100%, and also very high selectivity to carbon oxides. The highest selectivity to hexenes exclusively composed of 2-hexenes is 68.6% at a conversion of 3%.

Comparison of the two $NiMoO_4$ phases below the lower LFL showed that β-$NiMoO_4$ was more active than α-$NiMoO_4$ below 400 °C. Hence we can conclude that the operating conditions (*i.e.* fuel rich or fuel lean) also play an important role.

Comparison of the β-phase above and below the flammability range suggests that both the conversions and selectivity profiles for the catalysts change due to the different oxidizing environments.

β-$NiMoO_4$ catalysts were doped with 3.5 and 5.7% caesium and tested using the optimized conditions for best hexene selectivity obtained with the undoped catalysts. Incorporation of caesium reduced the activity of β-$NiMoO_4$ and higher loadings of the alkali metal resulted in further reduction in activity. The decreased activity was probably due to blockage of active sites on hexane by the caesium, which is reflected by the reduced surface areas of these catalysts.

Comparison of the unpromoted catalyst to the promoted catalyst showed that the promoter also reduced the selectivity to dehydrogenation products. Although the purpose of the dopant was to increase the basicity of the catalyst to improve the selectivity to the olefins by causing weak interactions between the hydrocarbon and catalyst surface, the overdoping effect is significant in having the opposite effect. This is because beyond a certain metal loading the increase in caesium oxide particles leads to a loss in dispersion instead of contributing to additional surface ionic conductivity which is associated with labile O^{2-} species and a decrease in hexene selectivity. Apart from basicity, electrical conductivity affects the selectivity to dehydrogenation products.

Finally it was proposed that the possible pathways for *n*-hexane ODH over $NiMoO_4$ are *via* 1-hexene, followed by ring closure and ODH to benzene or isomerization to 2- and 3-hexene.

References

[1] H. B. Friedrich, N. Govender and M. R. Mathebula, Appl. Catal. A, 297 (2006) 81.

[2] R. P. O' Connor and L. D. Schmidt, Chem. Eng. Sci., 55 (2000) 5693.

[3] C. Mazzocchia, C. Aboumrad, C. Diagne, E. Tempesti, J. M. Herrmann and G. Thomas, Catal. Lett, 10 (1991) 181.

[4] R. M. Martin-Aranda, M. F. Portela, L. M. Madeira, F. Freire and M. Oliveira, Appl. Catal. A, 127 (1995) 201.

[5] H. H. Kung, P. Michalakos, L. Owens, M. Kung, P. Andersen, O. Owen and I. Jahan, "Catalytic Selective Oxidation", American Chemical Society, Washington, 1993.

[6] M. E. Harlin, L. B. Backman, A. O. I. Krause and O. J. T. Jylha, J. Catal., 183 (1999) 300.

[7] A. Kaddouri, C. Del Rosso, C. Mazzocchia, P. Gronchi and D. Fumagalli, J. Therm. Anal. Calorim, 66 (2001) 63.

[8] P. Mars and D. W. van Krevelen, Chem. Eng. Sci. Special Suppl., 3 (1954) 41.

[9] O. Lezla, E. Bordes and P. Courtine, J. Catal., 170 (1997) 346.

[10] F. Cavani and F. Trifiro, Catal. Today, 24 (1995) 307.

[11] R. Burch and E. Crabb, Appl. Catal. A, 100 (1993) 111.

[12] F. J. Maldonado-Hodar, L. M. Madeira and M. F. Portela, J. Catal., 164 (1996) 399.

[13] P. Williams, "Hexene Isomers at Equilibrium", Personal Communication, Sasol, 2008.

[14] R. H. Perry and D. W. Green, Vol. Section 26, The McGraw Hill Campanies, 1999, p. 54.

[15] F. Cavani and F. Trifiro, Catal. Today, 51 (1999) 561.

[16] E. A. Mamedov, Appl. Catal. A, 116 (1994) 49.

[17] B.W. Wojciechowski, Catal. Rev. -Sci. Eng., 40 (1998) 209.

[18] A. Pantazidis, A. Burrows, C. J. Kiely and C. Mirodatos, J. Catal., 1997, 177 (1998) 325.

[19] J. Hagen, "Industrial Catalysis -A Practical Approach", Germany, 1999.

[20] G. C. Bond, "Heterogeneous Catalysis, Principles and Application", Oxford Science Publication, 1987.

[21] L. M. Madeira, R. M. Martin-Aranda, F. J. Maldonado-Hodar, J. L. G. Fierro and M. F. Portela, J. Catal., 169 (1997) 469.

[22] S. Albonetti, F. Cavani and F. Trifiro, Catal. Rev. -Sci. Eng., 38 (1996) 413.

[23] L. M. Madeira, M. F. Portela, R. M. Martin-Aranda and F. Freire, J. Mol. Catal. A: Chem., 111 (1996) 313.

[24] S. A. Driscoll, L. Zhang, U. S. Ozkan, S. T. Oyama and J. W. Hightower, American

Chemical Society; Washington DC, ACS Symposium Series No. 523 (1993) 340.

[25] S. A. Driscoll, D. K. Gardner and U. S. Ozkan, J. Catal., 147 (1994) 379.

[26] L. M. Madeira, J. M. Hermann, F. G. Freire, M. F. Portela and F. J. Maldonado, J. Catal., 58 (1997) 243.

[27] L. M. Madeira, M. F. Portela, C. Mazzocchia, A. Kaddouri and R. Anouchinsky, Catal. Today, 40 (1998) 229.

[28] L. M. Madeira, J. M. Herrmann, J. Disdier, M. F. Portela and F. G. Freire, Appl. Catal. A, 235 (2002) 1.

[29] C. Tellez, M. Abon, J. A. Dalmon, C. Mirodatos and J. Santamaria, J. Catal., 195 (2000) 113.

[30] T. Blasco, J. M. Lopez Nieto, A. Dejoz and A. Vazquez, J. Catal., 157 (1995) 271.

[31] P. M. Michalakos, M. C. Kung, I. Jahan and H. H. Kung, J. Catal., 140 (1993) 226.

[32] B. Grzybowska-Swierkosz, Appl. Catal. A, 157 (1997) 409.

[33] C. Kepel, C. Breitkopf and M. Standke, J. Mol. Catal. A: Chem., 210 (2004) 211.

[34] P. Meriaudeau and C. Naccache, Catal. Rev. -Sci. Eng., 39 (1997) 5.

CHAPTER 7

SUMMARY AND CONCLUSION

Nickel molybdenum oxide catalysts were synthesized and tested for oxidative dehydrogenation of *n*-hexane for feed/air ratios above and below the flammability limit. Two vertical fixed bed continuous flow reactors were designed and constructed for the catalytic testing.

The six catalysts tested were catalyst A: α-$NiMoO_4$ with excess MoO_3; catalyst B: α-$NiMoO_4$; catalyst C: α-$NiMoO_4$ with β-$NiMoO_4$ and NiO; catalyst D: pure β-$NiMoO_4$; catalyst E: NiO and catalyst F: MoO_3. The co-precipitation method was used to synthesize $NiMoO_4$ precursors (catalysts A-C) and several techniques were used to characterize these catalysts. ICP determined the chemical composition and XRD and IR spectroscopy showed the variation in phase composition. High temperature XRD showed that catalyst D after *in-situ* activation was composed of pure β-$NiMoO_4$. XPS showed that the Mo3$d_{5/2}$ and Ni2$p_{3/2}$ binding energy are typical of Mo^{6+} and Ni^{2+} oxidation states. BET surface areas were found to be influenced by the chemical and phase composition of the catalysts.

Products observed for all six catalysts were the carbon oxides (CO and CO_2), isomers of hexene (1-hexene, 2-hexene and 3-hexene), cyclic C_6 products (cyclohexene and benzene), cracked products: alkanes/alkenes (propane/ene, butane/ene) and oxygenates (ethanal, acetic acid and propanoic acid).

When the effect of phase composition of $NiMoO_4$ catalysts on their catalytic activity and selectivity to dehydrogenation products was studied in the temperature range 300-500 °C, it was found that at equal conversion, catalyst A gave the highest selectivity to cyclic C_6 products, catalyst E gave the highest CO_x selectivity, catalyst C gave the highest total cracked product selectivity and catalyst D gave the highest hexenes selectivity.

The two different modifications of $NiMoO_4$, which differ in the molybdenum coordination, clearly show different activity and selectivity. The pure β-phase was more active and selective toward the hexenes than the α-phase, whereas the α-phase with MoO_3 is more active. This suggests that the phase cooperation between the two phases (synergetic effect) plays an important role in modifying catalytic activity.

Hence the most selective catalyst for the synthesis of hexenes was the pure β-$NiMoO_4$, which gave 25% selectivity to 1-hexene and 10% selectivity to 2-hexenes and 3-hexenes at 9% conversion. Further experiments varying reaction conditions were performed in order to optimize the selectivity to hexenes. Changing the contact time at a constant temperature of 300 °C resulted in an increase in conversion. The highest conversion though was 6.8% at a contact time of 2.4 seconds. Above this contact time the CO_x's dominated.

When the feed was diluted with nitrogen conversion increased until 43% dilution. The hexene selectivity increased to 54.7%, while there was a drop in CO_x selectivity with the 43% dilution. The highest 1-hexene selectivity was 27.4%. Changing the fuel/air ratio did not show improvement in hexene selectivity. The optimum condition in terms of hexene selectivity (particularly 1-hexene) was a fuel/O_2 ratio of 2.2, dilution with 43% nitrogen and a contact time of 1.04 seconds at 300 °C.

β-$NiMoO_4$ when tested below the LFL gave the same product profile as that when the catalyst was tested above the UFL except that no 1-hexene was observed. Very high conversions and very high selectivity to carbon oxides were observed. The highest selectivity to hexenes exclusively 2-hexenes, is 68.6%.

BET surface area measurements, XPS and TPO-MS showed that used catalysts had coked and was the main reason for catalyst deactivation. This is also dependent on the oxidizing environment and N_2 dilution extended the onset of coking.

It can be concluded from comparison of the β-phase above and below the flammability range that the operating conditions (fuel rich or fuel lean, temperature, contact time, nitrogen dilution) all affect the catalytic performance.

Caesium-doped $NiMoO_4$ catalysts with different loadings were synthesized *via* the wet impregnation method. Catalytic results showed reduced activity of β-$NiMoO_4$ was due to incorporation of caesium which was correlated to the reduced surface area as measured by BET. The dopant also reduced the selectivity of dehydrogenation products and the possible reason for this was the overdoping effect.

The existence of homogeneous gas phase reactions, although significantly reduced in a carborundum-packed reactor must still be considered especially for the formation of cyclic products at elevated temperatures. Homogeneous-heterogeneous systems were considered in this study for the oxidative dehydrogenation of *n*-hexane over nickel-molybdenum oxide catalysts.

It was proposed the mechanism for *n*-hexane ODH over $NiMoO_4$ proceeded through 1-hexene *via* ring closure and ODH to benzene or isomerization to 2- and 3-hexene.

APPENDIX

EQUIPMENT USED DURING THE CATALYTIC TESTING

Karl Fischer Analysis

The determination of water in the liquid samples was done with the Karl Fischer method using a Mettler Karl-Fischer titrator DL35 (**Fig A**). The Karl Fischer reagent which is specific for water is composed of iodine, pyridine, methanol and sulfur dioxide. This method is based on the following principle: water reacts with iodine and a reactive component formed from the reaction of sulfur dioxide with an alcohol (methanol) in the presence of a suitable base.

Fig A: Karl Fischer apparatus used for water determination.

Fig. B: High performance liquid pump (HPLC) used for feeding n-hexane into the reactor.

Fig C: Wet gas flow meter to measure total volume of gas.

Specs for the wet gas flow meter (**Fig C**) are

Apparatus: Drum-type Gas Meter, TG1-PVS-PVC

Type: TG 1/5

Model: Casing of Polyvinlychloride, Measuring drum of Polyvinylchloride

Serial-no: 0.524.1 BJ

Fig D: Ohaus Adventurer^{TM} balance used for determining mass of hexane feed.

Fig E: A Grant LTD G -20 to 100°C chiller used for cooling products in catch pot.

Fig F: Perkin Elmer Autosystem XL GC used for the quantification of hydrocarbons.

Fig G: Varian 3700 GC used for carbon oxide separation and quantification.

Fig H: Reactor set up used for testing n-hexane below LFL.

Fig I: Reactor set up used for testing n-hexane above the UFL.

Fig J: Control board containing various components (pressure regulators, rotameters, pressure gauges, temperature controllers).

MSDS DATA FOR *n*-HEXANE[1]

General

Synonyms: n-hexane, normal hexane, hexyl hydride

Molecular formula: C_6H_{14}

Physical data

Appearance: colourless liquid

Melting point: -95 °C

Boiling point: 69 °C

Vapour density: 3 (air = 1)

Vapour pressure: 132 mm Hg at 20 °C

Specific gravity: 0.659

Flash point: -10 F

Explosion limits: 1.2% - 7.7%

Autoignition temperature: 453 F

Stability

Stable. Incompatible with oxidizing agents, chlorine, fluorine, magnesium perchlorate. Highly flammable. Readily forms explosive mixtures with air. Note low flash point.

Toxicology

May cause impaired fertility. Harmful by inhalation. Irritant. May cause CNS depression. Prolonged exposure may cause serious health damage.

Environmental information

Harmful in the environment - may cause long-term adverse effects.

Personal protection

Safety glasses. Effective ventilation. Remove sources of ignition from the working area.

1. Site: http://msds.chem.ox.ac.uk/HE/hexane.html

MSDS DATA FOR 1-HEXENE[2]

General

Synonyms: butyl ethylene, hex-1-ene

Molecular formula: $C_6 H_{12}$

CAS No: 592-41-6

EINECS No: 209-753-1

Physical data

Appearance: colourless liquid

Melting point: -141 to -139 °C

Boiling point: 62 to 63 °C

Vapour density: 2.9 (air = 1)

Vapour pressure: 412 mbar at 38 °C

Density (g cm^{-3}): 0.673

Flash point: -25 °C (closed cup)

Explosion limits: 1.2 - 6.9 % by volume

Autoignition temperature: 272 °C

Water solubility: 54 mg/l

Stability

Stable. Highly flammable - note low flash point. Incompatible with strong oxidizing agents, strong acids, combustible material.

Toxicology

May cause lung damage if swallowed or inhaled. Skin, eye and respiratory irritant.

Personal protection

Safety glasses, good ventilation.

2. Site:http://msds.chem.ox.ac.uk/HE/hexane.html

GAS CHROMATOGRAPHY PARAMETERS

1. GC 1: Perkin Elmer Autosystem (FID)

Carrier parameters:

Carrier gas: N_2 (HP grade), Supplier: Afrox

Vacuum compensation: OFF

Split control mode: FLOW Set point: 50.2 ml/min

Initial set point: 2 PSIG Initial hold: 8.00 min

Heater zones:

Injector: PSSI

Initial setpoint: 220°C Initial Hold: 999.0 min

Detector: 250°C

Oven Programme:

Initial Temp: 40°C Maximum Temp: 300°C

Initial Hold: 8.00 min Equilibration Time: 0.2

Ramp 1: 7.0°C/ min to 200 °C, hold for 2.00 min

Total run time: 32.86 min

2. GC 2: Isothermal Varian 3700 with TCD

Detector temperature: 130°C

Column temperature: 220°C

Injector temperature: 150°C

TCD filament temperature: 150°C

Output: Negative

Range: 0.5 mV

Carrier gas: Helium (instrument grade), Supplier: Afrox

GC COLUMN SPECIFICATIONS

1. Perkin Elmer Autosystem (FID)

Chromopak capillary column

Coating: CP Sil 24 CB

Dimensions: Length: 30 m

Inner diameter: 0.32 mm

Outer diameter: 0.45 mm

Maximum allowable temperature 225°C

2. Varian 3700 isothermal GC (TCD)

Pre-column

Stainless steel

Support: Chromosorb WHPSP

Dimensions: Length 1m

OD 1/8”

ID: 2.2 mm

Mesh range: 80/100

Liquid phases: OV-225 weight 10 %

Temperature range 20-275°C

Analytical column

Stainless steel

Support: carboxen ^{TM} 1000

Dimension: Length 2.5 m

OD: 1/8”

ID: 2.2 mm

Mesh range: 60/80

Maximum temperature: 225°C

CALCULATION OF THE CARBON MOLE BALANCE

In these studies a carbon balance was always calculated. The error for the results reported was always ± 5 %. The carbon balance was calculated as follows:

1) The hexane feed fed into the reactor was recorded on a balance and was used to calculate the moles of feed in.
2) To account for the products of oxidative dehydrogenation coming out of the reactor both online and offline analysis was performed.
3) All products from the gas stream including feed were calibrated on the GC with standards.
4) This gas had to pass through an online 500µl sample loop before entering the GC's FID (for organic products) and TCD (for the carbon oxides). The total moles of gas from reaction were quantified by scaling up to the volume recorded by the wet gas flow meter which measured the total volume of gaseous products produced during the reaction leaving the reactor.
5) The other source of products was from the sampling pot which contained organic and aqueous products which had condensed from the reaction. The mass of each sample was recorded and then subjected to Karl Fischer analysis to determine the amount of water that was present to determine the true mass of organic product.
6) Due to greater number of products contained in the liquid samples, instead of using calibration graphs for quantifying the product, response factors were used. The percentage areas from the GC trace were taken as representative of the mass percent of components in the organic and aqueous samples.
7) For the total number of moles of products produced, moles calculated from the gas stream was added to those calculated from the liquid stream for each product, followed by multiplying by the appropriate carbon numbers for each and then summed up.

SAMPLE CACULATION

	MASS OF ORGANIC PRODUCT	MASS OF PRODUCT	KARL FISCHER %
ORGANIC	0.91	1.01	10.19
AQUEOUS	0.14	0.61	76.87

	% AREAS											
	PROP	**BUT**	**ETHANAL**	**HEXANE**	**1-HEX**	**2-HEX (t)**	**2-HEX (c)**	**CYCLO-HEXENE**	**BENZENE**	**ACETIC ACID**	**PROPANOIC ACID**	**2,5-THF**
ORGANIC	0	0	0	97.51	0	0	1.61	0	0	0	0.01	0
AQUEOUS	0	0	0	0	19.48	6.79	0	0	59.99	0	0	0

*CORRECTED AREAS													
	PROP	**BUT**	**ETHANAL**	**HEXANE**	**1-HEX**	**2-HEX (T)**	**2-HEX (C)**	**CYCLO-HEXENE**	**BENZENE**	**ACETIC ACID**	**PROPANOIC ACID**	**2,5-THF**	**TOTAL**
RF	0	0	0.35	1	1.09	1.1	1.1	0.8	1.2	0.24	0.3	0.5	
ORGANIC	0	0	0	97.51	0	0	1.6905	0	0	0	0.003	0	99.2
AQUEOUS	0	0	0	0	21.3	7.5	0	0	73.0	0	0	0	101.8

*CORRECTED AREAS =% AREA x RF

*NORMALISED AREA													
	PROP	**BUT**	**ETHANAL**	**HEXANE**	**1-HEX**	**2-HEX (T)**	**2-HEX (C)**	**CYCLO-HEXENE**	**BENZENE**	**ACETIC ACID**	**PROPANOIC ACID**	**2,5-THF**	**TOTAL**
ORGANIC	0.00E+00	0.00E+00	0.00E+00	9.83E-01	0.00E+00	0.00E+00	1.70E-02	0.00E+00	0.00E+00	0.00E+00	3.02E-05	0.00E+00	1.00E+02
AQUEOUS	0.00E+00	0.00E+00	0.00E+00	0.00E+00	2.09E-01	7.35E-02	0.00E+00	0.00E+00	7.17E-01	0.00E+00	0.00E+00	0.00E+00	1.00E+02

*NORMALISED AREA = CORRECTED AREA/ TOTAL CORECTED AREA

*NO OF MOLES												
	PROP	**BUT**	**ETHANAL**	**HEXANE**	**1-HEX**	**2-HEX (T)**	**2-HEX (C)**	**CYCLO-HEXENE**	**BENZENE**	**ACETIC ACID**	**PROPANOIC ACID**	**2,5-THF**
MM	44.10	58.12	44.05	86.17	84.16	84.16	84.16	82.00	78.11	60.05	74.08	100.00
ORGANIC	0.00E+00	0.00E+00	0.00E+00	1.04E-02	0.00E+00	0.00E+00	1.84E-04	0.00E+00	0.00E+00	0.00E+00	0	1.10E-05
AQUEOUS	0.00E+00	0.00E+00	0.00E+00	0.00E+00	3.49E-04	1.22E-04	0.00E+00	0.00E+00	1.29E-03	0.00E+00	0.00E+00	0.00E+00

*NO MOLES = (NORMALISED AREA OF EACH COMPONENT/ TOTAL NORMALISED AREA) x MASS OF ORGANIC)/ MOLAR MAS OF EACH COMPONENT

OFF GAS FLOW/ ml	14950													
	FID												**TCD**	
	PROP	**BUT**	**ETHANAL**	**HEXANE**	**1-HEX**	**2-HEX (C)**	**2-HEX (T)**	**CYCLO-HEX**	**BENZENE**	**ACETIC ACID**	**PROPANOIC ACID**	**2,5-THF**	**CO**	**CO2**
RT	6.1	6.3	6.5	6.8	7.1	7..2	7.5	8.9	9.6	10.1	11.40	10.2	2.6	18.6
PEAK AREAS	0.49	0.19	133.59	451804.18	3168.98	4697.59	8768.81	130.57	527.23	179.17	0.00	0.00	34.98	27.13
EQUATION	y=1.86e+10	y=2.51e+11x	y=1.28E+10x	y=4.37E+11x	y=6.49E+10x	y=6.07e+10x	y=6.07e+10x	y=4.57E+10x	y=7.58e+10x	y=5.52e+10x	y=4.73e+10x	y=9.96E+10X	y=5.29E+7x	y=6.09E+7x
MOLES IN INJECTION VOL	2.63E-11	7.57E-13	1.04E-08	1.03E-06	4.88E-08	7.74E-08	1.44E-08	2.85E-09	6.95E-09	3.24E-09	0.00E+00	0.00E+00	6.61E-07	4.45E-07
ACTUAL MOLES	7.88E-07	2.26E-08	3.12E-04	3.09E-02	1.46E-03	2.31E-03	4.32E-04	8.53E-05	2.08E-04	9.70E-05	0.00E+00	0.00E+00	1.98E-02	1.33E-02

*ACTUAL MOLES = (MOLES IN INJECTION VOLUME x TOTAL GAS VOLUME (ml))/ 0.5 mL

TOTAL MOLES													
PROP	**BUT**	**ETHANA;L**	**HEXANE**	**1-HEX**	**2-HEX (C)**	**2-HEX (T)**	**CYCLO-HEXENE**	**BENZENE**	**ACETIC ACID**	**PROPANOIC ACID**	**2,5-THF**	**CO**	**CO_2**
7.88E-07	2.26E-08	3.12E-04	4.13E-02	1.81E-03	2.44E-03	6.16E-04	8.53E-05	1.49E-03	9.70E-05	3.71E-07	0.00E+00	1.98E-02	1.33E-02

HEXANE					FID	TCD		
MASS 1	**MASS 2**	**MASS ENTERING REACTOR (g)**	**MOLES ENTERING REACTOR**	**MOL C IN**	**MOL C OUT***	**MOL C OUT***	**TOTAL C**	**% C**
1142.62	1137.86	4.76	0.055	0.33	0.29	0.033	0.32	96.69

*MOLE CARBON OUT = MOLE OF EACH PRODUCT X CRABON NUMBER FOR PRODUCT

TYPICAL GC TRACE FROM THE FID

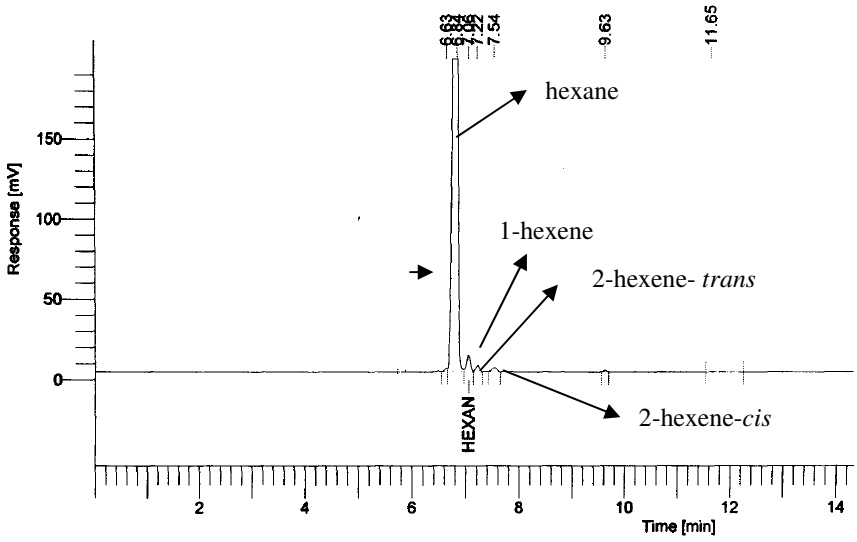

Fig K: GC trace from the Perkin Elmer Autosystem

LIST OF ENGINEERING SYMBOLS


filter


isocratic pump


non return valve


release valve

pressure gauge


ball valve


rotameter


cylinder


wet gas flow meter


sampling vessel


needle valve


three way valve

GC gas chromatograph


pressure regulator

heated line


hexane bottle

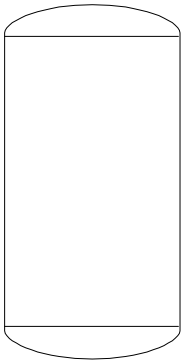
reactor